U.PORTO

FEUP FACULDADE DE ENGENHARIA
UNIVERSIDADE DO PORTO

Joining of light metals through diffusion bonding using cold rolled Ni/Ti multilayers

Omid Emadinia

Realized as the dissertation of

Integrated Master of Metallurgical and Materials Engineering

Supervisor: Professor Dr. Manuel Fernando Gonçalves Vieira

Portugal, Porto, March 2013

CANDIDATO	Omid Emadinia	*Código*	201004113
TÍTULO	Joining of light metals through diffusion bonding using cold rolled Ni/Ti multilayers		
DATA	15 de Março de 2013		
LOCAL	Faculdade de Engenharia da Universidade do Porto - Sala F103 - 14h30		
JÚRI	*Presidente*	Professora Doutora Filomena Maria da Conceição Viana	DEMM/FEUP
	Arguente	Professor Doutor Aníbal José Reis Guedes	DEM/EEUM
	Orientador	Professor Doutor Manuel Fernando Gonçalves Vieira	DEMM/FEUP

Acknowledgments;

Great thanks to my supervisor Professor Dr. Manuel Vieira who shared his research ideas to develop my thesis. I appreciate his kindly and patient direction, as well as his sympathy and positive point of view in difficult situations during the past two years.

I thank Professor Dr. Filomena Viana for her great suggestions which were so useful in developing the work. Her challenging mind influenced me and stimulated my ideas.

Thanks to Dr. Sónia Simões for teaching me how to work with equipment and use software as well as managing the tests and joints.

Professor Dr. Luís Filipe Malheiros, Head of Department, kindly provided me with access where needed.

Many thanks to Professor Dr. Carlos Silva Ribeiro who started teaching me in English at the time I began to attend FEUP. Without that I could not have completed this study.

The friendly personnel of the faculty provided non-stop assistance.

The Material Center of University of Porto, CEMUP, kindly shared their time and equipment.

To Laleh, my beloved wife, special thanks, and to Mandana my sweetheart daughter. They tolerated student life for the past two years while being far from the family.

Thanks indeed to my parents, brothers and brother-in-law In Iran for their help in many ways and at any time I needed them.

Finally, thanks to my friends and anybody else who directly and indirectly helped and inspired me on the way to my goal.

Abstract

Nitinol shape memory alloy and titanium alloys are light alloys used in different areas such as aerospace engineering, medical and defence applications that is why proper joining methods could promote their utilization. The shortcomings of the traditional welding methods could be improved by solid state joining techniques among which diffusion bonding (D.B.) has been selected for developing this master thesis. It has been claimed that reactive foils could reduce the required pressure and temperature for D.B process. This research deals with the fabrication of nano Ni/Ti multilayer through accumulative roll bonding. The fabricated foil was used as interlayer for joining TiNi to Ti6Al4V. This type of joint can preserve the shape memory or superelastic behaviors of the TiNi substrate in the interface because it will provide same chemical composition and microstructure across the joint.

Processed batches were composed of Ti (99.6%) and Ni (99.89%) foils with 200 μm and 125 μm thicknesses, respectively. That selection can provide equiatomic TiNi. Accumulative roll bonding (ARB) process was performed up to 15 cycles at room temperature by the strain rate of $20s^{-1}$. D.B was performed in a radiating furnace assembled with a LLOYD LR30K tensile machine under 10 MPa and 10^{-3} Pa for all experiments. Phase evolution and joint quality of Ti6Al4V to the nitinol alloy were investigated under 4 conditions. Two D.B. experiments were conducted with foils roll bonded for 10 and 15 cycles, at 800 °C/1h to evaluate the effect of deformation level and multilayer thickness on the joined zone. The two other D.Bs were made by using 10 cycle processed laminated foil, one at 700 °C for 1h and the other one at same temperature for 3h to evaluate the influences of the temperature reduction and the increase of diffusion time on the joints microstructure. Characterization of the laminated foils and joints were carried out by using DSC, OM, SEM, EDS, EBSD and microhardness measurements.

SEM observations of 10 cycles of ARB revealed ultra and nano alternated layers of Ni and Ti with small fragmentations. Some delaminated regions were seen. The increase of the cycles had improved the uniformity of the layers` reduction. A strong and brittle nanocomposite of Ni/Ti was produced after introducing the strain level of 11.55. High strain rate has a great influence on developing nano layers in comparison with the common rate of $\varepsilon^{\circ} = 0.1s^{-1}$, mentioned in the literature. Diffusion of constituents was observed in layers and it had increased by the growth of the deformation level. Intermediate phases, existing in the equilibrium diagram of the Ni and Ti, were observed in the laminated foil after heating processes. Kirkendall voids grow by temperature rise in the absence of pressure. Some parameters such as reduction of the thickness of the layers, temperature rise and the increase of the interval of the solid state welding were effective in reducing Ti_2Ni and $TiNi_3$ and in promoting the distribution and the formation of TiNi intermetallic phase as well.

Diffusion bonding is more effective at the interface of the multilayer and Ti6Al4V than that of the other substrate. Inclusions are observed at the joined region of the foil and nitinol substrate. The interlayer has found the chemical composition of a semi-equiatomic nitinol alloy. Both bonding time and temperature caused the formation of intermetallic grains with micrometric sizes.

Key words: ARB, multilayer, deformation, nano, diffusion bonding, intermetallic

Contents

List of figures;

List of tables;

Chapter one: Introduction

In this chapter the physical and metallurgical aspects of the materials used in this research will be explained as well as the techniques used to fabricate the intended product.

1.1 Solid state bonding

Applying joining technology is inevitable in man-made production. It encompasses any categories such as solid state bonding, soldering/brazing, fusion welding and adhesive bonding. This classification is based on the physical states of the parts. Those joining techniques are mainly used for metals and some can be utilized for ceramics and plastics. Joining aims at assembling two parts permanently through establishing a chemical, mechanical or metallurgical bonding between the faying faces. It has various applications, for large parts to micro-blocks, in medical, aerospace and defence industries [1].

It will be possible to join two solid surfaces without using any external material or energy if their surfaces are completely clean and atomically flat. It is fulfilled through a driving force resulted from the reduction of Gibbs free energy of the system, i.e. such flat surfaces have high free energy tending to reduce it e.g. silicon wafer bonding in tightly controlled environment [1]. It is very far to apply such method for engineering materials and industrial applications [2].

Solid state welding, SSW, joins two similar or dissimilar materials without using any filler that melts during the process. Pressure could also be used during the process and the process temperature reaches below the melting point of the base material. The process involves either deformation or diffusion. The latter case might include microscopic deformation in order to provide high quality joint. SSW is applicable in the case of metal joining when the phase diagram indicates that it is difficult to weld two parts together due to the formation of intermetallic or no solid solution. In this case the study of the joint area is very important because that region is most likely to failure. This evaluation is carried out by SEM and TEM. Solid state welding is also known as nonmelting process which includes friction welding, diffusion welding, explosion welding, roll welding and ultrasonic welding. For this research diffusion bonding will be used as the joining process of the light alloys and roll bonding will also be applied to develop the multilayer foil through accumulative roll bonding. Diffusion bonding is mostly used in aerospace industry particularly for Ti, Ni and Co alloys [2].

1.2 Diffusion bonding (DB)

Diffusion bonding accomplishes the joint without using any liquid state at the interface. The simultaneous application of pressure and temperature for a period of time will complete the joint under the following conditions;

- T_m (absolute melting temperature) of the base materials > Process temperature > ½ of the T_m;
- Applying pressure to introduce microscopic deformation at the faying faces;
- Using interface aids [2].

Bonding aids, such as foils or coatings, are used to avoid the formation of any intermetallic phase or any low melting temperature phase at the joining interface. When the constituents of the base have low diffusivity, the aid with elements having high mobility would promote the diffusion process. Ni-phosphorous electroless is a common aid. Another aim of this technique is to clean the surface in situ. Materials like Ti-alloys having high solubility of interstitial elements and could be used for this purpose. If the interlayer were soft, the contact area would increase. It is said that the 0.025 mm thick aid gives the highest strength and if the thickness increases the strength of the joint decreases [2]. The joining surface should be free of any large void or barrier otherwise the atomic bond is embedded. For example titanium at 850ºC dissolves its thin oxide layer and also absorbs gases on its surface or silver does so at temperatures above 190 ºC. Ta, W, Fe, Zr and Nb behave similarly. Metals showing high solubility of interstitial contaminants are well applied for DB while Al, Fe and Co base alloys are not easily solid state welded [2]. The mechanism of DB process involves three stages, they are not discrete but begin and end gradually, which are mentioned in the following [2];

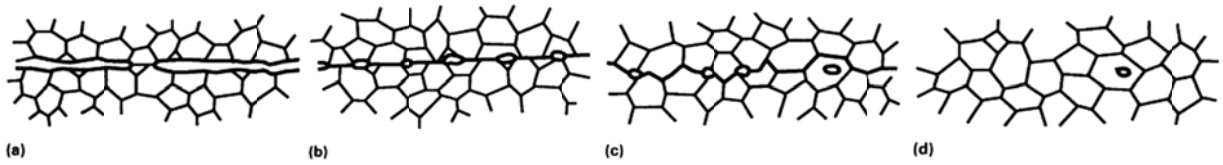

Figure 1 - Sequence of metallurgical stages in DB [2]

1. Initial contact and localized deformation; the interface is not completely planar and contains some voids. The intimate surface would change into new grain, figure 1-a. Factors such as surface roughness, yield strength, work hardening, temperature and pressure influence this stage, e.g. if high pressure is applied this stage will last shortly.
2. In the second stage the voids shrink and grain boundaries migrate to give a lower energy to the system because the surface area decreases. This reduction in the energy level provides

the force required for the solid bonding through mass transport process. Creep and diffusion mechanisms are effective here. Atoms flow along the grain boundaries; figure 1-b. Grain boundary migration towards an equilibrium configuration provides grains which are indistinguishable from other grains of the basis.
3. Atoms diffuse into voids in volume scale so voids should be no longer in contact with grain boundaries. In this stage the only diffusion path is the grain volume; figure 1-c and d and the higher the temperature, the lower the required pressure.

As it is seen in figure 2, there are micro-asperities on the faying surface so the real contact area is very small, that results in having a small microscopic deformation during the compression stage of the DB process. This deformation is limited if the material is work-hardened at room temperature but by raising the temperature this deformation increases because at recrystallization temperatures the work-hardening no longer affects and the creep mechanism controls the asperities deformation. Finally, the creep diminishes when the contact area increases because the locally acting stress decreases. The rougher the surface, the longer the time and the greater the temperature required to eliminate the voids [2].

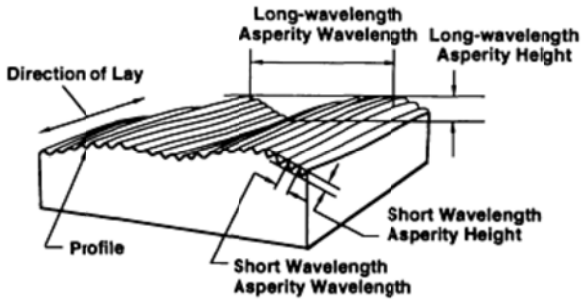

Figure 2 - The surface condition of the base metal [2].

1.3 Roll bonding/welding

Solid state welding is established between two stacked sheets, foils or strips through a sufficient deformation introduced by rolling. This process is known as cold welding generally used for ductile metals and alloys. This technique is faced with the strip separation during rolling especially in the case of thin foils. Therefore, it is needed to use either a deformation greater than the threshold required for welding (>60%), or to apply tack welding in several positions to ensure the alignment of the stacked foils during the process. It is reported that roll bonding is performed on Ni and Ti and their alloys [2]. This technique is described in the section of accumulative roll bonding.

1.4 Reactive foils

Local heat sources are used in the case of planar surfaces when the joining parts are difficult to join through conventional techniques because they are small or fragile [3]. They are used in joining techniques such as soldering and brazing [4], they can join ceramics, metallic glasses, metals/alloys, polymers and composites. The heat is generated from an exothermic reaction that could be called self-propagating high temperature synthetic; SHS [3, 5]. That reaction is synthesized through atomic diffusion and the energy released in such systems is very fast, i.e. 25 m/s. The heat released increases the temperature of the materials which can reaches 1500ºC and can even melt the filler metal [6].

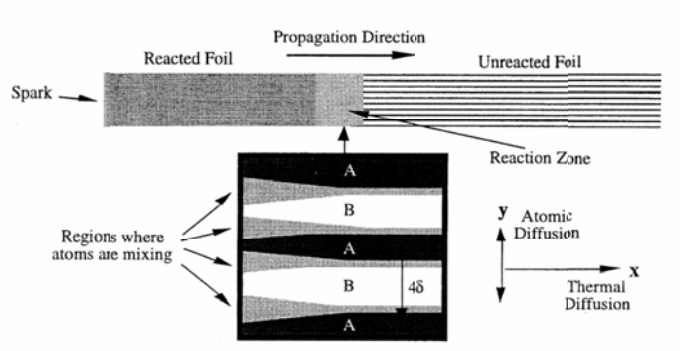

Figure 3 - Schematic illustration of a self-propagating reaction in a multilayer foil [6]

As it is seen in figure 3, when a reactive multilayer is burnt from one side the generated heat ignites the adjacent region, thereby the reaction travels along the entire film and it generates heat until the whole material reacts [3]. The heat should be generated faster than conducted away, i.e. a sort of adiabatic system [3, 7]. These materials are composed of nanolayers of alternated individual metals. The released heat, as the product of an exothermic reaction between those layers, is great because, the interatomic diffusion path between the reactants is significantly small; tens of KJ/mol energy is obtained by such phase formation. Reduction of chemical bonding is influenced by the interface reaction. Intimate contact between the layers promotes the thermal and atomic diffusion in the system. In the literature, it is said that the combustion reaction in such layers propagates faster than in powder systems with same composition. Self-propagating reactions have been reported in Ti/B, Ni/Si, Zr/Si, Rh/Si, Ni/Al, Pd/Al, Zn/Si, Ti/Al, Zr/Al, Nb/Al multilayers and Al/Fe_2O_3 and Al/Cu_2O as thermite compounds [6, 7]. It is said that such heating sources are controlled more easily than powder ones [5]. Joining methods using reactive multilayers has the following advantages;

- Gasless reaction;

- Facilitating the joining of temperature-sensitive compounds, e.g. glass-metals or the sealing of containers of microelectronics [5];
- Elimination of external heat sources;
- Avoiding the oxidation due to the speed of the reaction;
- Applicable under vacuum;
- Providing the least level of thermal stress to the workpiece;
- Joining of dissimilar materials with different thermal coefficient expansion, e.g. metals to ceramics [6].

Diffusion bonded parts using bond aids might fail due to the densification/debonding of the foil after reaction, to the non uniform expansion/contraction of the constituents or to the formation of brittle intermetallic compounds [3]. Individual alternated metallic layers are assembled to form a foil through different ways. The most used methods are deposition techniques, like physical vapor deposition and electron beam evaporation, and mechanical working techniques, as ARB, high pressure torsion (HPT) followed by cold rolling, and hot pressing followed by cold rolling [8]. In deposition techniques it is possible to have phase formation between the polycrystalline metal/metal multilayers. The thicknesses of the layers are controlled through the vapor deposition rate [6]. It is said that multilayer production through mechanical working is faster and cheaper than depositing techniques because they use simpler equipment, cheaper raw material and are capable of mass production [3]. It is also said that Ni/Ti laminated foil has some advantages over Ni/Al multilayer system as reactive foils; Ni/Ti performs higher thermomechanical properties and melting point which improve performance [5].

1.5 Pure nickel and nitinol alloy

Nickel metal is considered as a heavy metal and has been located in the periodic table as a transition metal, i.e. there is a strong cohesion between the atoms of nickel provided by the outer "d" electrons which justify its small interatomic distance. Nickel has faced centered cubic (fcc) structure which is constant from ambient temperature to the melting point [9]. Some nickel characteristics are presented in table 1. Nickel is prone to react with sulfur and oxygen so it is better to avoid exposing of any lubricant, SO_2 and H_2S. Annealing temperature for the pure nickel and nickel alloys is between 705 ºC and 1205 ºC. Stress relieving is done between 425-870 ºC depending on the chemical composition and the amount of work hardening [10]. There are three intermetallic compounds in the equilibrium phase diagram of Ni and Ti, figure 4; Ti_2Ni is formed through a peritectic reaction at 984 ºC plus TiNi and $TiNi_3$ that melt at 1310 ºC and 1380 ºC, respectively [12].

Table 1 - Pure nickel characteristics [11]

Properties	ρ (g/cm^3)	T_m (°C)	Atomic number	Atomic weight (emu)
Values	8.9	1455	28	58.69

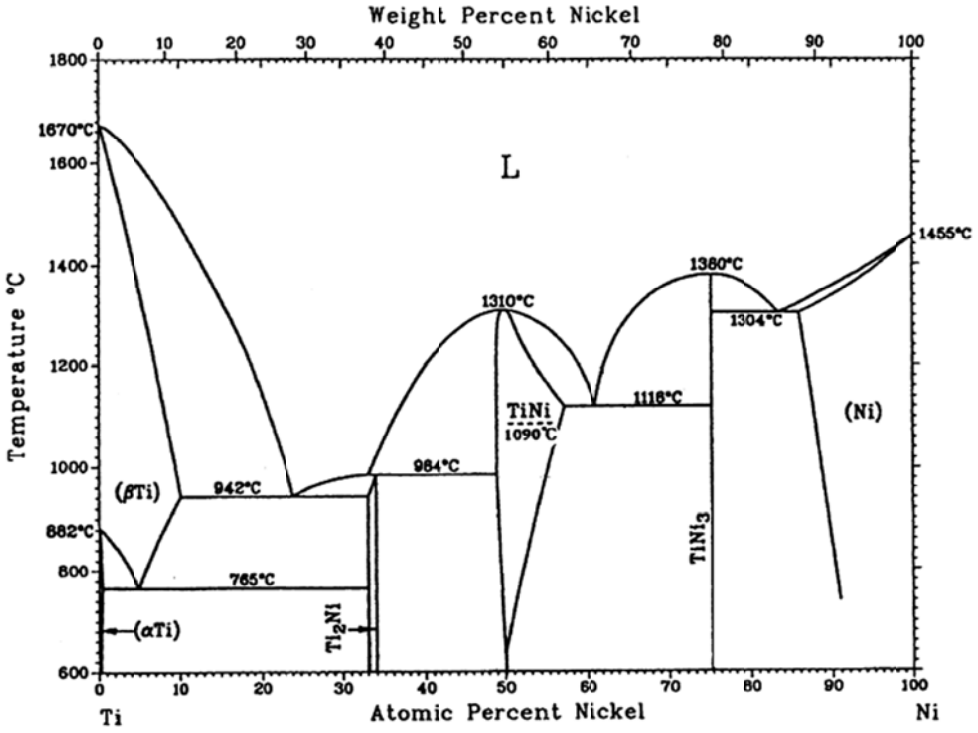

Figure 4 - Phase diagram of the Ti-Ni system [19]

Nickel-titanium shape memory alloys known as nitinol families have equiatomic or semi-equiatomic chemical composition [13]. This alloy has high strength, high ductility, high corrosive resistance, shape memory effect (SME), and superelasticity or pseudoelasticity [14]. As it is seen in figure 4, the equiatomic TiNi is embedded between two intermetallic compounds; Ti_2Ni at 33.3%Ni and $TiNi_3$ at 75%Ni content, these phases affect the alloy behaviors such as transformation temperature (T.T), and SME [13]. The equiatomic Nitinol is an extraordinary intermetallic compound because it has a solubility range for excess Ni or Ti and other metallic elements. This alloying ability improves the mechanical properties and the shape memory effect of nitinol; the excess nickel decreases the T.T and increases the yield strength of the austenite phase, adding Fe and Cr decrease the T.T; Cu lowers both the hysteresis and the martensitic transformation stress. Oxygen and carbon degrade the mechanical properties of the alloy [15]. Table 2 represents some properties of nitinol. The SME of the nitinol alloy is affected by the following factors; chemical composition, thermo-mechanical treatment and aging [14, 17]. The equiatomic or slightly Ni-rich compositions are superelastic and the slight Ti-rich alloy performs SME [5].

Table 2 - Characteristics and properties of as annealed equiatomic NiTi [15]

Properties	T_m (°C)	ρ (g/cm^3)	Corrosion resistance	Thermal conductivity		E (GPa)		Y_S (MPa)		σ_{UTS} (MPa)	T.Ts (°C)	Shape memory strain
				B2 (W/m.°C)	B19' (W/m.°C)	B2	B19'	B2	B19'			
values	1300	6.45	Similar to steels 300 series	18	8.5	83	28	195-690	70-140	895	-200 to +110	Max. 8.5%

Nitinol alloy is work-hardened extremely rapidly and frequent annealing is required during the cold rolling of that alloy. Machining or milling of Nitinol is difficult except by special tools. Welding, brazing and soldering of that alloy are also difficult [15].

1.6 Crystallographic structure of nitinol

This alloy has two main crystalline structures; cubic form known as parent phase, austenite or B2 and monoclinic phase, B19' or martensite, see figure 5. The latter phase is the product of the martensitic transformation, T_M, which is diffusionless and obtained through a cooling treatment; B2 → b19´ [19]. The crystalline structure of the nitinol is the origin of the stress induced and temperature induced deformations which are reversible and known as superelasticity and SME, respectively. SME is caused by a solid phase transformation between the austenite and martensite phases, i.e. phase B2 is stable at high temperatures but B19' is stable at low temperatures [18]. In other words; SME is the ability to return to the original shape when the alloy is heated [19].

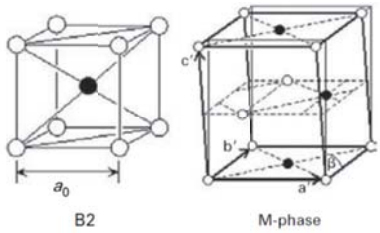

Figure 5 – Structures of crystals of B2 and B19' [13]

As it is illustrated in figure 6, in the case of SME the alloy has the structure of B19' in condition "b" and it is able to deform easily through aligning the rows of martensitic parallelograms by stress, condition "c". Heating transforms the structure to the parent phase which has already obtained the original shape condition "a" [19]. Superelasticity is the ability to withstand substantial deformation and then return to the original shape which occurs when the alloy has the austenite structure at the performing temperature. The performing

temperature should be lower than M_d[1] and greater than A_f, i.e. if any stress is introduced to the alloy at temperatures above M_d dislocations density increases and material will find unrecoverable deformation [5, 19].

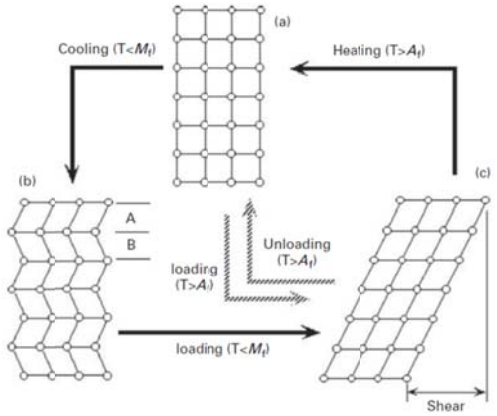

Figure 6 – An illustration of nitinol crystal structures upon cooling and heating or loading and unloading during the shape memory and superelastic behavior, respectively [13]

As it was already told the transformation of B2 to B19' occurs through either cooling or introducing stress over the material at temperatures above A_f. In both cases there is an interface between austenite and martensite which is not rotated or distorted which causes the minimization of the strain energy. Thereby, the lattice of that variant phase, B19', is to be twining which is reversible. Thus, this thermoelastic transformation results in elastic deformation through twinning [13].

1.7 Pure titanium and Ti6Al4V alloy

Pure titanium is a nonferrous metal and almost light; two times heavier than Al. Ti and its alloys are outstanding due to having high specific strength, high ratio of strength to weight, and excellent corrosion resistance. They have many applications in aerospace, chemical and medical industries. Pure titanium has an allotropic transformation at 822±2 ºC; below this temperature α phase, with hexagonal close packed (hcp) structure, is stable and the ß phase, with body centered cubic (bcc) structure, is stable until melting point. α is inherently more condensed than ß, thereby diffusion rate in the latter phase is higher than the first one. It means diffusion coefficient of α-Ti is smaller than that of ß-Ti [20].

Alloying elements in titanium alloys could be neutral, alpha or beta stabilizers. The latter elements are known as isomorphous or eutectoid. Nickel is placed in the last

[1] Md is defined as the temperature above which martensite cannot be stress-induced

classification which means that it is a eutectoid-forming element and intermetallic compounds could form even at very low volume fraction of Ni in titanium [20].

Alpha and beta have also different plastic deformation. α shows anisotropy in mechanical properties caused by its crystal lattice i.e. the single crystal of α will have a Young module of either 145 or 100GPa if the load is introduced either vertically to the basal plane or parallel with that plane, respectively [20].

Table 3 - Some characteristics of pure titanium [15, 11]

Properties	ρ (g/cm^3)	T_m (°C)	Atomic number	Atomic weight (emu)	α parameters (nm) at 25°C		ß parameters (nm) at 900°C	Y_S (MPa)		%EL	
								ASTM Grade 1	ASTM Grade 5	ASTM Grade 1	ASTM Grade 5
Values	4.51	1668	22	47.87	a=0.2950	C=0.4683	0.329	170	550	24	15

Commercially pure titanium contains the lowest amount of interstitial elements such as O, N and Fe. It has low mechanical properties but excellent corrosion resistance [21]. In table 3 the effect of impurities are seen on the mechanical properties of two grades. Impurities also influence the unit cell dimensions [15]. Titanium is a low thermal conductive metal [22].

Ti6Al4V is the most commonly titanium alloy used in industry due to a microstructure composed of the mixture of α and ß. This combination could provide variety of properties through thermomechanical processes. Welding the alloy could cause uncalled local thermal cycles resulting in improper properties in those regions.Ti6Al4V alloy has a maximum service temperature of 300 ºC. Al in the range of 2-7wt% is an alpha stabilizer and V in the range of 2-20wt% is beta promoter. This alloy has the ß transus temperature at 995 ºC [22]. The heat treatment and thermomechanical history of the alloy determine the microstructure and consequently the mechanical properties of the alloy [22].

Table 4 - Nominal chemical composition and the maximum of impurities of the Ti6Al4V alloy plus some mechanical properties [22]

Alloy	YS (MPa)	TS (MPa)	N (Wt%)	C (Wt%)	H (Wt%)	Fe (Wt%)	O (Wt%)	Al (Wt%)	V (Wt%)
Ti6Al4V	830	900	0.05	0.10	0.0125	0.30	0.20	6.0	4.0

About Ti; there is a limitation for α phase in comparison with ß in the case of plastic deformation [20]. It is even said that Ti is difficult to roll in comparison with steel, Al and Cu rolling. Ti might have the springback effect in cold forming and it is susceptible to the

Baushinger effect [21]. Metallic properties such as electrical conductivity and formability are resulted from having free mobile valence electrons in the crystal lattice. Different crystalline structures show different levels of deformation i.e. fcc > bcc > hcp in terms of ease of deformation. It is for two reasons; number of slip systems plus the length of the minimal slip path, b_{min} [20]. The discussion can be followed in table 5.

Table 5 - Characteristic parameters of metallic structure types [20]

Structure type	*N*	*CN*	*P*	*Slip planes / Slip directions*		*Slip system per unit cell*	*Atom density of slip plane*	b_{min}/a
				indices	*numbers*			
hcp (c/a=1,633)	6	12	74%	{0001} ⟨11$\bar{2}$0⟩	1 3	1×3=3	≈ 91%	1
bcc	2	8	68%	{110} ⟨111⟩	6 2	6×2=12	≈ 83%	1/2 $\sqrt{3}$ ≈ 0,87
fcc	4	12	74%	{111} ⟨110⟩	4 3	4×3=12	≈ 91%	1/2 $\sqrt{2}$ ≈ 0,71

N Number of atoms per unit cell
CN Coordination number
P Packing density
b_{min}/a Minimal slip component

Titanium is a ductile metal while having hcp structure because the ratio of c/a in Ti is close to 1.633, as it is seen figure 7, and the slip systems involve basal, prism and pyramidal planes. Moreover, in hcp metals twinning mechanism also plays an important role during deformation [23].

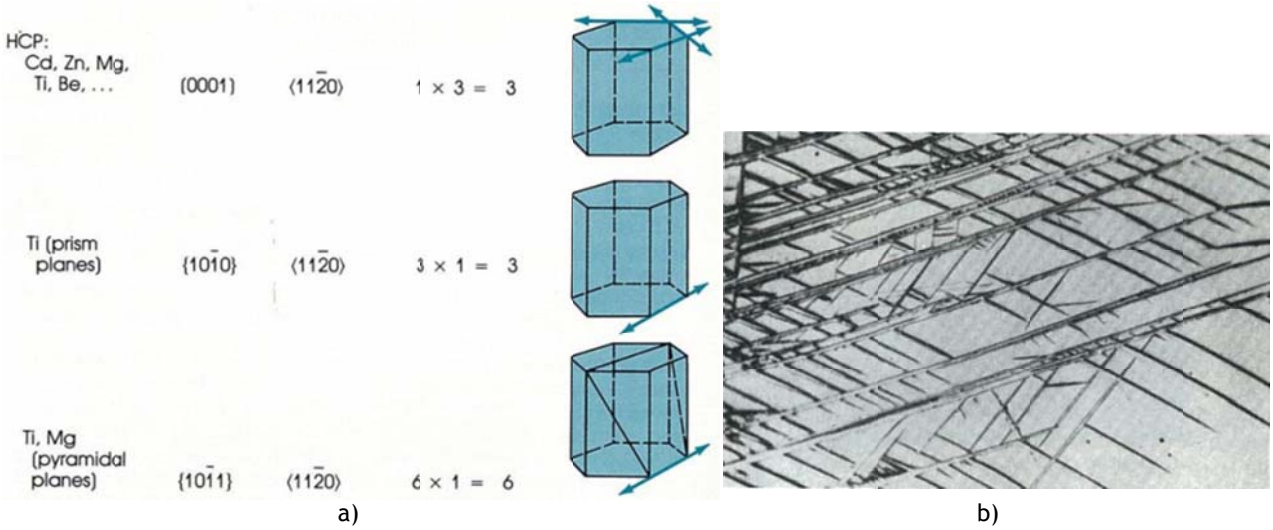

a) b)

Figure 7 – (a) Slip systems observed in hcp structure, (b) deformation twins in 99.77% Ti, 150X magnification [23]

Chapter two: Literature review

It was understood that metallic multilayers are produced for different purposes; reactive layers as local heat sources mentioned in previous chapter and alloy synthesis through mechanical alloying processes [4]. A new approach has been established to use multilayers as an aid foil in diffusion bonding technique in order to compensate the absence of surface flatness of the substrates and to lower the heat required in diffusion bonding [24]. In this chapter the following subjects are presented; fabrication of a multilayer Ni/Ti foil through cold rolling process, deformation mechanisms leading to ultrafine and nano structures and phase evolution during solid state diffusion processes.

2.1 Fabrication techniques of TiNi foil

Multilayer foils produced by sputtering deposition technique have been successful in producing microactuators in terms of stable shape memory and superelasticity behaviors. Such technique requires great control and specialized equipment. High purity of either nitinol alloy or individual pure Ti and pure Ni should be used as targets to produce an alloy with precise characteristics. In the case of using the alloy constituents, heat treating would be required to achieve the alloy. Sputtering technique is capable of producing foils having thickness less than 1 micron. Argon atoms accelerated by electrical field attack the target and deposit the atoms on a substrate. Equipment could be based on DC current or radio frequency. The first method has a higher production rate. Parameters that are to be considered precisely during the depositing process are as follows; quality of vacuum, smoothness of substrate, purity of gases and targets, substrate–target distances, magnetic field, and temperature. Electro-beam evaporation and CVD techniques have also been used to produce nitinol films more efficiently than physical evaporation deposition techniques [13]. Multilayer thin films produced by mechanical working have both high levels of plastic deformation and interfacial area. They are composed of elemental sheets that are folded or cut between each cycle of deformation if accumulative roll bonding technique is applied. During the cold rolling, the workpiece is in firm contact with the massive roll but the temperature increase of the material will be eliminated if the strain rate is small, i.e. it is suggested to apply $\dot{\varepsilon} = 0.1s^{-1}$. Such techniques have also been used to form amorphous phase in binary alloys e.g. Zr-Ni, Cu-Er, Al-Pt or Zr65Al7.5Cu17.5Ni10 has been produced when the rolling process is followed by annealing [8].

2.2 Accumulative roll bonding - ARB

Accumulative roll bonding is a sort of rolling process that could introduce large amount of strain on the rolled sheet/strip through repeating the process; moreover it establishes a joint at the facing surfaces of the rolled samples. As it is seen in figure 8 the workpiece is cut and restacked in each sequence. It is also possible to fold the sample than cutting it and then repeat the process.

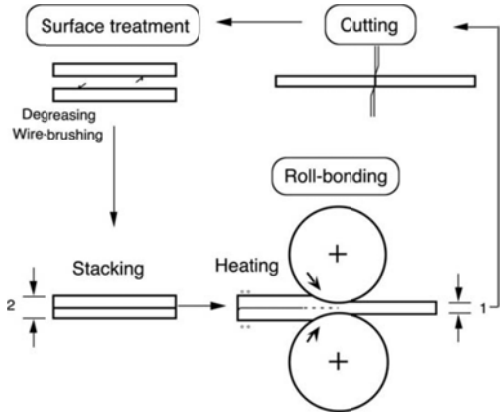

Figure 8 - Schematic of ARB process [25]

The final product of ARB should be solid. This job is performed in the following procedure:

- Providing equal strips of similar or dissimilar metals;
- Cleaning the surfaces of the strips including degreasing and brushing;
- Using no lubricant during the process;
- Stacking cleaned strips;
- Rolling the prepared batches;
- Reducing the thickness of the batches by 50% in each cycle;
- Cutting, cleaning and stacking the rolled strip;
- Repeating the process;
- Rolling can be repeated until edge cracks appeared [25, 26].

Cracking occurs during rolling when material gets hard and loses its workability, i.e. the material is too much strengthened [25]. Edge cracking also is the result of non-homogeneity due to the absence of lubrication. They appeared at the edges of the sample because stress is localized near that region. As the reduction percentage is growing, the edge cracking will increase [27]. Applying elevated temperature for the process improves both the bonding and workability of the material and causes less rolling force requirement. But it should not recrystallize the material [26]. Larger roll mills with greater diameters reduce the rolling

speed and also enhance the bonding effect [25]. Repeated rolling in each cycle increases the bond strength and decreases the delamination of rolled layers. At room temperature the strength of the bond depends on the cleanliness and closeness of the stacked foils. The maximum shear stress produced within the rolled strip is located in the direction of 45° because the tensile stress is treating at the center of the sample along with the direction of rolling and the compressive stress is perpendicular to that direction [27]. Total strain accumulated by "n" cycle equals 0.8*n because when 50% reduction is induced, the equivalent strain of that reduction is 0.8, calculated by von Mises criterion [25]. It is claimed that ARB is more favorable than other methods in producing laminated composites because it is rather a simple method and uses small deformation loads and low cost input materials, e.g. it does not need expensive mould. Such produced composites show high strength and low ductility. Input material might be of similar or dissimilar metal sheets. For similar layers it is believed that severe plastic deformation, SPD, imposes sub-grains and low angle grains followed by ultrafine grains with high angle boundaries. On the other hand a short coming effect is observed in multilayer foils fabricated by ARB which is multiple necking and rupture of one constituent, i.e. a soft metal has embodied the hard one. Necking occurs because the plastic instabilities have arised earlier in the harder layers and finally premature fragmentation forms. It is believed that multilayers composed of metals with same crystal structure suffer less from this problem especially in fcc structure i.e. they undergo co-deformation in several passes without necking [26].

2.3 Nanograins formation mechanisms plus the influences of rolling process on multilayers

Ultra-fine grained metals, UFG, have mean grain size less than 1μm. Metals with simple chemical composition and UFG structure are considered as advanced structural materials. They can be produced through SPD techniques such as ECAE/P, HPT and ARB or rolling and folding; R&F [25]. But the two latter methods are capable of fabricating multilayer foils. SPD imposes a large plastic strain on the bulk metal [26]. It is supposed to be almost impossible to produce such levels of strain by conventional rolling because the material thickness decreases while the deformation increases [25]. It is said that the difference between the crystal structures of the multilayer components influences the deformation process during rolling so that ARB and R&F products will be composed of nonuniform layers. Thus, it would be very difficult to define any modulation period like those produced by deposition techniques [25]. The crystal defects and the residual stresses affect the kinetics of the diffusion process required to have solid diffusion, e.g. in the case of producing nitinol through mechanical roots. Bulk nano structure metals produced by severe plastic deformation contain large grain boundary area as well as high dislocation content. Therefore, it is expected to have an

induced mixing at the interfaces of layers more significant than that of layers produced through deposition. Nano multilayers produced by ARB have less residual porosities and impurities than nano powders produced by ball milling. UFG bulk metals mainly have high angle grain boundaries obtained at low temperatures [25]. Mechanical attrition procedures are capable of synthesizing UFGs through refining the coarse-grained structures as the result of severe plastic deformation, SPD, unlike electrodeposition and gas-state condensation techniques which form nanostructures via cluster assembly [28]. There are several opinions about the formation of nano and ultrafine structures caused by SPD.

One of those explanations is based on ARB experiments of Al-sheets which demonstrate that shear strain plays a major role on UFGs formation. The grain size distribution across the thickness of the workpiece depends on the shear strain distribution in that zone. As ARB cycles increases, the amount of shear strain grows and distributes across the section complicatedly. This effect has been studied through the evaluation of equivalent strain, strain gradient and strain path. An experiment has been carried out by cold rolling of pure Ti to reveal the formation of nanograins; dynamic or quasi-static forces develop shear bands or high localized deformation. They are studied by electron back scattering diffraction in SEM and TEM techniques. Figure 9 illustrates such region. They even can lead to catastrophic failures [26].

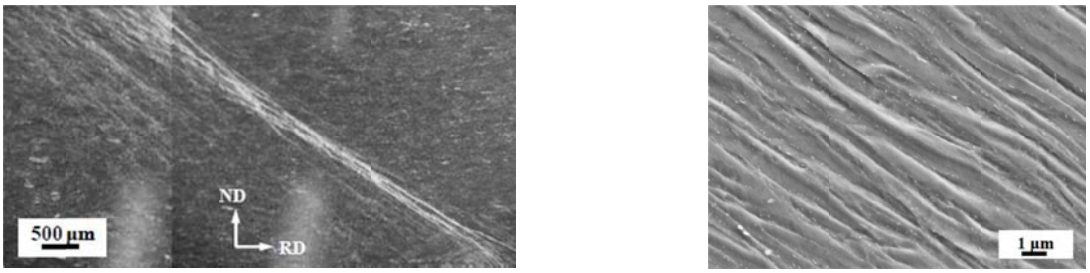

a) b)

Figure 9 - (a) the evolution of the localized shear band after 85% rolling deformation and (b) the microstructure inside the well-developed shear bands [26]

These shear bands experience very high levels of strain. In some cases they face high temperature rise that are called adiabatic shear bands. Thereby, the microstructure of those bands is often recrystallized and they might find phase transformations. But if that adiabatic region does not form, that process will contribute to the formation of sub-grains or fragments reaching the size of several tens of nanometers. Figure 10 is useful in understanding the above explanation. Thereafter, the slip of dislocations and the mechanical twinning both play important roles in plastic deformation. It was already mentioned that the number of slip systems in hcp is limited so, the beginning stage of deformation refinement in hcp metals

starts by the activation of twining through intersecting the twins and the formation of secondary and tertiary twins leading to the saturation of twinning. At high strains the dislocation slip dominates the process. It is hypothesized that the grains with the mean size of 80-100 nm are produced in this way [26].

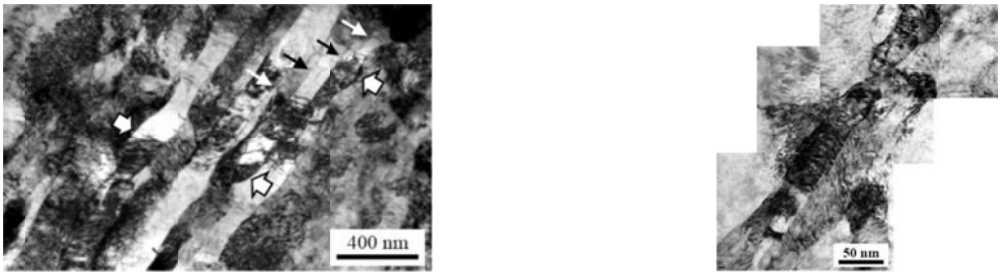

a) b)

Figure 10 - (a) TEM bright-field micrograph of the thin lath structure formed in a boundary region of the macroscopic shear band after 83% rolling reduction (b) the long laths breaking down into subgrains, through the formation of transverse dislocation boundaries, in a boundary region of the localized microscopic shear band after 67% rolling [26]

Ultrafine grains, UFGs, affect the mechanical properties like fatigue life and strength as well as the SME, superelasticity and hysteresis temperatures and stresses in nitinol alloys [18, 29]. It means that there is a strong correlation between the structure of the alloy and the shape memory behaviors [17]. In rolled multilayer foils the grain refinement is obtained through decreasing the thickness of the layers. The layer thickness reduction is confined to multiple necking and layer rupture [18, 29]. Figure 11 shows the fragments of Ni particles in the Al matrix. This fragmentation occurs in the early cycles of rolling. The metal of some layers finds necking in some parts and consequently two separate layers with same material composition will find each other and join together, consequently an island like Ni regions form. The reduction of such fragments during the next rolling stages is more difficult which is also detrimental for finding UFGs. In order to have uniform reduction of multilayers, it is better to stack metals with close rupture stress values. This material selection reduces highly localized necking or rupture [18].

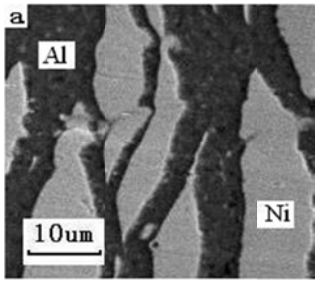

Figure 11 - Localized necking and rupture [6]

Localized necking is seen in harder metal and it is attributed to deformation instability of layers under large strain. It is also believed that layers composed of same crystal structures undergo co—deformation and they do not face failure [30]. Some believes that Ti/Ni system is an exception and both metals monotonously get thin by rolling [14]. It is reported that the ultimate tensile strength of the pure Ni and Ti is around 350 MPa [18, 14]. Optical microscope images reveal that the layers thickness fluctuates along the rolling direction that is due to the instability of plastic flow within the layers [31]. Excessive work hardening of the metals in these systems, as the result of several rolling cycles, not only increases the force required to continue the process but also it may cause explosion; work hardening promotes crack formation which enhances the Ti oxidation creating hot spots in the system. These points can provide sufficient heat to induce exothermic mixing reaction between Ni and Ti [18].

2.4 Solid state diffusion in Ni and Ti multilayer

Diffusion is very important and widely applicable in most metallurgical processes, for example solution treating, precipitation hardening or diffusion bonding. It is the result of the atoms movements within a solid state leading to the reduction of the total energy of processed system. Equilibrium, as a goal of any system, is provided through reaching the lowest level of energy by which diffusion helps; a thermodynamic and metallurgical principle [11]. A study was done in 1973 by Bastin and Rieck in Netherlands. They applied diffusion process at solid state and claimed that their results cover what they expected from the basis of Ti and Ni equilibrium. The procedure involved stacking the diffusion couples consisted of a Ti (99.97%) disc embedded by two Ni (99.99%) discs each in the thickness of 2mm placed in an evacuated silica capsule to avoid Ti degradation. Couples were joined then annealed at 930ºC for 504h under 10 Pa. They found the number of phases formed and determined the layer thickness of the interphases as the function of time and temperature. Microstructural observations revealed that at temperatures above 770 ºC diffusion layers are composed of Ti_2Ni, TiNi, $TiNi_3$ and solid solution of the Ti in Ni. Implemented markers at the interface (welding area) showed the displacement with respect to each other. None of the marks were at their primary places at the interface and those existed in the $TiNi_3$ layer were closer to the $TiNi_3$/Ni interface [32]. Figure 12 shows the image of a Ti-49.4%Ni multilayer. It contains the TiNi intermetallic and other intermediate compounds mentioned above [31].

During the attempts done to produce nitinol foil through annealing of the cold rolled multilayer strips it was observed that the thermal history of the multilayer strongly influences the phase evolution; when no heat had been applied during the fabrication of that metallic composite, no intermediate phase formation at the interfaces of those ultrafine layers had

been reported [18, 14, 29]. Whilst an average grain size of 20 μm is normal for commercial nitinol alloys, the materials produced by mechanical approaches show a grain size of 1-3 μm after final heat treatment. Some reports claimed that they could produce an equiatomic nitinol through selecting proper thickness ratio of the pure Ni and Ti layers [18] while it is reported that there was a deviation from equiatomic composition after annealing [33].

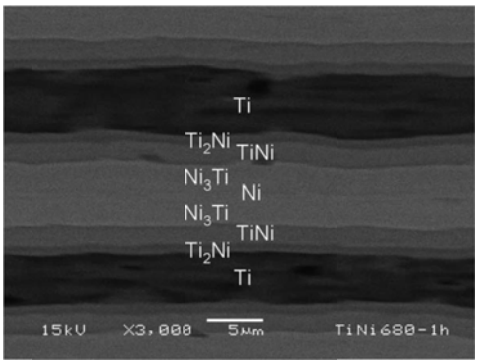

Figure 12 - Backscattering electron image of the Ti/Ni laminated sheet by roll bonding then heat-treated at 953 ºK for 1h [31]

In the case of multilayers of ultra or nano laminated Ni and Ti foils, it is said that when there is no interdiffusion between those layers, i.e. they have joined just mechanically. The bond strength will increase if fragmentation of layers is observed otherwise delamination would occur during annealing process. The separation of layers occurs due to weak bonding strength. The reason of that problem lies in the difference of thermal expansion coefficient between Ti and Ni; $13.5*10^{-6}$ and $8.4*10^{-6}$ K^{-1}, respectively. This different thermal response causes more deformation of Ni than Ti due to the induced thermal stress. Thus, the diffusion path between the Ni and Ti disconnects and they react no longer, thereby, as it is seen in figure 13, some pure regions of Ni and Ti are observed [14]. It is seen in literature that implementing temperatures above 500ºC during the rolling processes causes the formation of intermetallic compounds like TiNi, Ti_2Ni and $TiNi_3$ at the interfaces [33].

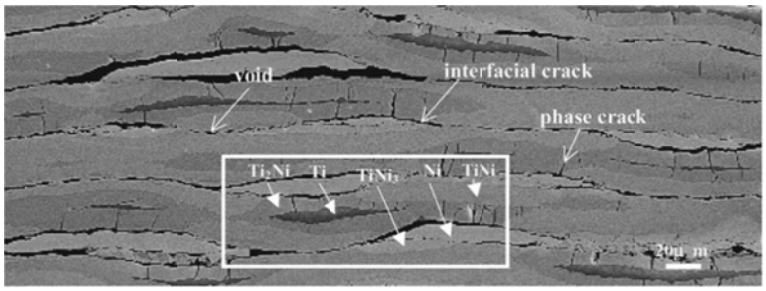

Figure 13 - Ti/Ni laminate sheet reduced for 76% after annealing at 730 ºC for 12h [14]

As it is observed in figure 13, some cracks exist in the intermediate phases are perpendicular to the interfaces and are highly observed in thicker layers. They have been resulted from incomplete stress relief of the thick layers. After annealing, the Ti/Ni laminate sheet submitted to greater reduction shows less defects of such like mentioned above which weaken the mechanical performance of the material, as can be observed in figure 14 [14].

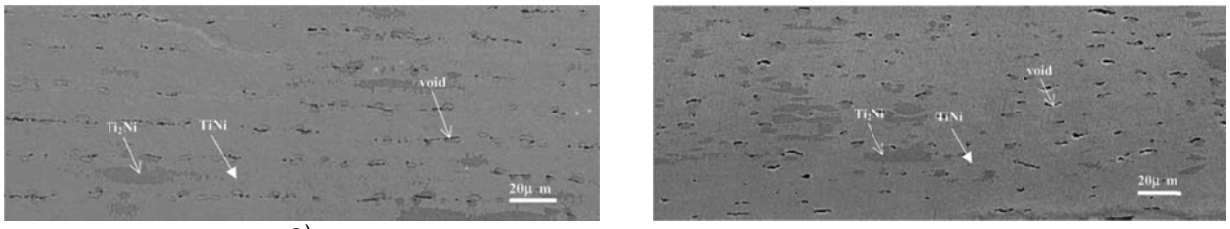

Figure 14 – SEM images showing the intermetallic and void distribution after annealing at 730ºC for 12h of samples reduced for (a) 88% and (b) 97% [14]

As it is seen in the SEM images presented in figure 14, the lamella structure of the as rolled multilayer has been disappeared after the annealing, i.e. a bulk material has formed through interfacial reactions [14, 17]. The final material has undesirable phases formed during heating stages, than TiNi [18, 29]. These phases were not formed in multilayers produced through depositing technique even after sufficient diffusion [31]. The minimum temperature to have inter-diffusion at the interfaces is 600 ºC, reported in the bibliographies of this research.

Some porosities are also produced after heat treating [14, 17, 33, 31] which are mostly located at the site of initial Ni layers [14, 17], as it was seen in figure 14-a; voids are aligned on a hypothetic line. The pores are believed to be the result of Kirkendall effect during the diffusion process between Ni and Ti because the diffusion velocity of Ni in Ti is faster than that of Ti in Ni [14, 17, 31]. It is concluded that;

- Multilayers produced by smaller reduction percentages have found less porosity, more interfacial cracks and more delamination. Such defects will influence the mechanical properties of the multilayered film;
- The increase of annealing time and temperature decreases the voids volume fraction [14];these conditions allows the annihilation of smaller voids through vacancy mechanism and it also increases the homogeneity of the foil reducing the quantity of $TiNi_3$ and Ti_2Ni (see figure 15) [17];
- Applying pressure on the outer surface of the foil during heat treatment inhibits the formation of the voids, e.g. voids were not observed when 3KPa load was used [31].

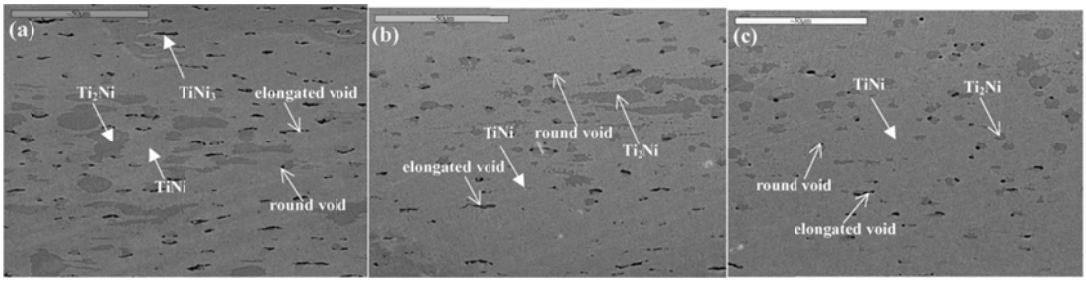

Figure 15 - SEM images of samples reduced for 97% annealed at (a) 650 ºC, (b) 730 ºC and (c) 800 ºC for 18h [14]

Microstructures and DSC results showed no phase formation or martensitic transformation neither in as rolled foils nor in foils heated at temperatures below 500ºC [33].

2.5 Joining of shape memory alloys and dissimilar welds

The growing need of joining SMAs to themselves or to other alloys is motivated by their various applications in aerospace, medical and defence industries and also for their poor formability. So far, both conventional and advanced techniques have been applied to join dissimilar metals. Study of such joints is interesting because some parameters affects the joint, like the heat flow due to different heat transfer rates, residual stress and chemical composition distribution and intermetallic compounds formation. Those affects become higher when the base materials are different [34]. Changes of the chemical composition of nitinol will affect its shape memory behavior as well as its superelasticity [35]. Outstanding defects might occur such as cracks caused by the formation of brittle phases; embrittlement due to the reaction of oxygen, nitrogen or hydrogen with the constituents of the weld pool; distortion or segregation if fusion welding techniques are applied [36].

An attempt has been carried out by L. Quintino and R. M. Miranda [34] to join TiNi to Ti6Al4V alloy through laser welding but an intense controlling procedure is required to avoid $TiNi_3$ formation within the Ti alloy side. This method gives a narrower weld zone than conventional welding techniques resulting in smaller thermal stresses. Arc welding processes such as GTAW, PAW and GMAW have tested to join the intended materials. Brazing and soldering processes and solid state welding techniques, like friction and explosion welding, have also been experienced on joining SMAs. Brittle phase formation has observed in brazing TiNi alloy. It is said that great deformation introduced to the SMA will affect the transformation temperatures and the superelasticity of the alloy [35].

Chapter 3: Experiments

In this chapter all the procedures carried out during this master thesis including material selection plus the evaluating techniques of the fabricated materials and joints will be explained in details. Here, it is better to repeat that the first aim of this research is to develop a semi-equiatomic Ni/Ti multilayer with an average thickness for individual layers in ultrafine or nano scale size. The second goal includes joining the two light alloys; nitinol and Ti6Al4V through diffusion bonding by using those fabricated laminated foils. Then it will be tried to improve the microstructure of the multilayer foil and provide a welded zone similar to the nitinol substrate in terms of microstructure and finally to decrease the process costs through restricting the temperature and pressure.

3.1 Primary material selection

Pure Ni and pure Ti foils with the thicknesses of 125 μm and 200 μm, respectively, are used as the input materials of the multilayer fabrication process in this work. They are to be in the annealed condition to get work-hardened as late as possible. To have a semi-equiatomic nitinol through rolling of individual stacked foils, it is important to calculate how much of each constituent is to be stacked to get the intended alloy. As it has been explained in appendix A the thicknesses of the selected foils used in this work are presented in table 6. In this table the Ni foil has been considered 0.125 mm, optionally selected from "Goodfellow" website, which gives the value of almost 0.202 mm for Ti foil. The available thickness by the supplier is 0.200 mm thick which is the closest thickness to the calculated one. There are varieties of different thicknesses offered by the supplier but that selection was done based on some considerations; the budget, working conditions and intended chemical composition, e.g. it is possible to obtain a semi-equiatomic nitinol alloy through other thicknesses that are thinner but they are more expensive.

Table 6 - Foils thicknesses, data except column 4 are extracted from Goodfellow website

Ni purity	Ti purity	Ni foil thickness (mm)	Ti foil thickness (mm)	Prices of Ni-20pcs		Ti foils (mm)	Prices of Ti-20pcs	
				50*50	100*100		50*50	100*100
99.98	99.6	0.125	0.202	312(261)	468(351)	0.2	384(274)	0(416)

* Numbers in parenthesis mean 10pcs per order than 20

3.2 Experiments

All experiments done in this work will follow the sequences presented in the diagram illustrated in figure 16.

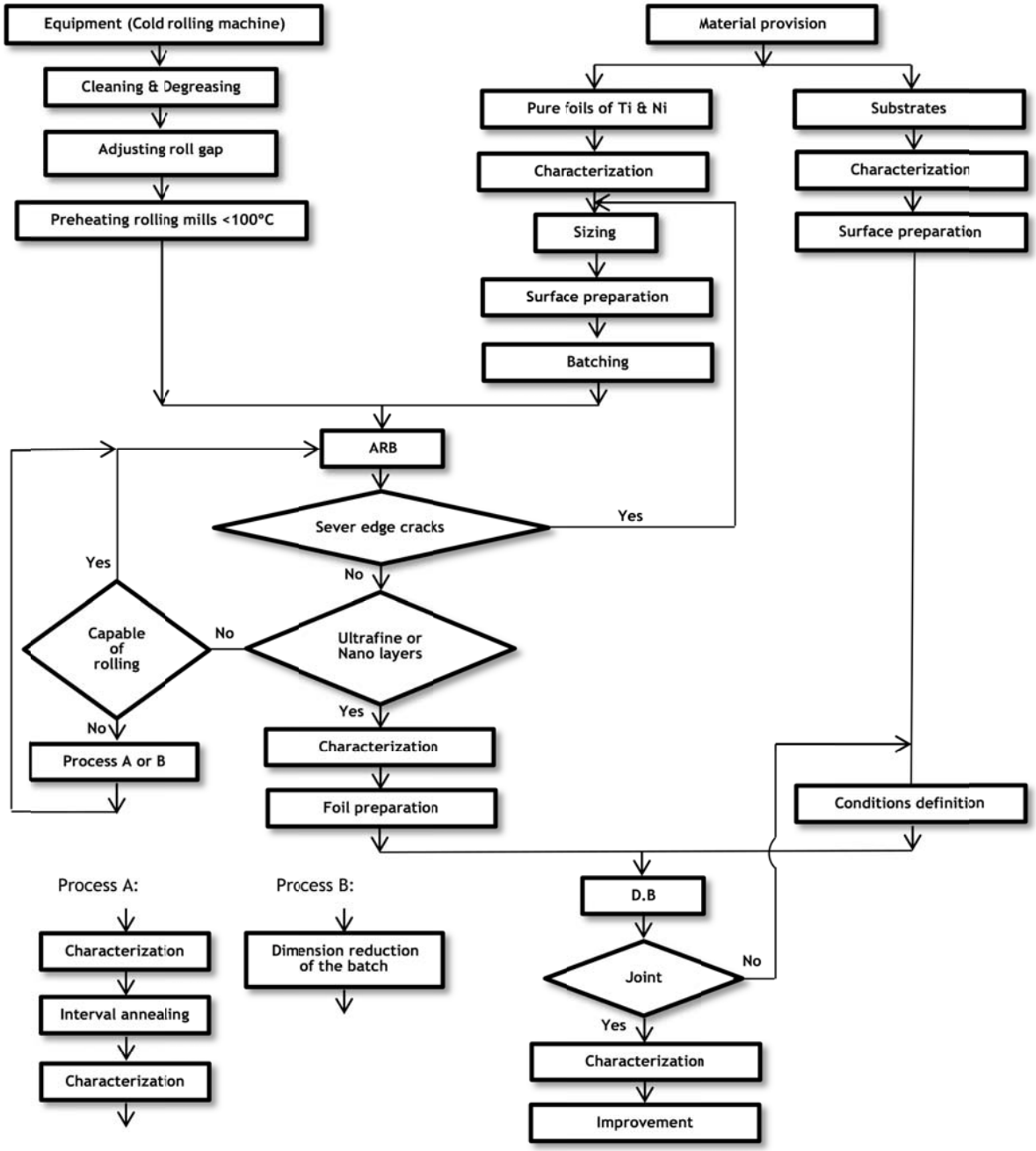

Figure 16 - The flowchart illustrating the sequences of experiments

3.2.1 Cutting and providing batches

Purchased foils are 100*100 mm and 50*50 mm of Ni and Ti, respectively. The difference has happened accidently by the purchase office so the maximum length of the strip could be 50 mm. It was arranged to prepare small strips of 10 mm, 15 mm and 20 mm wide to

experience the behavior of width variety during the ARB process. They were cut by iron scissors. Larger widths were not selected to have enough batches for doing more experiments. In this work one batch encompasses one strip of nickel and one of titanium due to easily handling and controlling the deformation process. They were staked without any supporter and were handled manually with plier during the process. Batches are to be stacked immediately after surface preparation and are to be rolled promptly otherwise good bonding will not occur. The batches of the last experiment are shown in figure 17-b.

3.2.2 Surface preparations and precautions

Surface preparation has a vital role in both roll bonding and DB processes because, this is a delicate work and even fingerprints or any other material containing salt, oil or contaminants containing halogen compounds should be removed [21]. Grinding will introduce defects at the surface that could promote the bonding process. As it was seen in the flowchart of figure 16 it is applied in several stages during the experiment and is explained in details in appendix B. This treatment

3.2.3 Rolling machine and deformation level

Available rolling machine in the Metallurgical department of University of Porto only works in ambient temperature and it has been designed for educational work shop purposes, as it is seen in figure 17-a. This machine transfers the rolling force by gear belt. As it has been calculated in appendix C, that machine can introduce a strain rate of 20 s^{-1}, which is much higher than what has been suggested in literature to perform ARB; 0.1 s^{-1}.

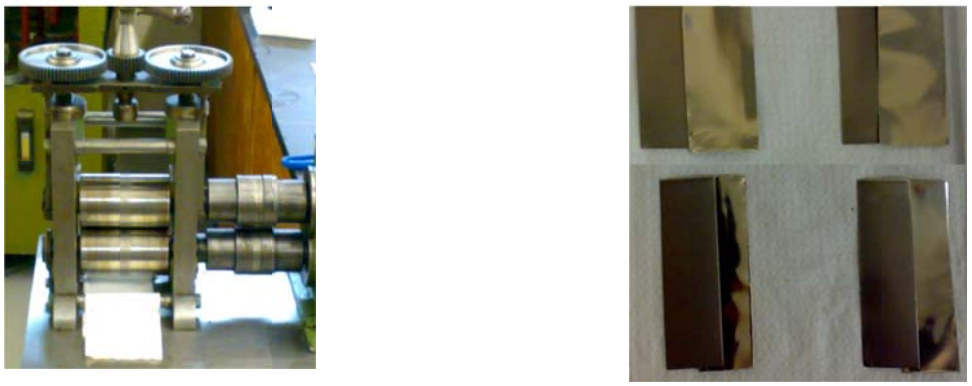

Figure 17 - (a) Available rolling equipment, b) four batches prepared, oscillation is easily seen in the nickel (bright) foils

In all experiments primary batches have the thickness of 325 μm (1 Ni foil + 1 Ti foil). Rolling process begins by a primary rolling then continued by ARB, i.e. the gap between the

roll mills is adjusted to introduce the primary reduction then it remains constant. The foil is cut in half and passed through the previous gap by which 50% reduction is provided. In this work, the term “cycle” starts after primary rolling and includes one cutting plus one 50% thickness reduction. This strategy of ARB could produce a thin multilayer foil that is to be used in diffusion bonding. As it was seen in the flowchart, it is tried to heat the roll mills surfaces. It is done by starting the machine and completely closing the gap between the rollers without introducing the material for 15 minutes; the friction between the surfaces makes the mills hot. This idea had not been considered in the earliest experiments but experience proved that it is very useful in bonding evolution among layers.

3.2.4 Heat treating

A sort of heat treatment was performed on the multilayer product during the ARB process which is difficult to be called stress relief because the selected temperature would provide phases formation in the bimetallic multilayer system. A relatively high temperature was intentionally selected to help the study of the phase evolution in the Ni/Ti system before making any joint. Heat treatment was applied when the material got strong during rolling so that the machine stopped during the process. It happened for the batches having the width of 20 mm in the 3^{rd} cycle and those 15 mm wide in the 4^{th} cycle. That heat treatment was carried out in a vacuum furnace (Termolab) under the pressure of 10^{-3} Pa; this level is selected because Ti is very reactive at high temperatures. Heating and cooling rates were always 5ºC/min to avoid delamination of layers due to the difference between the thermal expansion coefficients of Ti and Ni [14]. In order to do an accurate heat treatment, samples were located on a ceramic plate in the middle of the furnace tube. The temperature gradient of that part of the tube for a specific annealing temperature during an interval were recorded through an external thermocouple, testo 735, to find out whether the thermocouple of the furnace works precisely, e.g. 627 ºC (1000ºK) for 30 minutes revealed 40 ºC deviation. The temperature of 627 ºC was selected knowingly because it is very close to the minimum temperature, 630 ºC, mentioned in literature as the nitinol formation in Ni/Ti laminated layers [18, 37]. In this research intermediate annealing was done after 4 and 10 cycles of R&C i.e. 4 cycles of R&C then annealing and then 6 more cycles and again annealing. Samples must be cleaned to remove any finger prints by acetone before putting in the furnace.

3.2.5 Joining process

Diffusion bonding of the equiatomic nitinol alloy and Ti6Al4V alloy was done in a radiating furnace assembled with a tensile machine (LLOYD LR30K), figure 18-a. Three joining

conditions were applied; 800 ºC/1h, 700 ºC/1h and 700 ºC/3h, all under vacuum level of 10^{-3} Pa, heating rate of 10 ºC/min and 10 MPa pressure. Substrates and interlayer foils were prepared as it was mentioned in surface preparation section. Nitinol sample is a 10*9 mm parallelepiped and the titanium alloy is a cylinder with a diameter of 10 mm. As it is illustrated in figure 18-b the interlayer foil was a bit larger than those blocks. Edge cracks are to be removed before joining.

a) b)

Figure 18 – (a) LLOYD LR30K tensile machine and (b) the joint constituents before assembling.

A sandwich of two blocks involving the foil is placed between two molybdenum punches of the universal testing machine in the compression mode. After assembling the complete system, a primary pressure of 300 N is introduced, then the vacuum is established until it reaches the pressure of 10^{-3} Pa, afterwards the furnace starts heating. As it has been calculated in appendix D the required force to introduce 10 MPa on the sample is 785 N. The material expands during the heating stage through which required pressure is obtained. That load even exceeds 785 N which requires complete controlling until the end of the diffusion process. During cooling no pressure is applied.

In this work 800 ºC was selected for DB because in previous work [36] the same alloys were joined using Ni/Ti nanolayers deposited on both the base materials and it has been shown that the best results were obtained at that temperature. On the other hand it is tried to decrease that temperature not only to decrease the costs but to reduce the deformation of the base materials.

3.2.6 Evaluation techniques

Structural and mechanical characterization of the primary materials, of the fabricated foils in the as rolled and annealed conditions, and of the joined zones was carried out by the following equipment and techniques.

3.2.6.1 Differential scanning calorimetry

DSC is helpful in studying the reactions and phase formations within any reactive layer during a heating stage, i.e. it not only can record the amount of the heat released or absorbed during the reaction but can identify the temperatures at which any phases form. Thereby, it could be helpful to find proper stress relief temperature for the work hardened foils through which no phases form during the heating process so that a higher level of any probable reactive energy would be available during the solid state diffusion process. This test will also help the study of the microstructural evolution of a metallic system at a specific temperature, i.e. the sample is heated up to a specific temperature and then cooled as fast as possible. The heated sample could be evaluated by OM or SEM. The equipment used in this work is Labsyst^{TM}, TG-DTA/DSC model, available in the department lab. The maximum rate of the heating and cooling can be 40ºC/min. Samples from different batches and cycles have been tested. It is better to select the sample from a well bonded part. In all the tests the heating and cooling rate is considered 20ºC/min. Argon gas is used as the shielding atmosphere and the system is cooled by water. DSC sample size is almost 2*2 mm; the sample was ultrasonically cleaned by acetone, weighed and placed in an alumina crucible. For this research samples were prepared from the batches of 4, 10 and 15 R&C cycles. If small heating and cooling rate, like 5ºC/min, is selected, it will be almost impossible to recognize any change on the graph because the interval temperature on the graph will be wide, i.e. the higher the heating and the cooling rates, the sharper the peak revealed on the graph.

3.2.6.2 Sampling

Specimens were selected from raw materials and fabricated foils after each stop during the processes such as intermediate annealing, final laminated product and joints. Transverse cross section specimens were selected from sound parts of the samples.

3.2.6.3 OM and SEM/EDS/EBSD

These techniques could evaluate the effects of deformation and heat on the material in terms of structural development and phase evolution. Metallography samples require perfect

surface preparation, especially for the SEM. Scanning electron microscopy was done in CEMUP, Center of Materials of University of Porto. The equipment used is "FEI QUANTA 400 FEG / EDAX Pegasus X4M"; a High Resolution (Schottky) Environmental Scanning Electron Microscope with X-Ray Microanalysis and Electron Backscatter Diffraction Pattern Analysis. All characterizations are done at an accelerating voltage of 15 keV. Some images were taken by Secondary-Electron mode and some others by Backscattered Electron mode. In the latter condition the greater the atomic weight, the brighter the observing zone. It should be mentioned that the obtained chemical composition by EDS is influenced by the volume interaction effect. It means that a larger volume underneath the intended surface is analysed by EDS therefore the result has been influenced by the adjacent region [36]. Surface preparation of the specimens was started with 230 mesh silicon carbide grinding paper followed by 600, 1000 and 4000 using water. Then they were polished by 1 micron diamond suspension on very clean smooth cotton cloth for 10 to 15 minutes for each sample and finally were polished by 0.5 micron colloidal silica on a synthetic leather cloth for 10 minutes. It is important to wash samples by water and soap followed by ultrasonic in a solution of water and soap for 5 minutes between each stage. Polishing cloths should be washed repeatedly otherwise a surface without any scratches is not obtained. This difficulty of surface preparation is due to the entrapped particles in the delaminated regions and the gaps between the sample and the mounting material.

3.2.6.4 Micro and macro hardness measurements

Micro hardness evaluation was done by "Struers-Duramin; Ver 0.08". Selected loads were 0.01, 0.05 and 0.1 Kgf. Macro hardness measurement was also done to measure the global hardness of the interlayer foil in the joined region with 1 kgf indenting load by "Emcotest/DuraVision" equipment. Both tests were performed at ambient temperature (23 ºC±2) according to the manuals of the equipment. Microhardness was done to evaluate the effects of the following processes; strain hardening, annealing and joining on the multilayer foil. Macrohardness was carried out to see which joining conditions would provide a global hardness as close as to the nitinol substrate. It was tried to measure the hardness of the phases formed during the processes by microhardness as well as the effect of strain hardening on the individual metals by macrohardness.

Chapter four: Results and discussions

In this chapter the characteristics of the products evaluated by SEM and OM observations, chemical analysis obtained by EDS, structural information given by EBSD and micro and macro hardness measurements are presented. The results of different processing conditions will be compared with each other as well as what has been claimed in the literature. Evaluating of selected samples was done after any stop during the multilayer fabrication or joining process.

4.1 Primary materials characterization

The microstructure of pure Ni and Ti foils as well as the nitinol and Ti6Al4V alloys used in this research were observed under optical microscope. The etchants selected from literature and ASM handbook metallography section are presented in table 7.

Table 7 – Etchants used to reveal the microstructure of the alloys [38, 39]

Alloy	Pure Ni	Pure Ti	Nitinol	Ti6Al4V
Etchant	Equal parts of HNO_3, H_2O & CH_3COOH	Kroll's reagent: 1.5cc HF, 4cc HNO_3 & 94cc H_2O	1 part HF, 5 parts HNO_3 & 5 parts CH_3COOH	Kroll's reagent: 1.5cc HF, 4cc HNO3 & 94cc H2O
Polishing	Mechanically, as mentioned in sample preparation section			
Etching technique	Repetitive polishing and etching in 10s	Repetitive polishing and etching in 20s	Immersing sample for 10s	Immersing sample for 1 to 2 min

As it is illustrated in figure 19-a, microstructure of pure nickel consists of equiaxed grains showing the annealed or normalized condition. Average grain size obtained by Lietz software is 10 based on ASTM-E112. The differences in color are the results of different grain orientations. Pure titanium grain structure consists of equiaxed alpha grains revealing the annealed or normalized condition, figure 19-b. Comparison between the microstructure of two metals shows that the Ti grains are finer than those of Ni.

Metallography of Ti6Al4V reveals a matrix of very small equiaxed alpha (α) grains; intergranular beta (β) phase (dark regions) is rather uniform distributed in the matrix, figure 20-a. The nitinol alloy was composed of coarser equiaxed grains than titanium alloy, figure 20-b. Those grains looks like austenite revealed by Kroll`s reagent. The grain size of the alloy in average is 7 in ASTM-E112. Brighter grains are the effect of grain orientation under directed light. The alternative etchant presented in table 7 has revealed other morphology

for the nitinol alloy which is seen in figure 20-c&d. Fine and coarse martensite plates/needles are easily recognized.

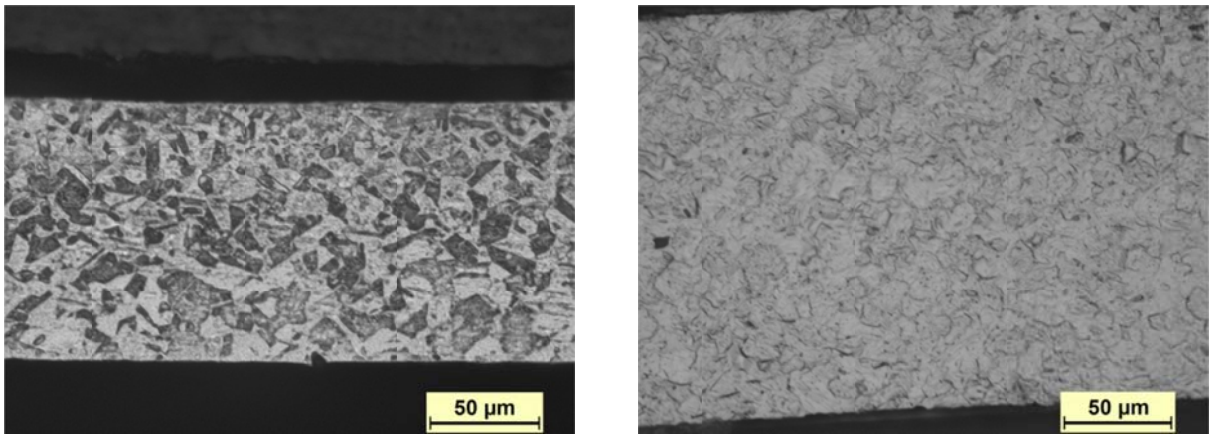

a) b)

Figure 19 – (a) Pure nickel grain structure and (b) pure titanium alpha grain structure.

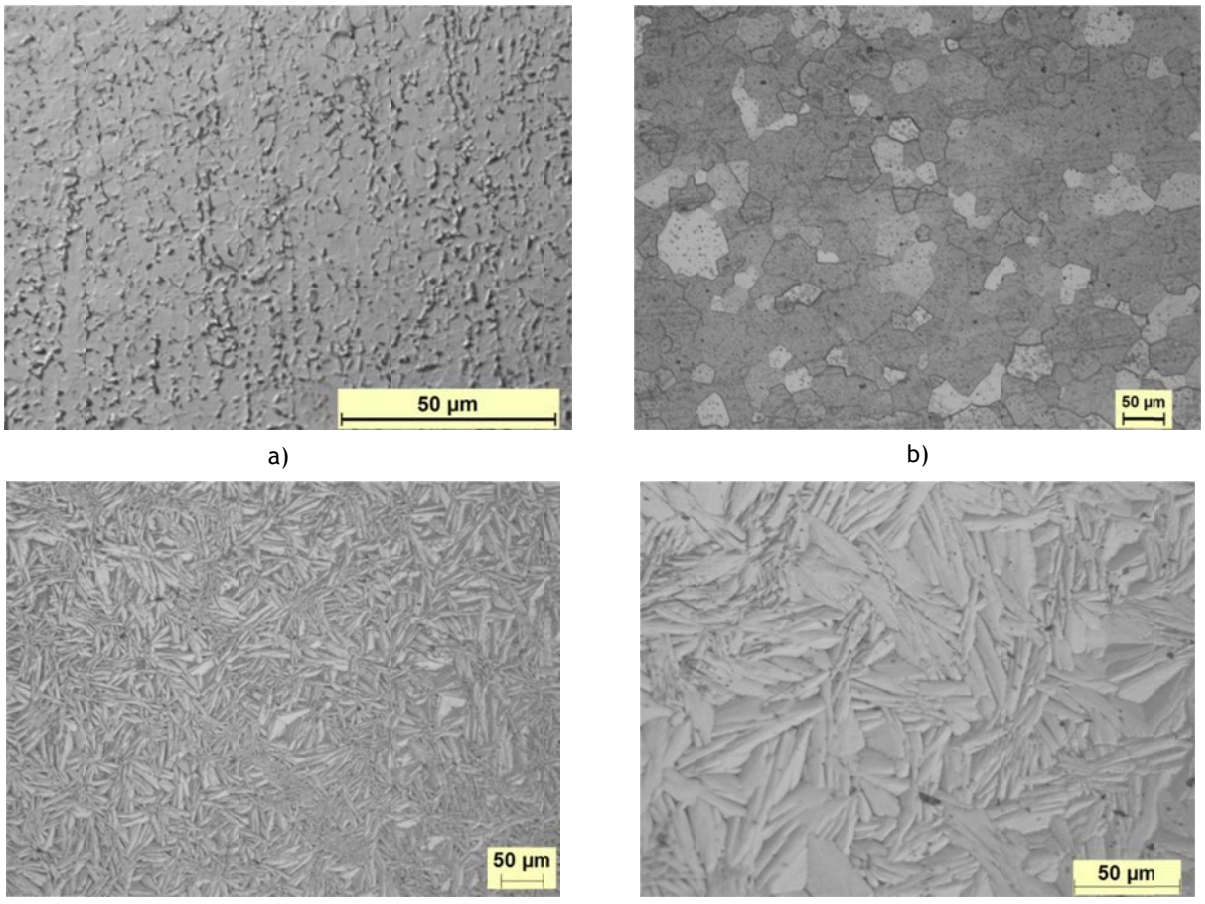

a) b)

c) d)

Figure 20 – (a) Ti6Al4V alloy with α-β structure, (b) equiaxed grains of nitinol alloy, (c) martensitic needles and (d) magnification of (c).

4.2 Macroscopic evaluations of the multilayer foils and joints

There are different ways to reveal the quality of any type of joint even in the cases of roll bonding and DB. First approach is visual inspection and manually bending and splitting the stacks, as it is seen in figure 21-a; the least wide sample on the right side of the image has not well bonded through ARB but the two other stacks are acceptable. In figure 21-b it is illustrated that nearly half of the stack has not roll-bonded during the last cycle. In the case of joint between the light alloys, figure 21-c shows that the material has moved in the earliest stage of the compression during diffusion bonding process and caused an incomplete joint between the substrates, but they were not separated by hand. As it is seen in figure 21-a, the batch with 10 mm width would be useless after ARB processing due to the formation of edge cracks. Other selected widths, 15 mm and 20 mm could be used as a final product.

a) b) c)

Figure 21 - Both well and weak roll bonded foils a) surface view, b) lateral view and c) incomplete joint between two light metals.

Macroscopic or microscopic evaluations of the cross section of the joint could involve the second approach. It is also possible to recognize whether a good joint has been established during sample preparation; in particular, during cutting. For this work samples were cut by iron scissors for both DSC and structural evaluations. If the layers were not well bonded, they would get separated. As it is seen in figure 22-a, b; structural evaluation through OM reveals that there are some internal regions that have not bonded. It is also possible that OM cannot show any defect but they are easily appeared under SEM, like image 22-c. As it was seen in figure 21-b; it is common for Ni/Ti system in the ARB process that the bond of the last rolling stage will be completed and improved in the further cycles and the roll bonding process should be continued fast and clean even with the non-bonded foils. Roll bonding might fail either all along the strip or only along the end part of the strip during the ARB process for the following reasons;

- Insufficient induced roughness;

- Non-ground regions on the surface due to the oscillation of the strip during the primary cutting process;
- Movement of foils over each other during the rolling process due to high strain rate ;
- Inherently ununiformed rolling process;
- Contamination from the working environment, e.g. operators` hands.

a) b) c)

Figure 22 - Unbounded zones revealed by microscope; a) within the foils and b) between the substrates and (c) two non-welded regions revealed by SEM

4.3 Failure during multilayer fabrication

If the surfaces of the primary foils are not well ground, a fish tail-like strip will form after the first cycle; figure 23-a. It is required to cut that part away to continue the process which is material loss. The only way to avoid the formation of this defect was a primary reduction greater than 30% as well as a perfect surface preparation. That defect occurs due to the movement of the strips over each other during passing the rolling gap, i.e. the roughness of the surfaces is not enough to establish the mechanical bonding during thickness reduction. The high strain rate, 20 s^{-1}, also promotes the formation of that end shape. It was one of the reasons for choosing 600 mesh grinding paper for Ti foil than 1000 mesh. If the ARB process pauses for some minutes to do any measurements or any other evaluations, roll bonding will not form in further cycles. Some failures are observed in figure 23-b and c. The following reasons justify the multilayer formation process rate;

- As the material contains pure titanium experiencing high levels of deformation it is prone to oxidize at the process temperature, thereby, formation of any surface compounds will eliminate the roll bonding process;
- Any delay will also promote the propagation of micro cracks which have already formed during the previous rolling stages;
- Any long pause between cycles might provoke the delamination of weak bonded regions due to the residual stress that remained in the multilayer system.

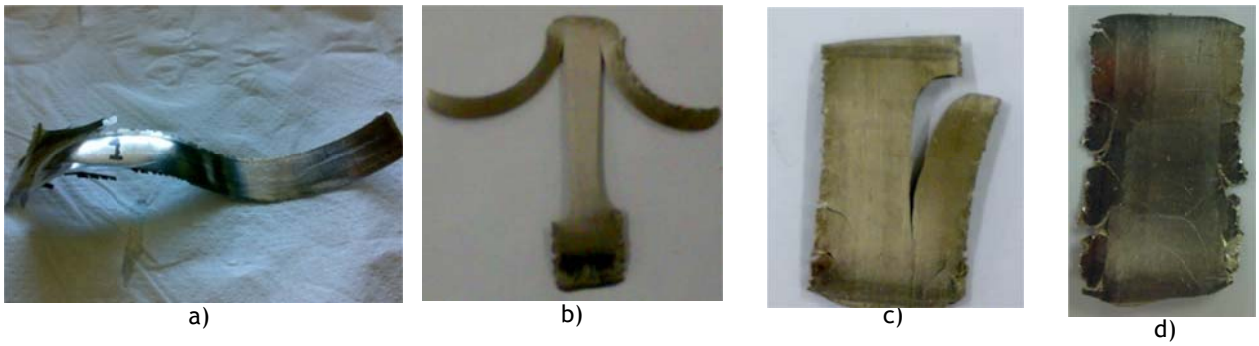

a) b) c) d)

Figure 23 - Different types of deffects occurred after (a)1st cycle, (b)11th cycle and (c) 1st rolling after 2nd intermediate annealing and (d) 3rd cycle, look at macroscopic bumps on the foil surface

Edge cracking occurs during rolling when material gets hard and loses its workability [25]. ARB could be better repeated until edge cracking is appeared [25, 26]. However, in this work it was continued even after small cracks were appeared. The author has experienced that when the material is soft that can be bended easily by hand, if any cracks without open mouth form during the process, most likely they will be eliminated in the next cycle. As it is seen in figure 23-d, there are some macroscopic bumps on the foil surface, adapted from the roll mills surface. They could promote the propagation of edge cracks. It is very difficult to predict sever failures, e.g. in the case of figure 23-b there was no sever cracks on the edges of the sample after the tenth cycle but the foil failed drastically in the eleventh cycle.

4.4 Deformation level

As it was described it was very difficult to control the deformation process through recording the changes of dimensions during the process. The evaluation of the mechanical terms, such as equivalent strain and reduction in each cycle, has not been the aim of this work otherwise more material and time was needed. It was also difficult to maintain the gap, the distance between the roll mills of the available machine, during the period of this thesis because that machine was used for other projects. Before the beginning of ARB process on the Ni/Ti system some experiment was carried out on Al and brass foils. Some data obtained are presented in table 16, appendix E. These results show that it is possible to claim that ARB process on such dimensions can provide plain strain condition, i.e. the difference of the width of the strips before and after each rolling stage is very small and it is possible to ignore it. But two materials behave differently under same plastic deformation conditions so it is impossible to adjust the gap by one material and then using it for another one. For example, under same conditions, temperature and gap distance, foils of Al, Ni and Ni/Ti with thicknesses of 60 μm, 90 μm and 230 μm were produced, respectively.

According to the literature in earliest experiments almost 30% reduction, less than 50%, was introduced which caused material loss for the intended material system, as mentioned before in details. To avoid the occurrence of that problem it was possible to apply a primary diffusion bonding before any rolling but it required especial mould and more time. Therefore it was tried to perform roll bonding in the earliest stage but it was very difficult to adjust 50% reduction, it required more Ni and Ti which are expensive materials. In the latest multilayer fabrication experiment a primary deformation of 69.2% was done which is seen in figure 24-a. During several experiments two interesting subjects were noticed;

- It was observed that nickel deforms more than titanium during primary rolling. This point is observed in figure 24-a; brighter portion in the end part of the strip located on the left side of the image. This part should be preserved during the cycles otherwise the predesigned chemical composition will not be obtained;
- When one cycle is repeated, the strip will become longer in the second stage but the result depends on the quality of the bond, i.e. the strip would be elongated if there was already a good bond otherwise it would be delaminated, as it is seen in figure 24-a.

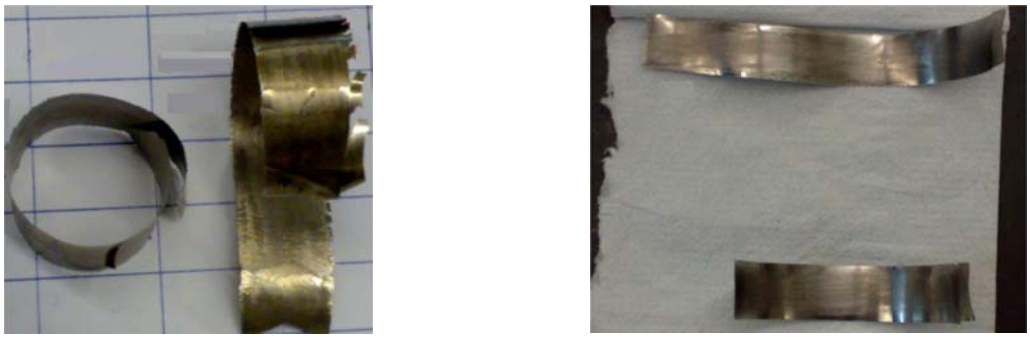

a) b)

Figure 24 - (a) Complete delamination after repeating a cycle plus the effect of greater deformation of Ni than Ti, (b) longer strip resulted from repeating a cycle

The elongated strip made through repeating the cycle is illustrated on the top part of figure 24-b. It seemed that it had lost its spring like behavior increasing rigidity which could be the effect of reducing a bit more the thickness. Thus, in general it is possible to claim that repeated rolling increases the bonding strength and decreases delamination [27]. It was also difficult to have products with almost equal thicknesses because as the process continues the roll mills get hot and hotter and the same gap gives thinner foil than the earliest stage. For example, in one day after 10 cycles of R&C a foil with almost 230 μm was produced and the next produced foil become almost 100 μm thick. It reveals that the material processing is

carried out at temperatures above ambient temperature and that increase enhances the thickness reduction.

Table 8 – Estimated deformation and layer thickness for the several R&B experiments (average dimensions)

Laminated product	Number of layers N!	Layer thickness in average (nm)	Number of couples (Ni/Ti)	Couple thickness in average (nm)	Strain of one couple after cycles
4 cycles	32	10156	16	20312	4*0.69=2.76
10 cycles	1024	317	512	634	10*0.69=6.9
12 cycles	4096	79	2048	158	12*0.69=8.28
14 cycles	16384	20	8192	40	14*0.69=9.66
15 cycles	32768	10	16384	20	15*0.69=10.35

- Primary foils have the thicknesses of 0.2 mm plus 0.125 mm = 0.325 mm
- It is supposed that each layer suffers equal deformation
- Each cycle of ARB introduces 50% reduction in Ni/Ti system that gives the strain of 0.69
- Primary rolling will introduce the strain of 0.35 and 1.2 if the reduction is 30% and 70%

In this work it was almost impossible to record the thickness variations during the process and control the deformation process through strain; moreover cold rolling inherently introduces nonuniform deformation. So the information presented in table 8 has been obtained approximately based on the thickness of the primary material and number of cutting and folding cycles. The product is a foil composed of two different materials with different properties and behaviors by which provides that problem. Results presented in table 8 could be ensured through appendix F. According to the approximations presented in table 8, the product of 10 cycles of cutting and rolling has already found an ultrafine laminated structure and the ARB processes foil after 14 cycles could be considered as nano laminated composite. When the processed material got strong and the rolling machine stopped during rolling, two alternative approaches were applied, to overcome that problem;

- Intermediate annealing and continuing the rolling;
- Shrinking the rolled sample to smaller size and continuing the rolling.

The first approach requires more time, energy and precautions to avoid oxidation and intermetallic phases` formations as well. This was the method used when an explosion occurred in the earliest stage of the 11^{th} cycle of rolling after second intermediate annealing. The second approach includes removing the edge cracks, as illustrated in figure 25, when this approach is applied the machine will provide the required rolling pressure because the rolled area has decreased. This method is more feasible and more reasonable than applying

intermediate annealing because it consumes less energy and time. It was possible to reach 15 cycles of R&C but it is important to keep the mills surfaces clean during the process.

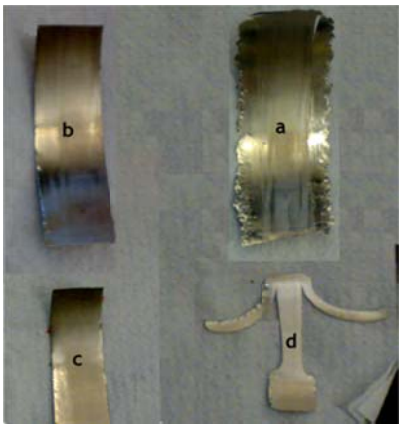

Figure 25 - Sequences of applying second approach; (a) foil after 4 cycles, (b) after cutting the edges to reduce the width of the foil, (c) second time of width reduction after 10th cycle and (d) failure after 11th cycle

During ARB process of the Ni/Ti system, material loss is observed due to:

- The formation of brittle chips on the edges and its separation during the process;
- Fish tail-like formation that should be cut to continue the process;
- Edge crack removal to eliminate intermediate annealing.

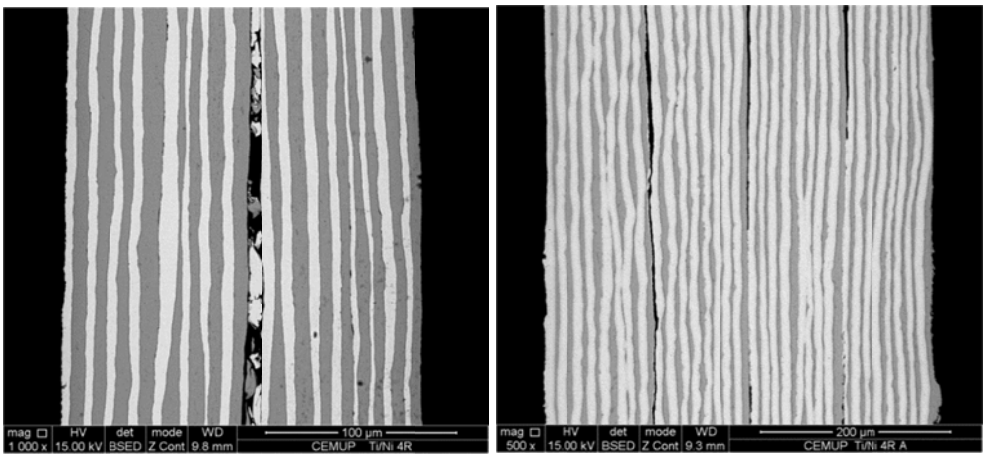

a) b)

Figure 26 – Transversal cross section showing (a) the fluctuation of layers after 4 cycles of R&C, and (b) non uniformed thickness reduction, delamination is observed in each 16 layers

Delamination provides difficulties of grinding and polishing. The trapping of fine particles inside the gaps causes scratches during surface preparation for OM and SEM. Microstructural evaluations revealed cold rolling process cannot introduce a uniform

deformation not only at a macroscopic level (thickness reduction) but also at a microscopic scale (layers experience fluctuation along the rolling path). These two problems are easily recognized through the following evaluations;

- Thickness measurement along the rolled sample; thinner thicknesses in the earliest length of the foil and close to its edges than in the middle part of the sample which might have been caused by the geometry of the roll mills;
- Microstructural images from longitudinal cross section reveal fluctuations and variation of thicknesses of the layers, as it is seen in figure 26;
- A complete bond in region provides thinner section than unbounded parts of the strip.

4.5 Structural characterization of multilayers during deformation;

4.5.1 Structure of Ni/Ti multilayer after 4 cycles of cutting and rolling;

The analysis of the microstructure after 4 cycles show ultrafine elongated grains in the Ni layer (figure 27). Grains are not visible in the Ti which might be caused by the formation of nano grains. Further observations, namely by TEM, are required to characterize these layers.

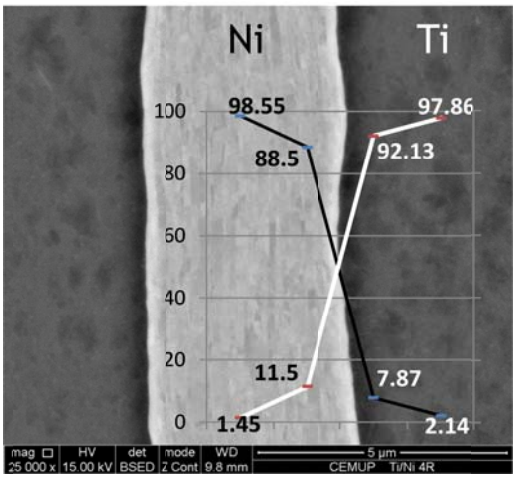

Figure 27 - Ni (white layer) and Ti layers after 4 cycles. The chemical composition determined by EDS is also shown

This structure is similar to the one described in literature for much higher deformation; 20 cycles. This achievement at this stage could have been resulted from introducing a very high strain rate. Having finer grains in one constituent, under same working conditions, might be resulted from;

- Greater activation of twinning mechanism deformation in Ti due to having hcp structure in comparison with Ni having fcc structure;
- Experiencing a bit more strain hardening in Ti;
- Primary Ti foil was composed of finer grains than primary Ni.

Unlike hot rolling, recrystallization of the grains does not occur in cold rolling due to low working temperature. Those elongated grains resulted from the dislocation movements [23]; it is also claimed that the formation of subgrains by the accumulation and rearrangement of dislocations through intense cold rolling produce fine and elongated grains. Rearrangement of dislocation goes for lowering the strain energy of the system [28]. SEM was also helpful to evaluate whether any solid state diffusion has occurred within the layers. This purpose was fulfilled by using SEM/EDS technique that determines the chemical analysis of the intended regions, as it is illustrated in figure 27. The graph matched with the picture shows the analysis results at the interface of two layers and in the middle of those layers. The Ni content in the middle of the Ti foil is 2.14at% while Ti content in the middle of Ni foil is 1.45at%. This difference expresses the principle saying that the diffusion coefficient of Ni in Ti is greater than the reverse direction state [14]. It is also observed that the closer to the interface, the higher the diffusion level. The particular features of this rolling process help explain this solid diffusion at low temperature. Fabrication of multilayers through severe plastic deformation processing routs introduces high levels of strain so that each individual metallic layer will experience the increase of structural defects, such as voids, dislocations and grain boundaries [17]. Moreover; the material is not deformed at ambient temperature because ARB does not consume any lubricant so, the amount of heat produced by friction will grow. On the other hand high strain rate does not allow the system to have enough heat transfer. The latter condition was experienced so that the rolled piece and roll mills surface burns fingers` operator at the point of touch. This point has also been confirmed in the literature [3]. Therefore, as a general rule, atoms of every metallic system move at the ambient temperature by self-diffusion mechanism through void mechanism [11].

4.5.2 Structure of Ni/Ti multilayer after 10 cycles of cutting and rolling;

The structure of an as rolled sample after 10 cycles of R&C is presented in figure 28. It has been produced without using any intermediate heat treating. SEM/EDS was also hired to identify the chemical composition of the multilayer and it gave a composition of 50.71at%Ni. Such produced multilayer was achieved through taking the following precautions; rolling mills are to be maintained clean, no stop during the process and removing edge cracks. OM could not reveal the formation of nano layers; it was only possible to observe few thick nickel

regions within the structure. These thick regions are clearly seen by SEM, figure 28-a, plus some other thick Ti regions that have the maximum thickness of 2 µm. However, SEM revealed the formation of laminated metallic composite of Ni/Ti in the size of nano scale in the majority of the foil. As it is seen in figure 28-b, there are layers having thicknesses smaller than 20 nm. Layers are continuous and small fractions of fragmentations are observed (figure 29), unlike Ni/Al laminated structure [6]. As it has been claimed in the literature [14, 19], Ni and Ti have suffered almost equal work hardening so that they have suffered same level of localized necking, they have close values of ultimate strength. As it is seen in figure 29-a, even some fragments are composed of multilayers of Ni and Ti. Ni and Ti foils have been folded in those regions due to either the non-uniformity effects of the rolling or the presence of inclusions, like oxide particles formed during the process.

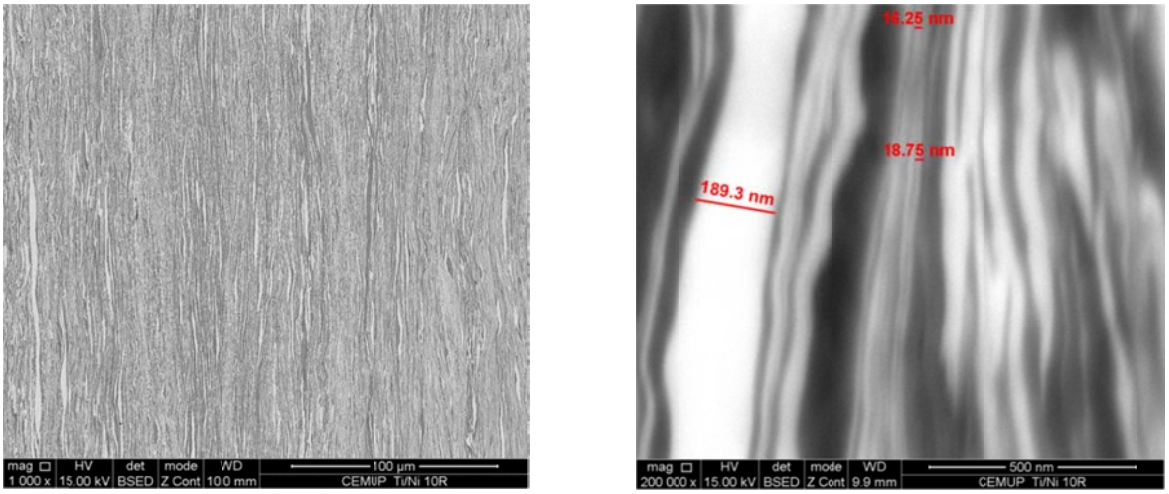

a) b)

Figure 28 - SEM images of a multilayer after 10 R&C cycles

The produced laminated structure could be summarized as in the following;

- Layers are almost uniform distributed;
- Fluctuation of layers is observed due to the non uniform distribution of stress during rolling process;
- Thickness reduction along a layer is not uniform that is a sign of localized necking without rupture;
- As it is seen in figure 29-b, Ni nano grains have formed inside the thick layers (thickness of almost 1.5 µm) unlike what has been proposed in the literature [28] saying that the formation of nano grains occurs after transforming the thicknesses of the layers into nano scales;

- Presence of solid state diffusion, with same explanation and justification brought in previous section, presented by the adapted graph on the image of figure 29-b;

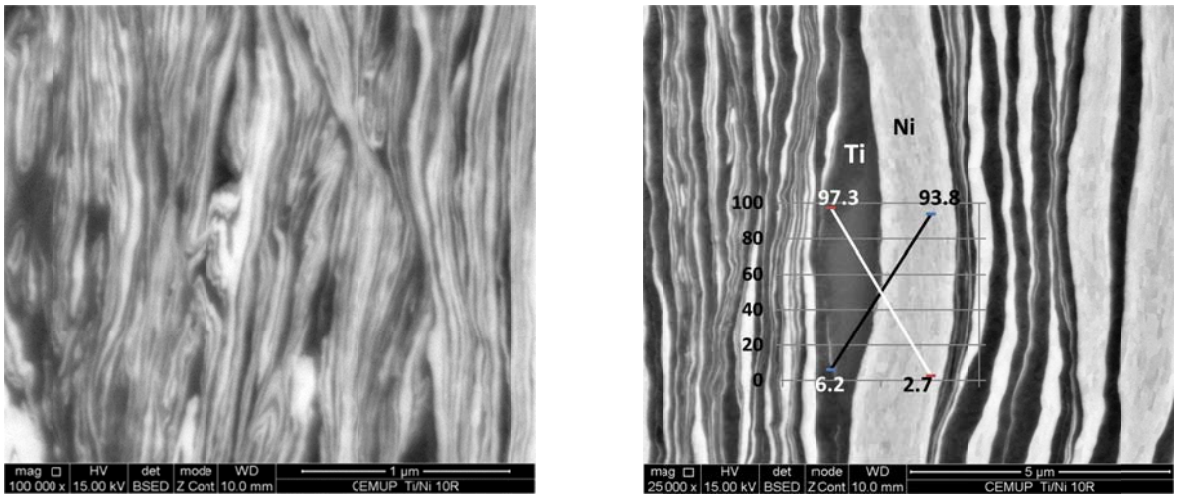

a) b)

Figure 29 – (a) Vortex like zones composed of multilayers (b) diffusion in the layers and nonuniform reduction

As the graph depicts, the diffusion rate of both elements has increased in comparison with the values presented in figure 27; increase rate of Ti is almost 3% and for Ni is 1.9%. It shows that higher deformation increases the diffusion rate; the diffusion can be promoted by the formation of nano grains which results in the growth of the diffusion rate through boundary mechanism [8, 25].

4.5.3 Structure of Ni/Ti multilayer after 15 cycles of cutting and rolling;

After 15 cycles of R&C, it seems that both the distribution and thickness reduction of lamellas have become more uniform in comparison with the foil produced by 10 cycles but some micro cracks have been appeared, see figure 30. As it is illustrated in figure 30-b, the propagation of cracks is observed in both directions; perpendicular to the lamellas and along them which might be the effects of process and strain. Figure 31-a, shows the thickest Ni layer observed in that sample that is almost 2 µm thick. It was not possible to recognize any grains in that region by SEM in that magnification. As it was seen in figure 30-a; there are also some Ti regions having the thickness of almost 2 µm. Such laminated structure was not observed by OM. As it is illustrated in figure 32-a; one shear strain line was appeared between two brackets in the SEM image. Global chemical analysis was also determined by SEM/EDS. Figure 32-b illustrates the graph of EDS revealing the intensities of the Ni and Ti in the analysed region. It gave a chemical composition of Ti-50.13at%Ni.

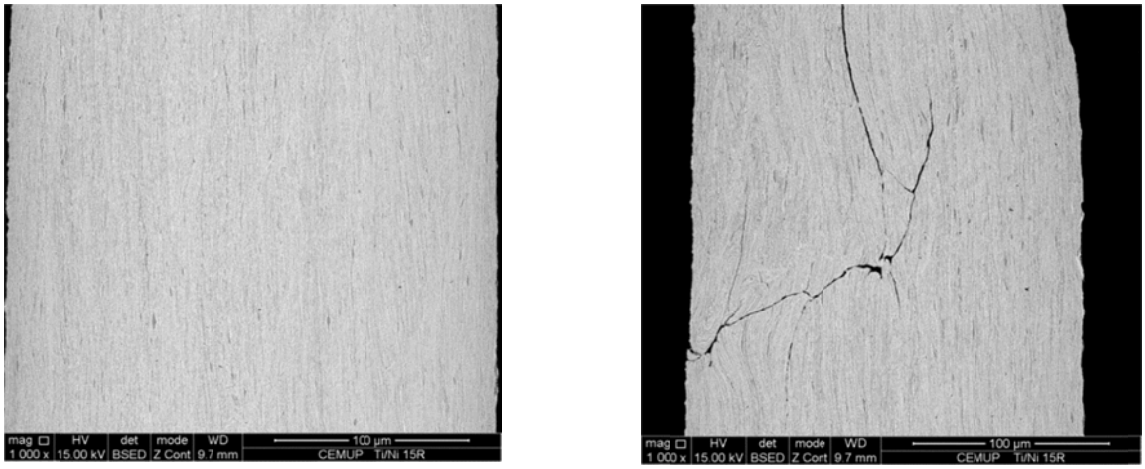

a) b)

Figure 30 – (a) Uniform distribution of layers and (b) cracks formation across the section of the sample after 15 cycles of R&C

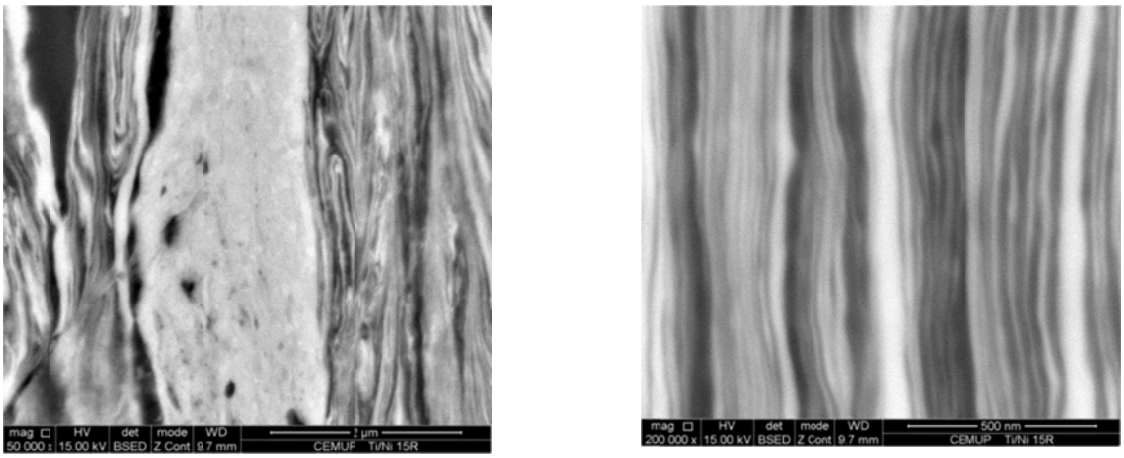

a) b)

Figure 31 – (a) Thick Ni layer plus folded lamellas and (b) layers of almost 5 to 40 nm thick

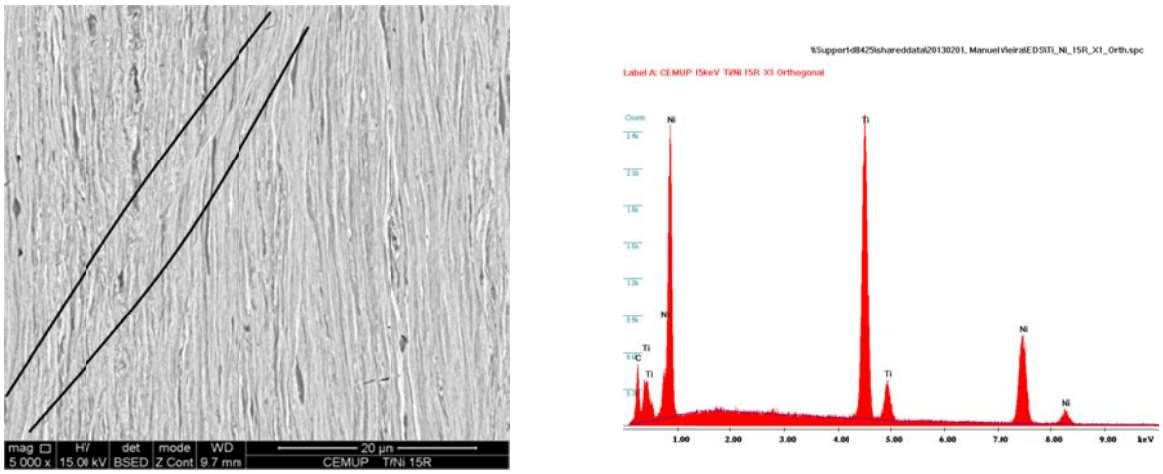

a) b)

Figure 32 – (a) Shear strain line and (b) EDS qualitative analysis graph

4.5.4 Comparison between different strain rates

Figure 33-a&b has taken from a multilayer produced by the strain rate of $20s^{-1}$ after 10 and 15 cycles, respectively. They have had primary materials with the thicknesses of 200 µm and 125 µm, while figure 33-c&d reveals Ni/Ti multilayer after 20 cycles fabricated by strain rate of $0.1s^{-1}$ [18]. Their primary materials were 32 µm and 7.5 µm thick. This comparison reveals that the increase of strain rate enhances the reduction rate.

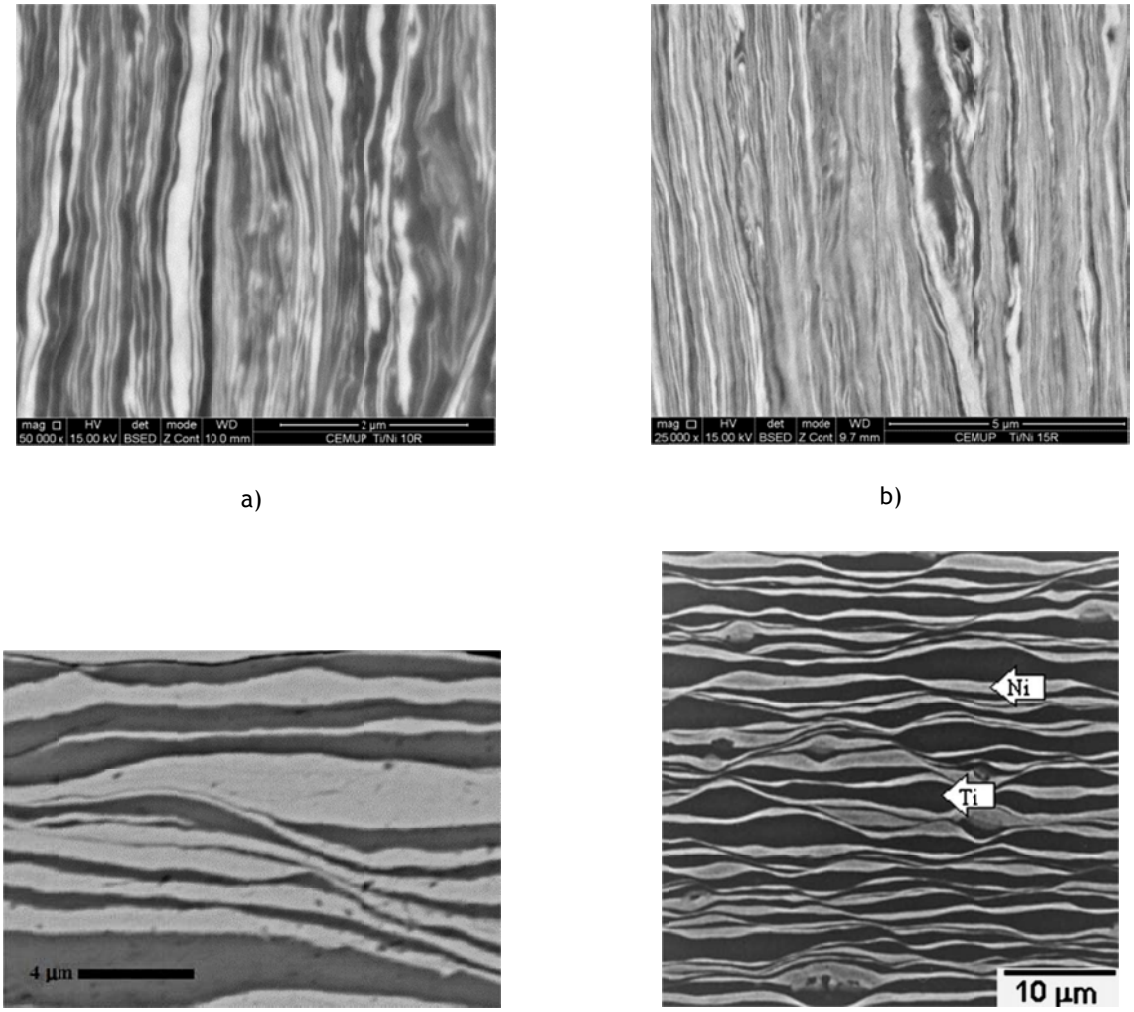

a) b)

c) d)

Figure 33 – (a) and (b) Ti/Ni layers of this work produced with a strain rate of $20s^{-1}$ after 10 and 15 cycles, respectively, (c) and (d) Ti/Ni layers with 20 cycles but produced with a strain rate of $0.1s^{-1}$ [19]

4.5.5 Differential scanning calorimetry evaluations;

As it was already mentioned DSC was performed to determine the amount of heat released during the reaction between Ni and Ti layers and also to identify the initial temperature at which any phases form. The latter result could be useful to select a proper

stress relief during the fabrication of the multilayer foil at which no intermetallic phase form, i.e. heating at a temperature below the initiation of phase formation.

In this study it is aimed to evaluate only the intermetallic phase formation on heating and so the graphs of figure 34 are of the heating part of the DSC test. From the analysis of these graphs, plus the extracted data presented in table 9, the following information could be extracted;

1. Two peaks appeared in the graph of 4 cycles, red graph, depicting exothermic reactions which may be associated with the formation of intermetallic phases. Those phases might form at the same time or not, depending on the energy of formation [14, 40], that will be discussed later in details.

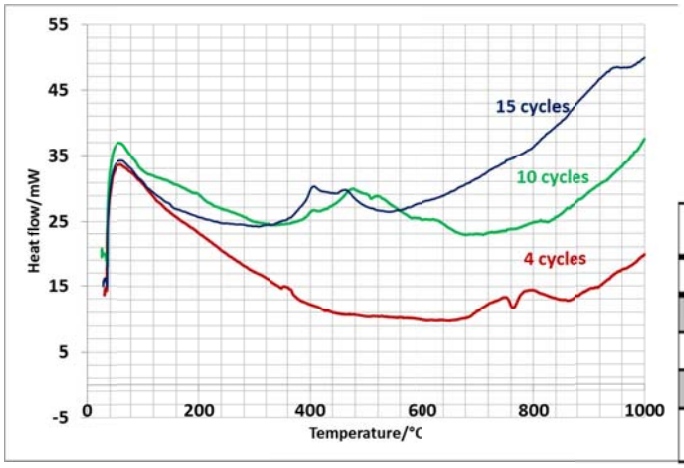

Table 9 - Information of DSC graphs extracted from the equipment

Exothermic reactions			
	4 cycles	10 cycles	15 cycles
Peak (°C)	790.88	476.37	407.06
Onset (°C)	685.65	437.73	374.34
Enthalpy (J/g)	-180.32	-132.20	-166.03

Figure 34 - DSC graphs of test started at ambient to 1000ºC at a rate of 20ºC/min.

2. As it is seen in other graphs, the temperature of phase formation decreases by increasing the deformation level. It indicates the effects of both layer thickness and the structural defects at the ignition of exothermic reaction, i.e. the thinner the layers, the lower the temperature required to ignite the reaction. As the reaction takes place through the diffusion of Ni and Ti atoms within the layers, both high number of grain boundaries and high density of dislocations, pipe diffusion mechanism, have increased the diffusion process [17].

3. According to the literature it was expected to reach high levels of energy through reducing the thickness of layers [7], but table 9 does not show that growth. This discrepancy should be investigated increasing the number of DSC experiments. DSC was done only for one sample from each batch while it should have been better to have three samples from each batch.

4. There is a concave region on the red graph in figure 34 between two separate peaks. It has the endothermic peak around 764 ºC, close to the eutectoid reaction at 765 ºC. It will be

discussed in next section that it could be the endothermic reaction due to formation of ß-Ti [41]. As it will be seen in the graph of figure 35, the peak observed on the cooling curve around 760 ºC could prove that claim. In general there are some parameters affecting both the propagation and the heat of the reaction as in the following;

- Delamination of two layers disconnects the reaction of those two adjacent layer and results in omitting the path of diffusion;
- Fracture of the layers caused by strain hardening impedes the propagation of the ignition along the layers.

4.6 Solid state diffusion within Ni/Ti bimetal system

Before continuing the study of phase's evolution during any heating process it is better to evaluate the diffusion of Ni and Ti atoms within the possible system. According to the equilibrium diagram illustrated in figure 4, there could be three intermetallic compounds present in any bimetallic system composed of Ni and Ti. As all the heating processes in this work were applied at temperatures between 600 ºC and 800 ºC, the diffusion process will be studied within that range. However, only data belongs to 700 ºC and 800 ºC were obtained in literature. Diffusion in the solid state is a function of temperature, $D = D_{0^*} \exp(-Qd/RT)$. D_0 is a temperature-independent (m^2/s), Qd is the activation energy for diffusion (J/mol or eV/atom), R is the gas constant, 8.31 J/mol-K or 8.62 10^{-5} eV/atom-K and T is absolute temperature (K). The driving force of diffusion process is fulfilled by the concentration gradient at the interface of the faying joint [11]. The diffusion coefficients of the constituents in different systems are calculated based on date presented in table 10 through previous equation. Diffusion coefficient and the required energy needed for diffusion process at temperatures between 750 ºC and 900 ºC are presented in that table as well.

Literature claims that Ni diffuses in Ti faster than Ti does [14, 17, and 31]. Table 10 also gives the following results;

1. This is the order of titanium diffusion: Ni > Ti6Al4V > $TiNi_3$ > TiNi > Ti_2Ni;

2. This is the order of nickel diffusion: Ti6Al4V > Ti_2Ni > TiNi > $TiNi_3$;

3. Diffusion rate of Ti is rather greater in intermetallic compounds than that of Ni in those compounds except Ti_2Ni;

4. $D^{Ti}_{Ti6Al4V} > D^{Ni}_{Ti6Al4V}$;

5. Diffusion rate of Ti and Ni is greater in Ti6Al4V than that of in nitinol.

Table 10 – Diffusion coefficients and activation energies of the mentioned compounds at different temperatures [values of D_0 and Q_d from 40]

	D^{Ti}_{Ni}	D^{Ti}_{TiNi3}	D^{Ti}_{TiNi}	D^{Ti}_{Ti2Ni}	$D^{Ti}_{Ti6Al4V}$
D_0 (m^2/s) at 750 °C - 900 °C	$1.6*10^{-6}$	$1.4*10^{-8}$	$1.6*10^{-8}$	$2.3*10^{-8}$	$2.0*10^{-8}$
Q (kJ/mol) at 750 °C - 900 °C	132	231	251	272	125
D (m^2/s) at 700 °C	$1.3*10^{-13}$	$5.5*10^{-21}$	$5.3*10^{-22}$	$5.65*10^{-23}$	$3.86*10^{-15}$
D (m^2/s) at 800 °C	$6*10^{-13}$	$7.85*10^{-20}$	$9.53*10^{-21}$	$1.3*10^{-21}$	$1.63*10^{-14}$
	-	D^{Ni}_{TiNi3}	D^{Ni}_{TiNi}	D^{Ni}_{Ti2Ni}	$D^{Ni}_{Ti6Al4V}$
D_0 (m^2/s) at 750 °C - 900 °C	-	$2.2*10^{-9}$	$1.5*10^{-9}$	$6.6*10^{-9}$	$8.6*10^{-5}$
Q (kJ/mol) at 750 °C - 900 °C	-	286	275	257	257
D (m^2/s) at 700 °C	-	$9.6*10^{-25}$	$2.54*10^{-24}$	$1.04*10^{-22}$	$1.35*10^{-18}$
D (m^2/s) at 800 °C	-	$2.6*10^{-23}$	$6.05*10^{-23}$	$2*10^{-21}$	$2.61*10^{-17}$

According to those results and the claims mentioned in the literature the following conclusions could be made:

- Greater D_{Ni} than of D_{Ti} in Ti/Ni interface [14, 42] means that an excess of vacancies will accumulate in nickel side. After accumulation of such empty places, voids will be formed. They are located in Ni layers and are known as Kirkendall voids. Thus, it is expected that the increase of temperature will increase the number of those voids. That difference of diffusion coefficient might justify the formation of $TiNi_3$ in the earliest time of the diffusion process than two other intermetallic compounds;
- The formation of intermetallic phases will behave as a barrier and impede the diffusion process thus, implementing any homogenizing treatment requires large soaking time and higher temperature;
- Ti and Ni atoms tend to diffuse to the substrates. It would be difficult to trace the addition of Ti in Ti6Al4V and of Ni in nitinol.
- As Ti diffuses faster than Ni, the transformation of $TiNi_3$ into TiNi is faster than that of Ti_2Ni which explains why Ti_2Ni is more abundant in microstructure than $TiNi_3$;
- The diffusion of Ni and Ti in Ti6Al4V should be greater than in nitinol.

Thermodynamically, it is possible to predict the probability of the formation of the intermetallic compounds in the Ni-Ti bimetal system. It is said that due to the thermodynamic equilibrium of Ni and Ti it is very difficult to have only TiNi phase in a bimetal system. According to the literature [14, 40] tables 11 and 12 present the data calculated in appendix G depicting that $TiNi_3$ forms at the interface of DB zone more rapidly than two other intermetallic phases at 700 °C and 800 °C.

Table 11 - Gibbs free energy formation of the mentioned compounds based on equations 6 to 8		
	At 700 °C	At 800 °C
G(TiNi)(kJ/mol)	-268.2	-291.5
G(Ti_2Ni)(kJ/mol)	-385.3	-422.0
G($TiNi_3$)(kJ/mol)	-490.4	-537.5

Table 12 - Gibbs free energy formation of the mentioned compounds based on equations 9 to 11		
	At 700 °C	At 800 °C
G(TiNi)(kJ/mol)	-37.0	-35.1
G(Ti_2Ni)(kJ/mol)	-34.1	-30.7
G($TiNi_3$)(kJ/mol)	-41.7	-38.5

4.7 Phase evolution of multilayers during heating processes;

4.7.1 Phases evolutions within the DSC samples

Two more DSC tests were conducted to evaluate the phase formation in terms of priorities and temperature influences, as in the following; selected samples tested at equal heating rate, 20 °C/min, one heated up to 726 °C and the other one up to 791 °C and both cooled rapidly, 40 °C/min, the results are presented in figure 35. Microstructure of the higher temperature DSC sample is illustrated in figure 36. Figure 36-a shows a lamellar structure, zone 1.This zone is the product of the eutectoid reaction ß-Ti →α-Ti + Ti_2Ni. EDS results are presented in table 13; the phases identified in each region according to the equilibrium phase diagram, as it is illustrated in figure 37, are listed in the same table.

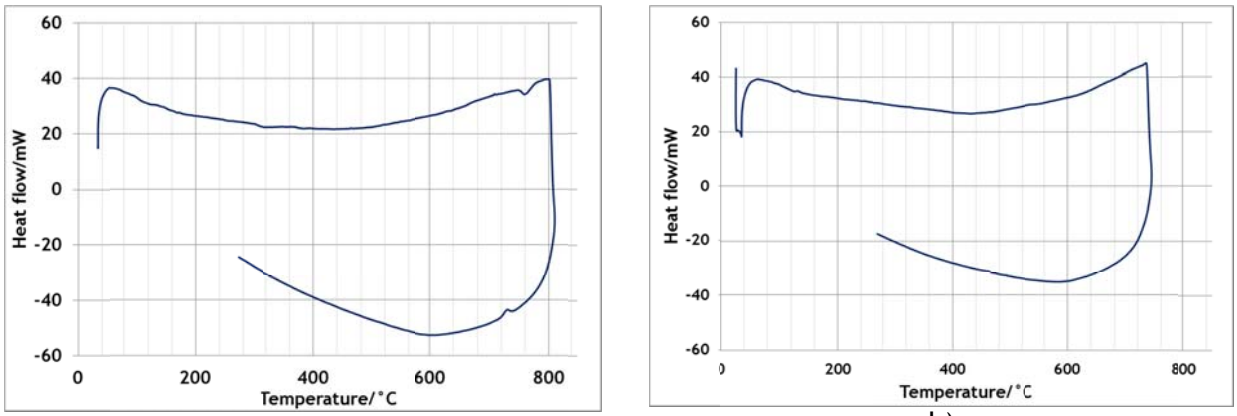

Figure 35 - 4 cycles of R&C heated at 20°C/min then cooled at 40°C/min (a) up to 791 °C and (b) up to 726 °C

In the earliest stage of any phase identification through using equilibrium diagrams it should be said that the products of solid state diffusion have not produced under equilibrium conditions because the structures are in ultrafine and nano scales, pressure of the atmosphere is not 10^5 Pa (1 atm) but almost 10^{-3} Pa and in DB process the material is compressed. The image analyzer of the software of the SEM equipment calculated the amount of white phase in region 1, which is Ti_2Ni, as 26%. In appendix H it is illustrated that it is close to the value calculated through level rule; 23%.

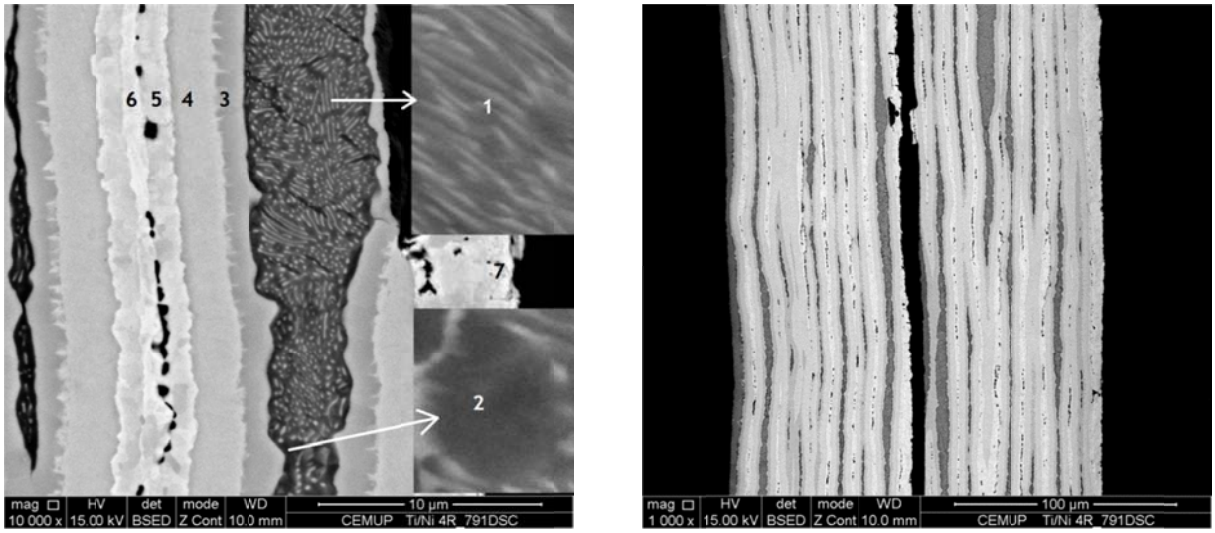

a) b)

Figure 36 – SEM images of the DSC sample heated up to 791 °C and cooled rapidally by the rate of 40 °C/min (a) shows the analysed region (b) reveals the voids and likely interfacial cracks

Table 13 – EDS results in atomic percentages and the phases identification based on the equilibrium diagram, regions are illustrated in figure 36-a.

Regions	Ni-at%	Ti-at%	Ratio of Ni/Ti	Equivalences
1	7.9	92.1	0.086	α-Ti + Ti_2Ni
2	6.06	93.94	0.065	α-Ti + Ti_2Ni(caused by interaction volume)
3	35.76	64.24	0.557	Ti_2Ni + TiNi(caused by interaction volume)
4	50.2	49.8	1.01	TiNi
5	70.22	29.78	2.36	$TiNi_3$ + TiNi(caused by interaction volume)
6	88.01	11.99	7.34	Ni + $TiNi_3$(precipitated)
7	93.26	6.74	13.83	Ni

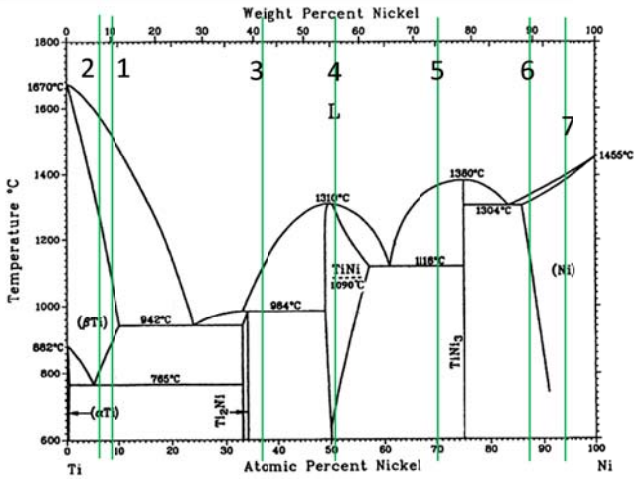

Figure 37 – identifying of the zones 1 to 7 illustrated in figure 36-a in the equilibrium diagram of Ni-Ti

As it is seen all possible intermetallic compounds formed at the interface of the layers are $TiNi_3$, TiNi and Ti_2Ni and the amount of TiNi in the microstructure is observed greater than others` by which it is justified through diffusion coefficients. As it is illustrated in figure 36-b Kirkendall voids are considerable and they are only seen in the Ni sites [17]. There are some elongated voids, they might be either the interfacial cracks [14] caused by the difference of thermal expansion coefficient of Ni and Ti or the accumulation of Kirkendall voids. As it is seen in figure 36-a; there are only three distinguishable layers between each individual pure metal but the results presented in table 13 show the presence of two phases in each layer. This problem has been resulted from the volume interaction effect caused during EDS (close to 1µm in the phases analysed [36]). Therefore the phases that probably exist in the analysed zones from 1 to 7 are titanium and Ti_2Ni, Ti_2Ni, TiNi, $TiNi_3$, and nickel. Figure 36-b also shows some regions only composed of Ti_2Ni and TiNi which means that heating up to 791 ºC has provided enough energy for the diffusion of Ti atoms and has eliminated the $TiNi_3$ phase.

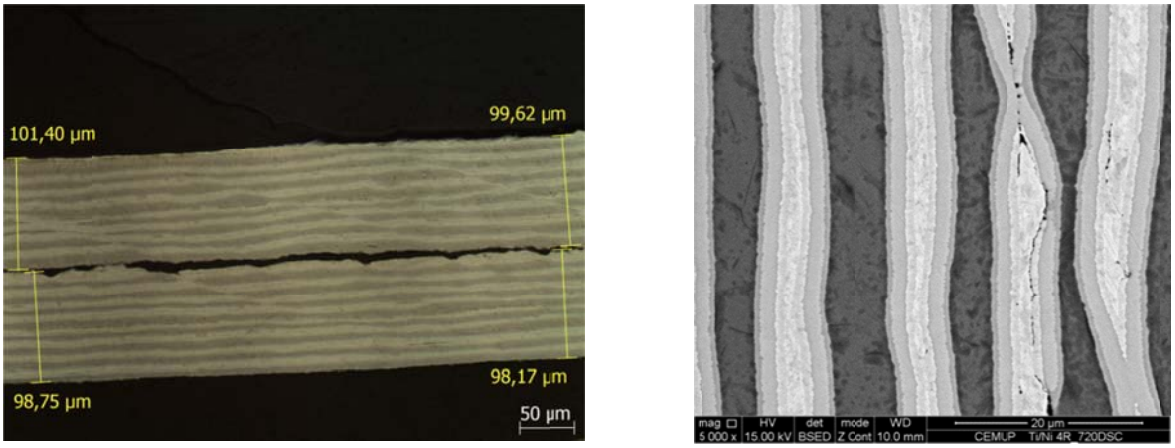

a) b)

Figure 38 – (a) shear strain bands visible in longitudinal cross section samples after 4 cycles, (b) elimination of $TiNi_3$ in the shear strain regions

Another DSC test was carried out on the 4 cycle R&C sample to evaluate the phase formation before the concave area illustrated in the red graph of figure 34. It was heated up to 726 ºC and cooled rapidly under same conditions selected for the previous one. SEM evaluation revealed same phase evolution like previous test but some differences are observed as in the followings;

- As the temperature of the test has been selected below the eutectoid reaction the lamellar structure has not been observed;
- As the temperature is lower than the previous test, the number of Kirkendall voids and interfacial cracks has considerable decreased due to reduction of diffusion;

- It seems that the amount of $TiNi_3$ in this test is greater than the previous test. It was not possible to evaluate quantitatively the amounts of this phase in each case because the image analyzer available, Leica LAS version 4.1 was not able to distinguish the difference between the colors of the intermetallic phases.

Shear strain zones are observed in figure 38-a, obtained by OM. The shear strain lines has been reported in literature after higher deformation levels [26]; the observation of this macroscopic strain localization effect with only 4 cycles of R&C could resulted from the application of high strain rate, $20s^{-1}$. SEM evaluation of that region shows the absence of $TiNi_3$ in thinner sections, figure 38-b. It might be the effect of either thickness reduction or the effect of the level of the strain energy in that region. The first condition has caused the presence of less Ni in those regions and resulted in decreasing the probability of $TiNi_3$ formation. The latter proposal might result in higher migration of Ti atoms to the Ni site. The question is that if the elimination of $TiNi_3$ is mostly due to the thickness reduction why in foils having ultrafine layers, further sections, the formation of $TiNi_3$ is observed. Another interesting result is that the non uniform distribution of structural defects could affect the formation and distribution of voids. This problem could be observed in figure 38-b in which Kirkendall voids are seen only in the two layers that might have had higher levels of defects. In the literature [14] it was mentioned that voids have increased by the growth of deformation level in both Ni/Ti and Al/Ti multilayer systems.

4.7.2 Phase evolution during intermediate heat treatments

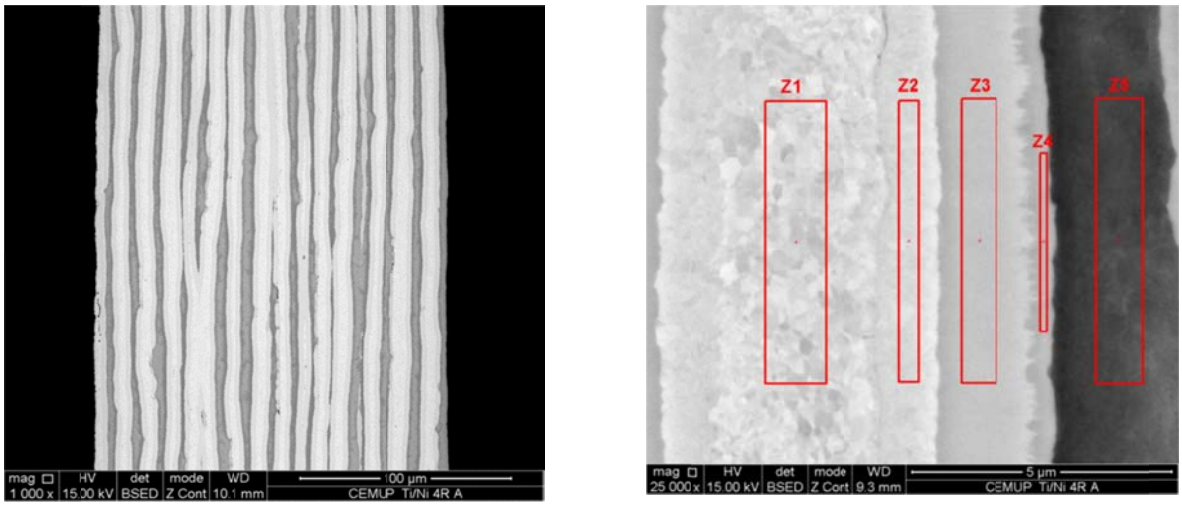

a) b)

Figure 39 - 32 layers of Ni/Ti after 1st intermediate heat treatment, (b) analysed regions of an interface produced during 1st heat treatment

This treatment was done at 627 ºC under 10^{-3} Pa for half an hour on a sample after 4 cycles of R&C (according to figure 34 and table 9 the formation of intermetallic phases is not expected). SEM and EDS evaluations revealed same formation order of phases like what had occurred in DSC tests but there were some differences in terms of voids formation and grain size. As it is illustrated in figure 39-a, number of voids and interfacial cracks have decreased at 627 ºC/30 min in comparison with heating at 726 ºC or 791 ºC in DSC equipment.

Table 14 - EDS results of regions illustrated in figure 39-b in atomic percentages and the phases identification based on the equilibrium diagram

Regions	Ni-at%	Ti-at%	Ratio of Ni/Ti	Equivalences
Z1	96.66	3.34	28.94	Ni
Z2	72.27	27.73	2.61	$TiNi_3$ + TiNi
Z3	51.40	48.60	1.06	TiNi
Z4	32.53	67.47	0.48	Ti_2Ni + TiNi
Z5	4.79	95.21	0.05	Ti_2Ni + Ti

If volume interaction effect of the EDS is considered, the phase identification of the regions illustrated in figure 39-b, obtained from the atomic percentages presented in table 14, will be pure Ni for Z1, $TiNi_3$ for Z2, TiNi for Z3, Ti_2Ni for Z4 and pure Ti for Z5. It is also curious that grain structure is seen only in pure nickel and $TiNi_3$. If this image is compared with figure 27, the recrystallization of grains during annealing is easily recognized, they have turned to equiaxed grains but they are still in ultra-fine scale. The following conclusions could be made from the comparison of previous treatments;

- Effect of temperature on the formation of diffusion products is greater than the effect of time, i.e. formation of greater amounts of voids and intermetallic phases, more TiNi, are seen at higher temperatures which shows the direct proportion of diffusion with increase of temperature;
- By comparing the Ni grains of DSC samples, figure 40-b, with heat treated samples, figure 40-a, it is revealed that temperature has also more effect on recrystallization kinetics than time; DSC samples were heated at higher temperature with much smaller soaking time;
- Possibility of elimination of $TiNi_3$ is greater in higher temperatures due to higher diffusibility of Ti than Ni;
- Grain size of $TiNi_3$ phase is similar to the nickel grains, the grain size in the other phases is not visible and visible grains have maintained ultrafine sizes.

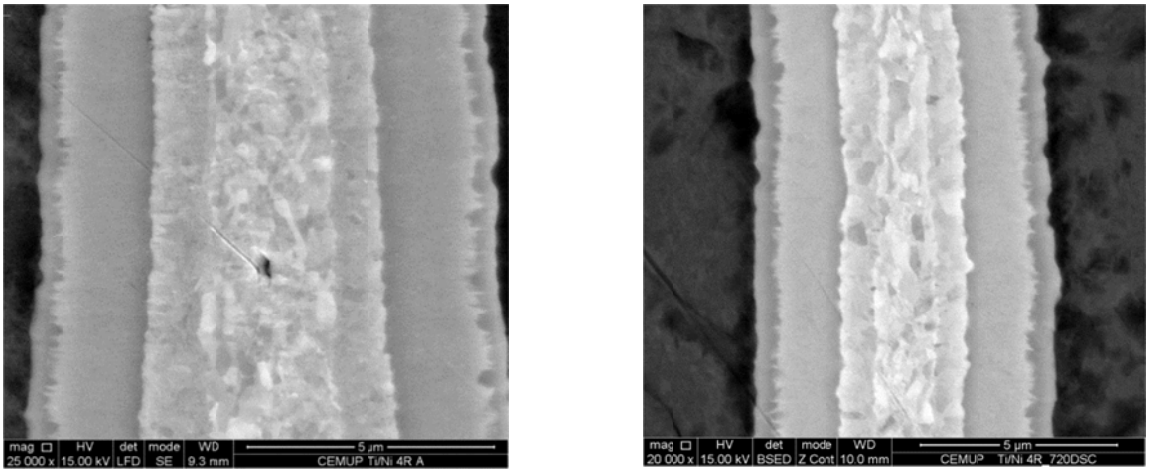

a) b)

Figure 40 – (a) Secondary electron mode image reveals the grain structure of the pure nickel and $TiNi_3$ annealed at 627 ºC/30 min, (b) same grain structures in a DSC sample heated up to 726 ºC

Investigation on samples processed by further deformations revealed that the increase of deformation through more rolling and cutting cycles, 6 more cycles of R&C, on the samples that have already been rolled for 4 cycles and experienced one intermediate heat treating would provide the following effects on the microstructure;

- Non-uniform thickness reduction of layers is observed more than the time they had been rolled without using intermediate heat treatments;
- Intermetallic phases have tolerated less deformation, experienced localized necking and appeared in fragments; as it is illustrated in figure 41, failure is observed in $TiNi_3$ as transverse cracks;
- Ni grains have maintained the equiaxed form and they have not been refined anymore.

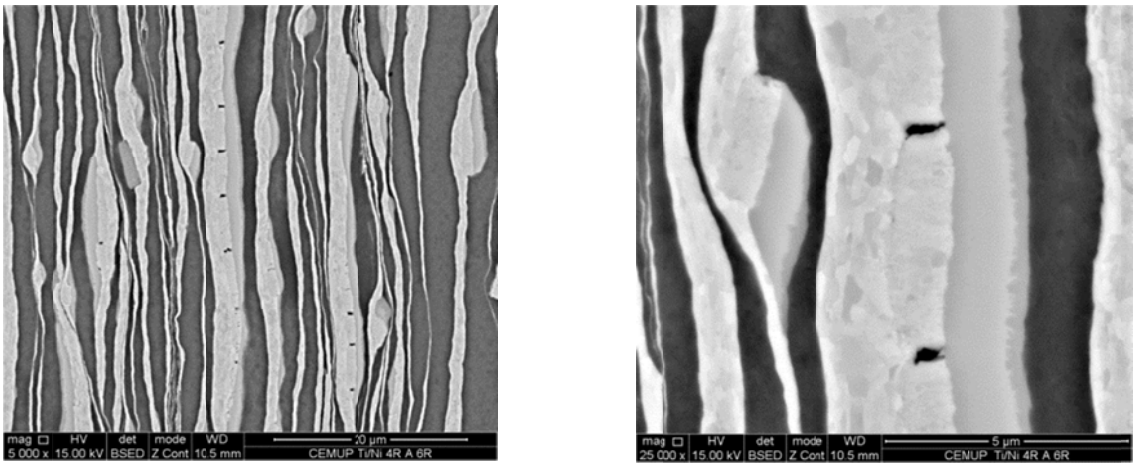

a) b)

Figure 41 – (a) nonuniform deformation after introducing 7.25 strain and crack formation, (b) equiaxed Ni grains and fragments of intermetallic phases

4.7.3 Second intermediate heat treatment

After first intermediate heat treatment of 4 cycles rolled sample, the ARB process was continued until 10 cycles, i.e. 6 more cycles. The machine did not stop during rolling but it seemed that edge cracks were becoming severed so the second intermediate annealing was done again knowingly at 627 ºC.

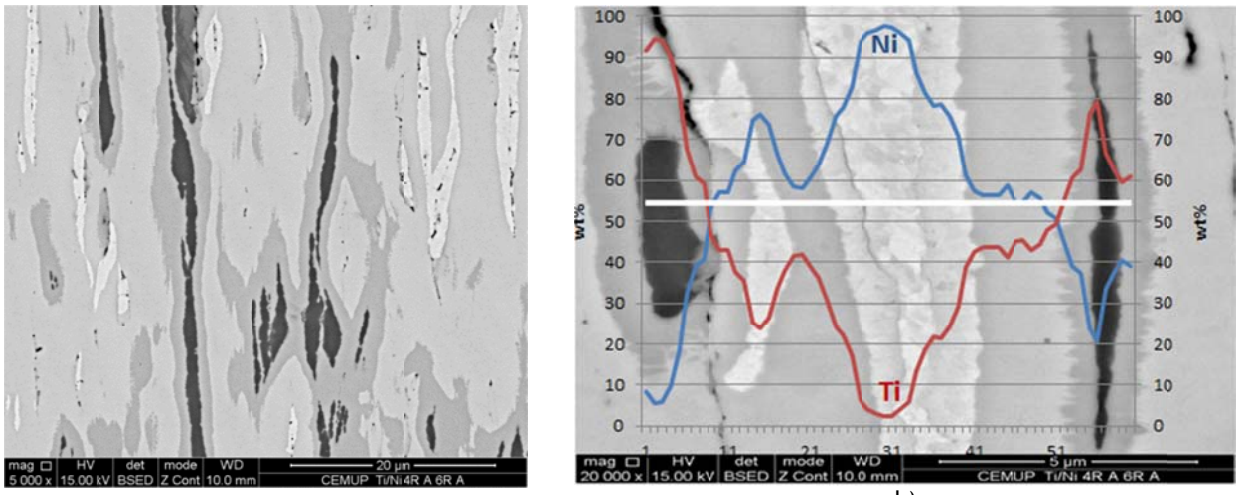

a) b)

Figure 42 – (a) Distribution of intermetallic phases and presence of voids and interfacial cracks, (b) variation of chemical composition between two Ti sites

Microstructural observations revealed that no lamellar structure is observed after second intermediate heat treatment. This indicates the progress of diffusion process. As it is illustrated in figure 42-a; Kirkendall voids and interfacial cracks exist in the structure as the products of diffusion process. Cracks are mainly located along the elongated nickel regions. Those cracks might have been resulted from the difference between the thermal expansion coefficients of Ni, Ti and intermetallic compounds as well. SEM/EDS evaluations confirmed the presence of the five phases had already presented in previous experiments, the graph adapted on figure 42-b depicts the variation of chemical composition along a line with the length of 9.46 µm between two Ti sites. Those oscillations indicate the need of greater diffusion time to find a complete matrix of TiNi phase. After second intermediate annealing the sample was cleaned by acetone and rolled but in the earliest time of rolling, it exploded. A blue and yellow sparkle was seen between the roll mills and it broke into small particles. This could be justified through the work hardening of the alloy that promotes the crack formation which enhances the Ti oxidation creating hot spots in the system. These points can provide sufficient heat to induce exothermic mixing reaction between Ni and Ti [18]. However, OM images from exploded sample shows no differences in microstructure after explosion (figure 43).

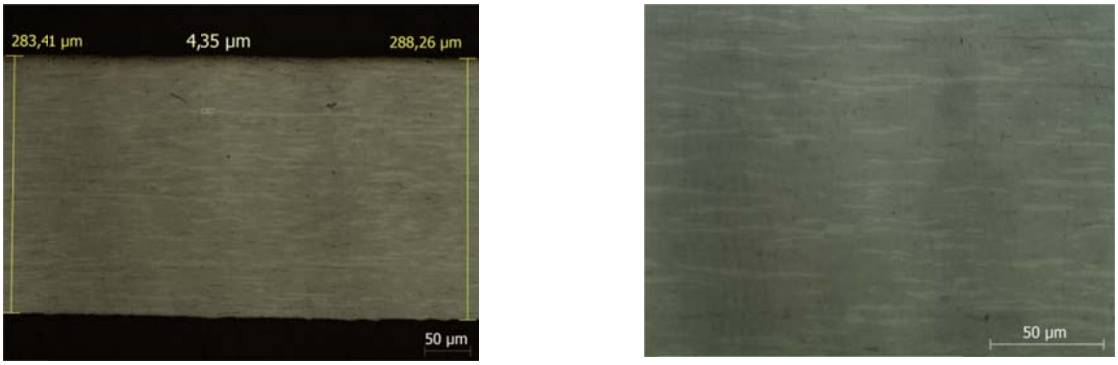

a) b)

Figure 43 - OM images from exploded sample

4.7.4 Evaluation of phase formation at the interface of the 1st joint produced by DB

Materials: Ti6Al4V, Ti/Ni multilayer foil fabricated by 10 cycles ARB and Nitinol alloy

Joining conditions: 800 ºC (10 ºC/min) /10 MPa/60 min

Different techniques such as OM, SEM and EDS were applied to evaluate the phase's formation during the DB. Results of SEM are presented in Figures 44 and figure 46 plus table 15. Global analysis of the foil was obtained by EDS. It determined the chemical composition of Ti-50.71At%Ni for that interlayer.

According to the observations seen in figure 44 and the results presented in table 15, the following conclusions could be made;

- Laminar structure of the multilayer foil has been completely eliminated;
- No pure Ti and pure Ni zones have left in the evaluated zones and TiNi, Ti_2Ni and $TiNi_3$ have formed within the interlayer ;
- Small amounts of voids and interfacial cracks have formed during the process in comparison with applying intermediate heat treatments on the foils;
- Some voids are observed at the interface of multilayer and nitinol substrate while no void was observed at the other interface;
- At the interface of interlayer and Ti alloy; Ti_2Ni has formed than $TiNi_3$ because $D^{Ti}_{Ti6Al4V}$ is greater than $D^{Ni}_{Ti6Al4V}$;

According to the results of table 15; thick layer of Ti_2Ni has formed between the interlayer and Ti6Al4V while very thin layer of an intermetallic exists at the interface of the interlayer and nitinol. This resulted from the grater diffusion coefficients of Ni and Ti in Ti6Al4V than in nitinol, as already discussed.

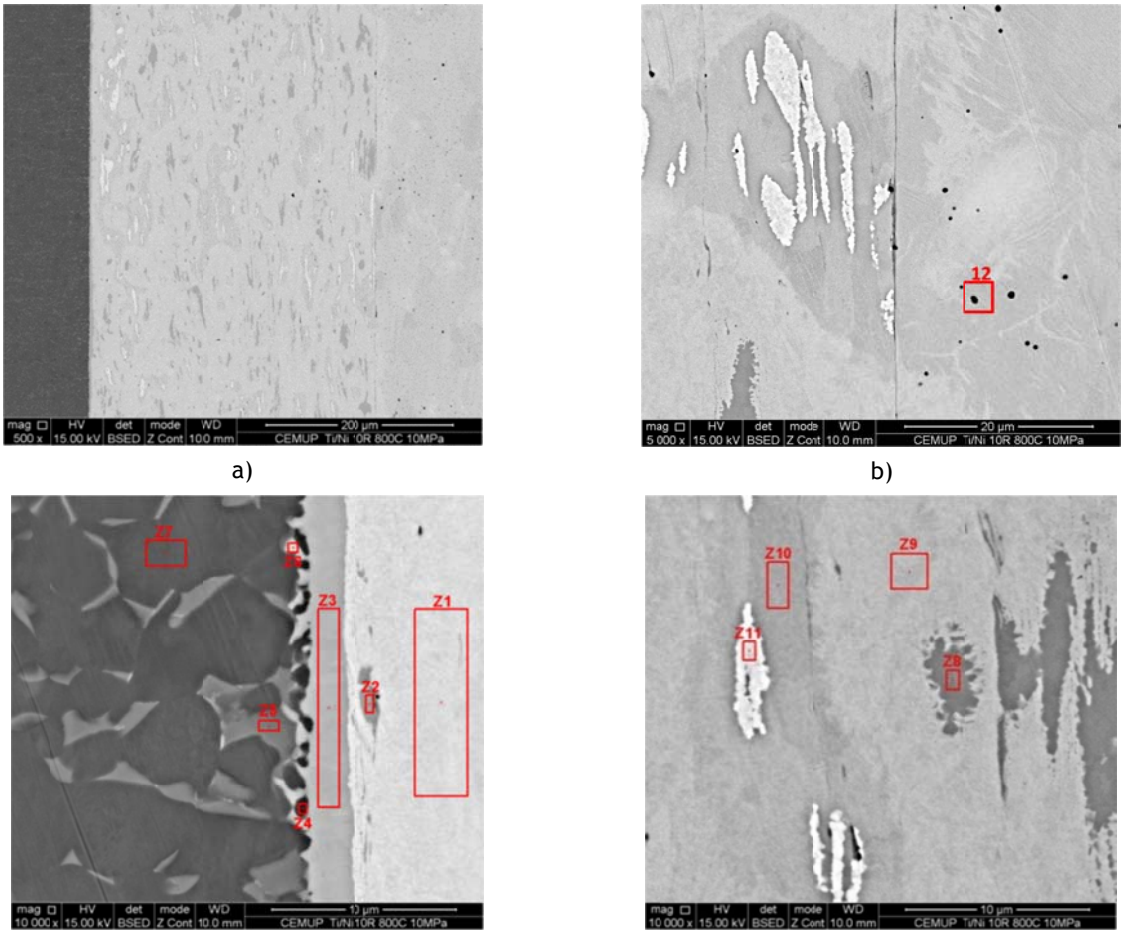

a) b)

c) d)

Figure 44 – (a) Phases distribution in the interlayer used in joint, (b) interface of the nitinol base metal and interlayer, (c) interface of the interlayer and Ti6Al4V and (d) intermetallic phases formed during the diffusion process plus the Ti-rich zone in the base nitinol, Z12. The composition of the phases marked are given in table 15

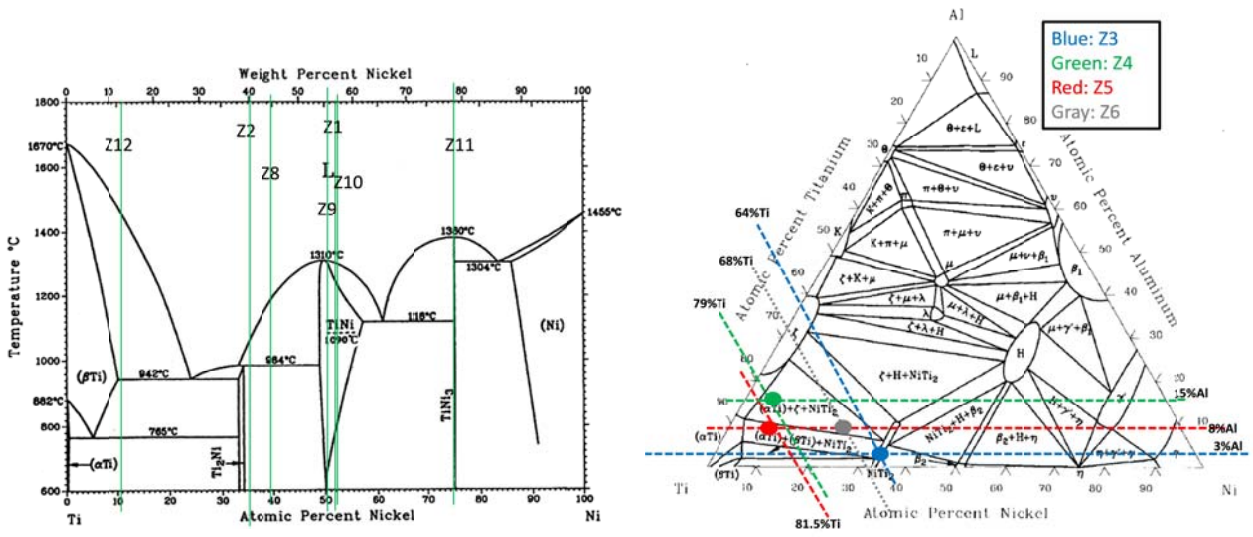

a) b)

Figure 45 – (a) Binary and (b) ternary equilibrium, at 800 °C, diagrams used in phase identification [16, 43]

Table 15 – EDS results and phase identification of Z1 to Z12 illustrated in figure 44 using diagrams of figure 45

Zones	Ni-At%	Ti-At%	Al-At%	V-At%	Ratio of Ni/Ti	Equivalences of the identified phases
Z1	51.21	48.79	-	-	1.05	TiNi
Z2	34.96	65.03	-	-	0.54	Ti_2Ni + (TiNi)
Z3	32.75	63.91	3.34	-	-	Ti_2Ni
Z4	5.85	79.35	14.81	-	-	(α) + ζ + (Ti_2Ni)
Z5	10.48	81.35	8.17	-	-	(α + β)+ ζ + (Ti_2Ni)
Z6	24.46	67.70	7.84	-	-	(α)+ ζ + (Ti_2Ni)
Z7	1.16	89.73	7.38	1.74	-	α -Ti6Al4V**
Z8	36.88	63.12	-	-	0.75	Ti_2Ni + (TiNi)
Z9	50.61	49.39	-	-	1.02	TiNi
Z10	51.81	48.19	-	-	1.07	TiNi
Z11	74.83	25.17	-	-	2.97	$TiNi_3$
Z12	10.74	89.26	-	-	0.12	Ti + (Ti_2Ni)

*Phases indicated between the parenthesis are not observed in the SEM images but they have been appeared in the EDS results due to the interaction Volume.

**According to binary phase diagram of Ti-V [16],V is solid soluble in alfa phase upto almost 2 at% while zone 7 is most abundant in the image.

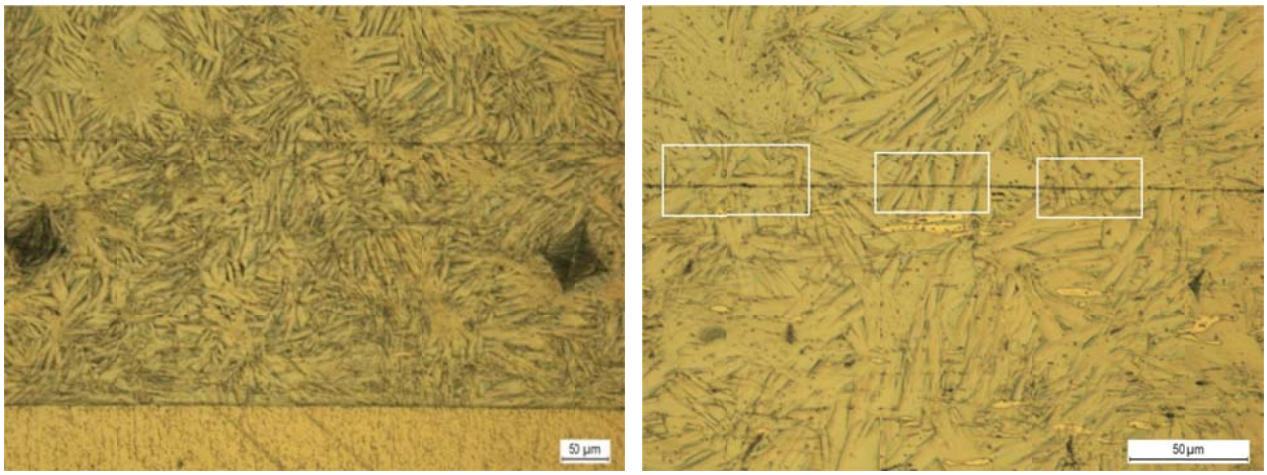

a) b)

Figure 46 – OM images of the first joint (a) HV indentation effects and two visible interfaces, (b) epitaxial growth of the martensite needles between nitinol and interlayer

In comparison with intermediate heat treatments, Kirkendall voids have decreased due to high temperature [14] resulting in promoting the movements of atoms and vacancy mechanism, i.e. diffusion growth. In comparison with DSC test specimen, voids have considerably decreased that might be the result of applying pressure during process [31].The promotion of diffusion process due to higher temperature and giving time have transformed all constituents to the intermetallic phases but two unwanted intermediate phases (Ti_2Ni and

$TiNi_3$) still exist. In comparison with the results of second intermediate heat treatment the amount of $TiNi_3$ has considerably decreased due to the associated effect of high diffusion coefficient of Ti in intermetallic, high temperature and greater soaking time. OM images were taken by etching the samples after SEM (figure 46). Martensitic needles in the interlayer are thinner than those of the substrate. It is easily recognized that the growth of martensite blades are epitaxial, i.e. atoms of the surface of the interlayer have followed the orientation and order of the atoms of the surface of the substrate which gives the morphology observed in those images. This is not observed at other interfaces that does not have equal crystallographic sites [2].

4.7.5 Evaluation of phase formation at the interface of the 2nd joint produced by DB

Materials: Ti6Al4V, Ti/Ni multilayer foil fabricated by 10 cycles ARB and Nitinol alloy

Joining conditions: 700 ºC (10 ºC/min) /10 MPa/60 min

For this experiment no EDS analysis was done because it is obvious that the phase evolution will follow the former discussions. Microstructural characterization, figures 47 and 48, revealed results similar to first joint except the differences that will be explained in the following;

- Almost sound joint was obtained;
- Some pure Ni and Ti regions exist in the structure;
- Pure Ni grains are larger than previous tests;
- Large cracks, 120 µm, to very small ones are distributed along the phases;
- No laminar structure is seen in the cross section of the joint but intermetallic phases are elongated;
- It seems that greater amount of $TiNi_3$ exist in the microstructure in comparison with the first joint;
- A thinner interdiffusion layer is seen at the interface of Ti6Al4V and interlayer than the first joint;
- Some voids are present at the interface of interlayer and nitinol;
- Global analysis indicates the chemical composition of Ti-49.9 at%Ni.

According to the discussions presented in section 4.6; lower temperature has preserved some unreacted constituents in the structure of the joint. As it was seen in figure 47-d, Ni grains have grown due to the process temperature and soaking time. As those grains had already transformed to ultrafine sizes due to the severe plastic deformation, they could have been

recrystallized at lower temperatures than normal pure Ni due to having high levels of strain energy.

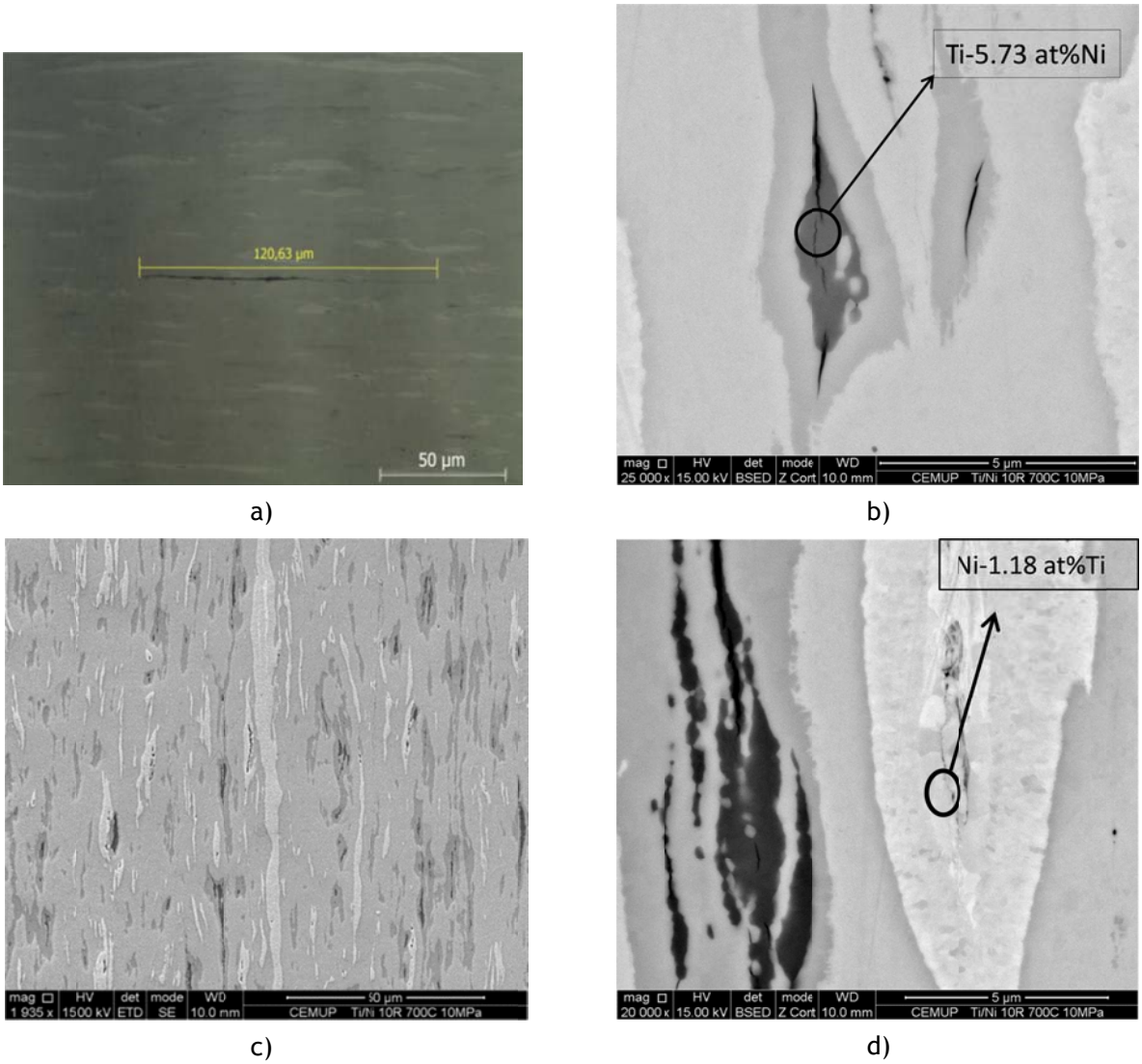

Figure 47 – (a) Large microcrack in the OM image, (b) interfacial cracks in the pure Ti region, (c) phase distribution within the interlayer between two substrates and (d) recrystalized Ni grains and the onset of Kirkendall voids in the Ni site

As it was seen in figure 47-c, intermetallic phases are observed a bit elongated due to lack of diffusion and consequently smaller amount TiNi intermediate phase has formed. The amount of $TiNi_3$ in comparison with the first joint is high because temperature has been low and diffusion coefficients are smaller than the first conditions. According to same justification presented in the results of the first joint, the interdiffusion layer at the interface of the Ti/Ni multilayer and Ti6Al4V is thicker than that of nitinol and multilayer. The intermetallic layer

observed in figure 48 is smaller than that of first joint due to lower temperature which reduces the diffusion rate.

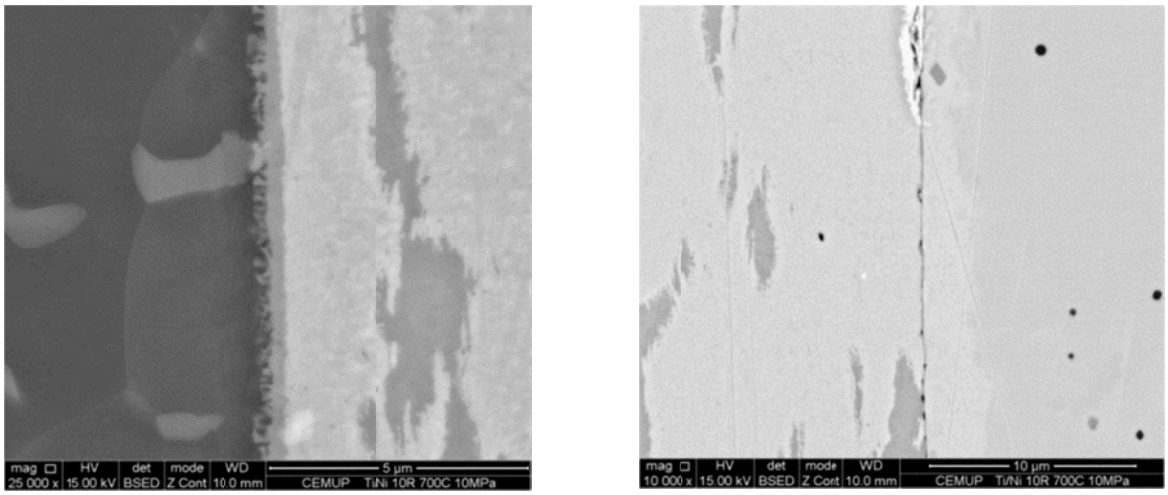

a) b)

Figure 48 – Comparison of interdiffusion layer between Ti/Ni multilayer and the two substrates (a) Ti6Al4V alloy and (b) nitinol

Cracks do not seem to be Kirkendall voids due to their morphology, sharp tips, and for applying the pressure during the process. They could have already existed in the microstructure as delamination, due to lack of bonding strength between the layers, or interfacial cracks resulted from the difference of thermal expansion coefficient of Ti and Ni or brittleness of the surrounding phase. This problem was not seen in the first joint because the interlayers used in the diffusion bonding process were not from the same batch.

Same explanations as brought for the metallography test of the 1st joint are acceptable here for images of figure 49.

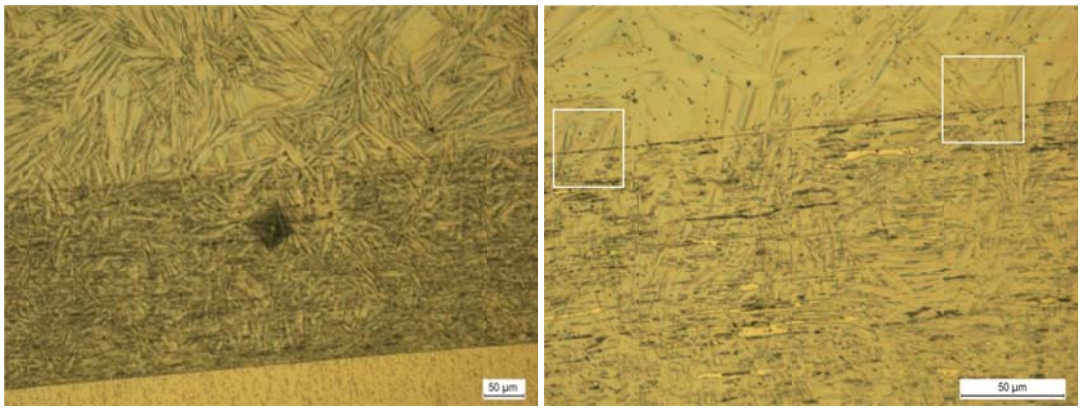

Figure 49 - OM images of the second joint (a) HV indentation effects and two visible interfaces, (b) epitaxial growth in the martensite needles between substrate and interlayer

4.7.6 Effect of 3h dwell time on the microstructure of the joined zone

Materials: Ti6Al4V, Ti/Ni multilayer foil fabricated by 10 cycles ARB and Nitinol alloy

Joining conditions: 700 ºC (10 ºC/min) /10 MPa/180 min

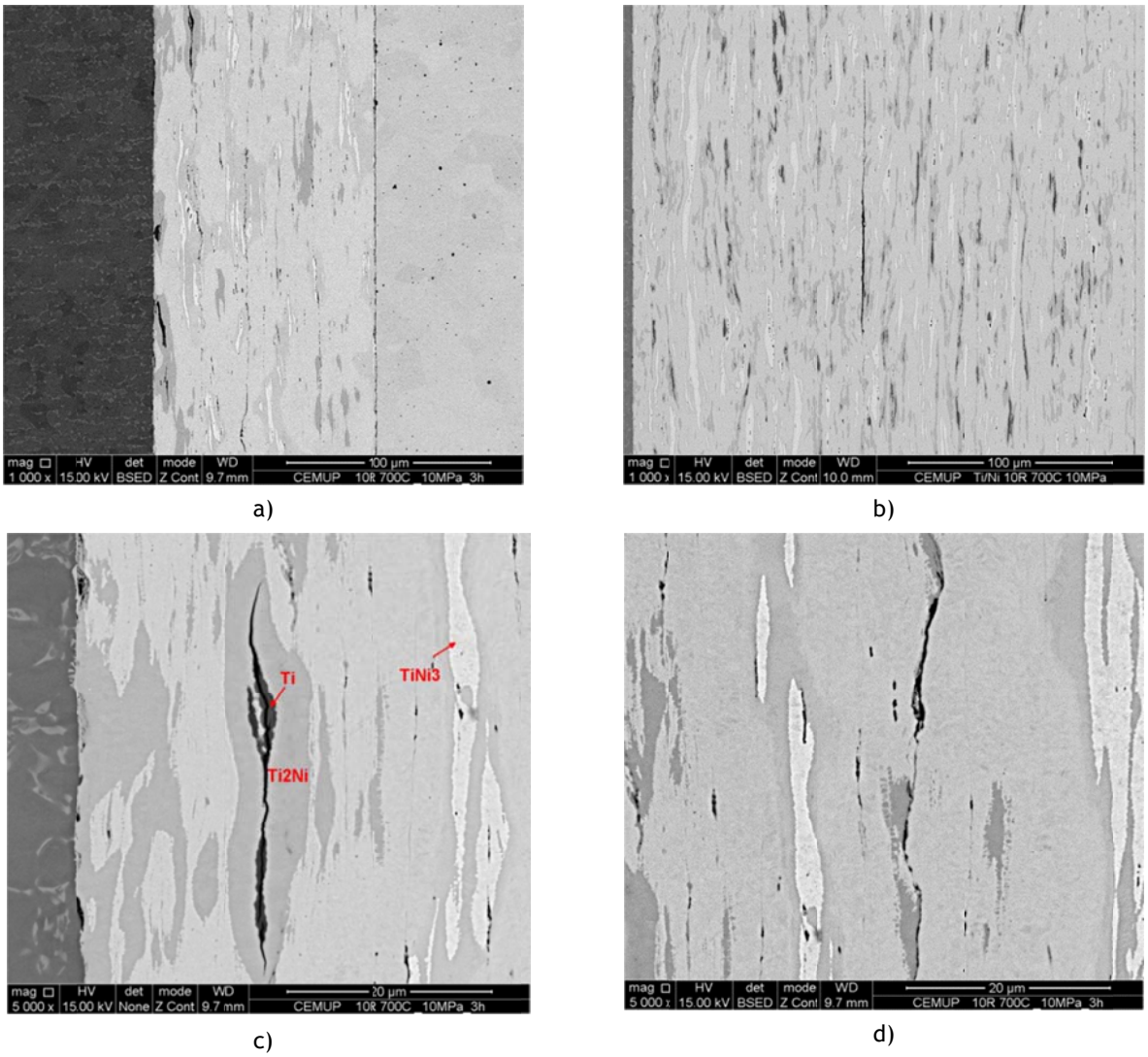

a) b) c) d)

Figure 50 – Diffusion bonded regions heated at 700 ºC under 10 MPa pressure for (a) 3 hours and (b) 1 hour and (c, d) Interfacial cracks observed along the layers with 3 hours.

As it is illustrated in figure 50-a&b, the comparison between two different soaking time reveal that the greater time has promoted the diffusion of the constituents, i.e. no pure nickel region was found in the investigated regions and it seems that the amount of $TiNi_3$ has decreased. It is also observed that the amount of interfacial cracks in the interlayer is greater than in the previous experiment. OM observations of the as-rolled foil used in the present joint showed that there have already been some delaminated regions between the Ni/Ti layers and the number of them has grown after heating due to the difference of thermal

expansion coefficients of the constituents. As it is recognized from the figures, the interlayers have different thicknesses, in comparison with previous experiments the interlayer in thinner. Such differences occurred due to the short time of performing this master thesis and having no foil from same batch while they all have experienced 10 cycles of R&C but the present foil has suffered greater strain. This problem has happened because during the ARB the roll mills get hot and hotter by passing time and it provides greater deformation. Therefore, the foil could have become harder than the previous conditions so same surface preparation conditions (600 mesh grinding paper) has not been enough to produce required scratches on the surface of the foil to establish good diffusion bonding. EDS also identified the global analysis of Ti-50.15 at%Ni for the interlayer as well as the presence of some pure Ti regions. As it is seen in figure 50-c, a crack exists in this titanium region. This sort of crack is only observed in Ti-rich regions, another example was illustrated in figure 47-b. They might have been resulted from the brittleness of surrounding phases, Ti_2Ni. OM characterization of the samples revealed the epitaxial growth at the interface of nitinol and interlayer and it seems that martensitic needles have turned thicker due to greater diffusion time.

4.7.7 Effect of higher levels of strain on phase evolution

Materials: Ti6Al4V, Ti/Ni multilayer foil fabricated by 15 cycles ARB and Nitinol alloy

Joining conditions: 800 ºC (10 ºC/min) /10 MPa/60 min

Another joining experience was done with a multilayer foil that had experienced strain of 11.55 with the minimum average layer thickness of 10 nm. SEM investigations, figure 51, revealed that phase's distributions are more uniform than the first joint, 10 cycles. No pure Ni and Ti were found. Ti_2Ni and $TiNi_3$ phases have decreased, especially in the thinner region of the foil. EDS results identified the Ni-rich- TiNi phase for the matrix of the microstructure. That foil is hard and also brittle and same surface preparation like the first joint has been done on it. Observation (figure 52) show that a good joint was not obtained probably due to improper scratches on the faying surface. It has caused less mechanical deformation and less contact area between those surfaces. Another consequent of harder interlayer might be higher sensitivity to the presence of stress concentration factors which can explain the occurrence of cracks, as it is seen in figure 52-b. Needle like morphology observed in figure 52-a is the result of burned Ti6Al4V sample during cutting process before joining. It was used due to time limitations. It was proved by OM images as illustrated in figure 53-b.

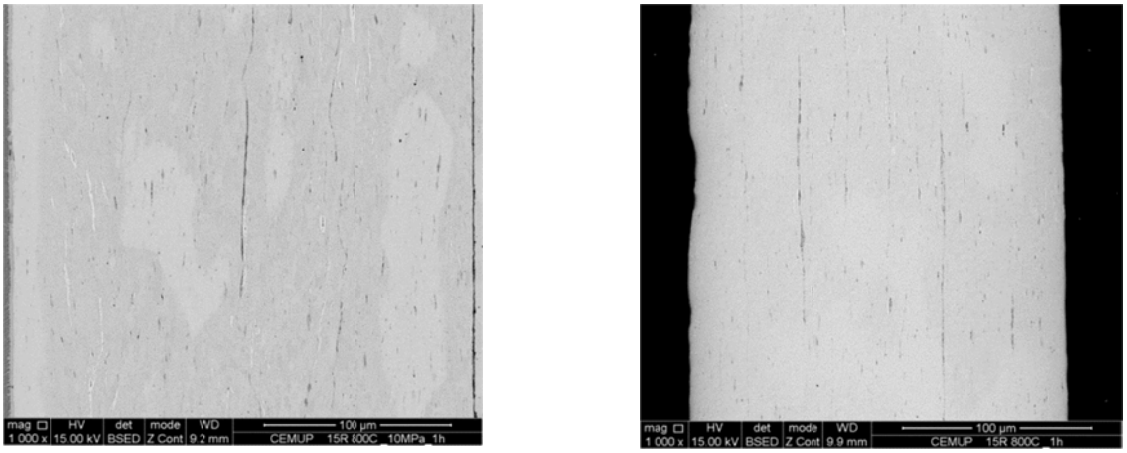

a) b)

Figure 51 - Phase distribution in the interlayer at (a) thicker and (b) thinner sections

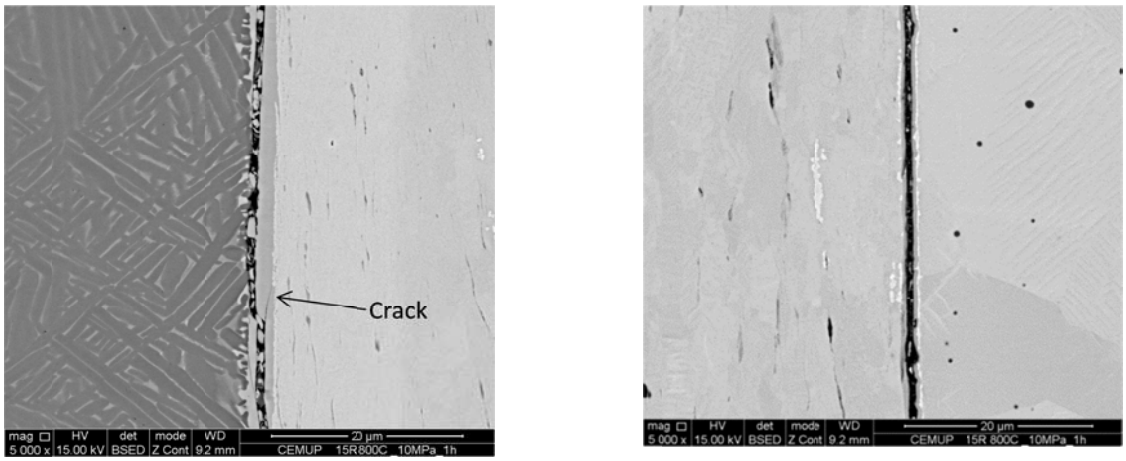

a) b)

Figure 52 – (a) Interdiffusion region between Ti6Al4V and multilayer and (b) unbound region and concentration of Ni at the interface of nitinol and multilayer

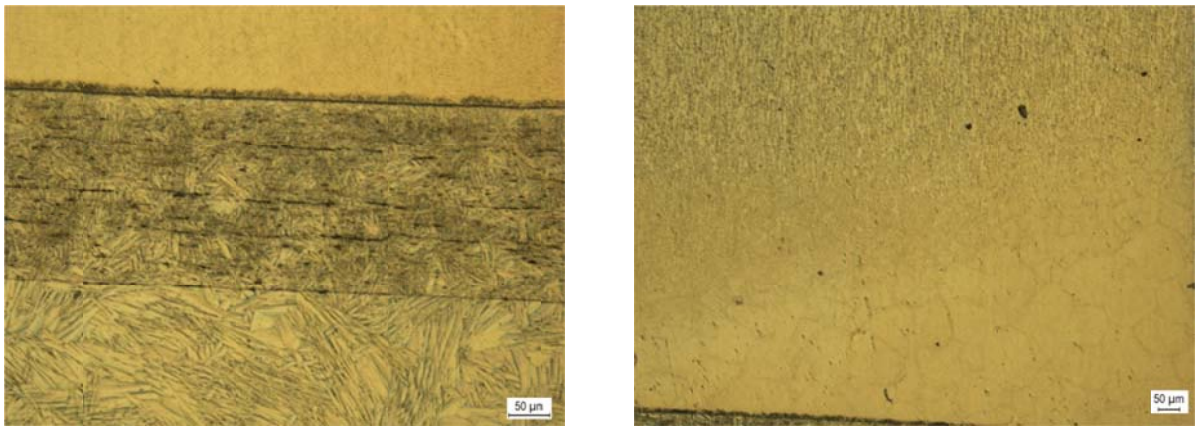

a) b)

Figure 53 – OM images of the joint interface showing (a) epitaxial growth, cracks and (b) burnt part of the substrate.

4.8 EBSD test of the interlayer of 15 cycled R&C for the joint at 800 °C/10 MPa/1h

Crystallographic information of a surface in the depth of almost 50 nm is revealed by electron backscatter diffraction technique. Phases present in the evaluated surface are identified by the indexation of the Kikuchi patterns obtained by EBSD. Unlike SEM and EDS, samples are placed in an angle of 70° with horizontal for EBSD [36]. According to the data extracted from the software of the equipment, 91% of the total length of the grain boundaries of the selected area are high angle which are illustrated as blue lines in figure 54-a. The average grain size of that area is 1.04 μm which means that grains have lost their nano size. It is obvious that both the reaction between the atoms of the nano laminated layers and the heat introduced through joining process have caused the formation of new grains that have had enough time to grow. As it is seen in figure 54-b; most grains are blue or green; as each color specifies a crystallographic orientation so it is depicted that the interlayer has a weak texture. They have formed with a preferential crystallographic orientation because they nucleated between or within nanolayers and the energy along the layers has influenced the direction of the growth.

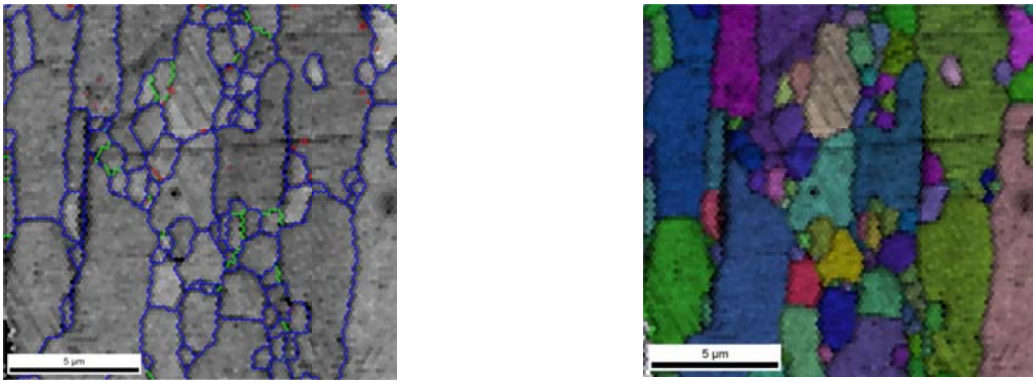

a) b)

Figure 54 – (a) Rotation angle of the grain boundaries, (b) grain orientations indicated by color

4.9 Mechanical properties of the fabricated foils and joints

As it was mentioned before, deformation influences the mechanical properties of the processed material through strain hardening caused by dislocations behavior, i.e. high levels of deformation provides the accumulation of dislocations behind grain boundaries and their movement becomes difficult thus strengthening the material [23]. In this work, due to time and material restrictions, work hardening of the fabricated composite was not traced by performing tensile test and it was controlled by hardness tests. Microhardness measurements were done by different loads such as 0.01, 0.05 and 0.1 Kgf. All the results are presented in

appendix I but in the following those which was good traceable will be used to discuss and characterize the mechanical properties of the fabricated products. As it is illustrated in figure 55 the measurements were done across the transverse cross section of the selected samples to follow the distribution of hardness in those sections and to see how strain has introduced to the foils in terms of distance from the roll mills surface. Results are presented in figures 56 and 57. As it was told before, two approaches were considered to produce ultrafine laminated composite of Ni and Ti. The first one used intermediate heat treatments to decrease the strength of the foil that the available rolling machine could continue the process and formation of edge cracks delayed. The second one was reducing the dimensions of the rolled foils to provide enough pressure because the amount of force introduced by the machine was constant. The graphs presented in figure 56 depicts that deformation is not completely homogeneous on cross sections of the samples.

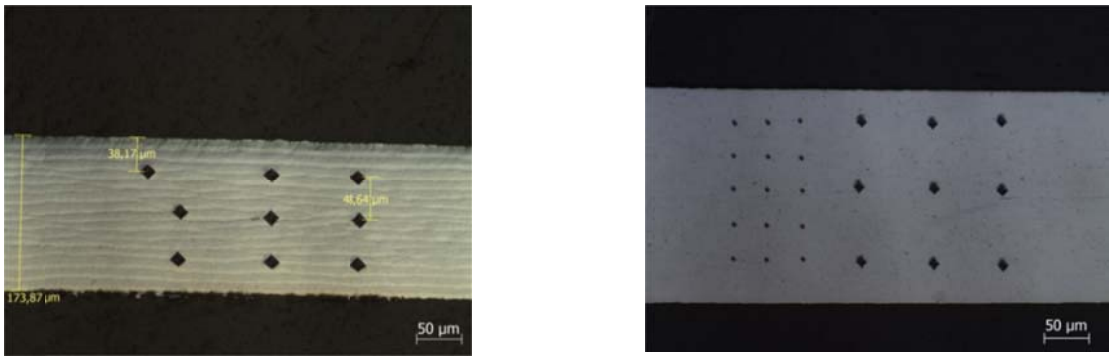

a) b)

Figure 55 - Indentation on cross sections of multilayers (a) after 4 cycles and (b) after 15 cycles

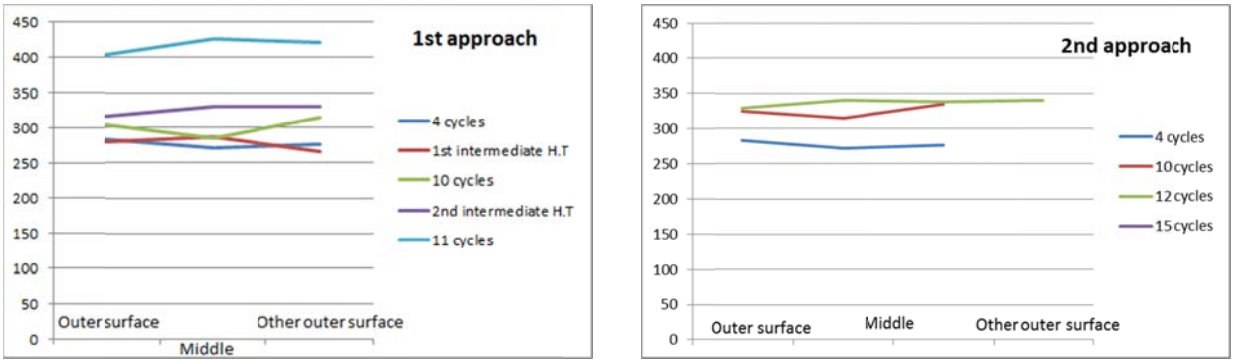

a) b)

Figure 56 - Hardness distributions across the transverse cross section during ARB process (a) 1st approach used intermediate heat treatments and (b) samples in 2nd approach are as-rolled

The results of microhardness measurements presented in figure 57-b show the hardness growth of the fabricated foil by increasing the deformation level. The first approach, with intermediate annealing, has enhanced the hardness as well, i.e. applying high temperature leads to the formation of intermetallic phases in the microstructure which partially compensates the softening effect of the annealing. This explains why the hardness values of as-rolled batch and heat treated samples of that batch are similar, figure 57-a.

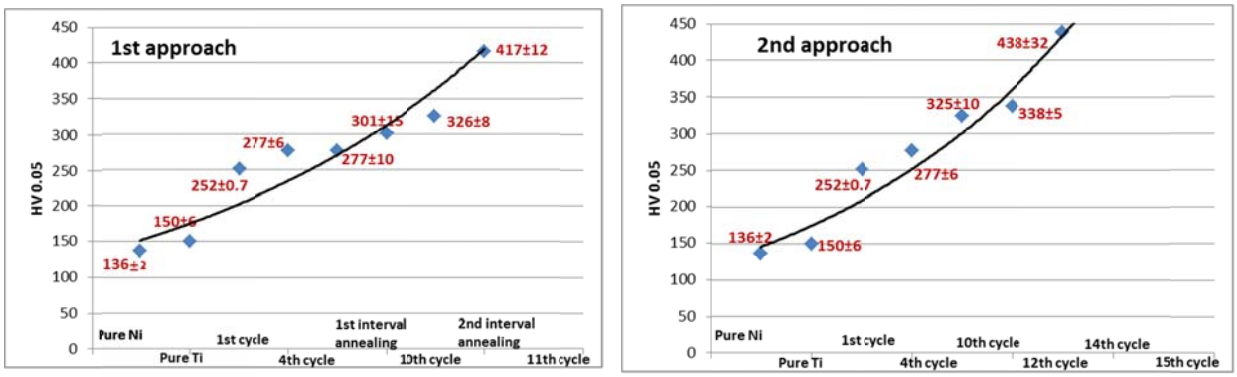

a) b)

Figure 57 - Effects of phase evolution and strain hardening on the fabricated foils produced by using intermediate heat treatments (a) and dimension reduction approach (b)

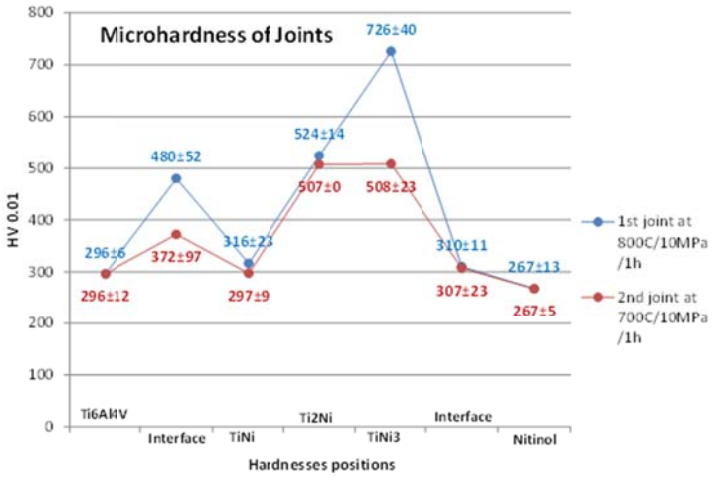

Figure 58 - microhardness of the intermetallic phases plus interfaces of the joint at 800 °C/1h (blue line) and 700 °C/1h (red line)

After identification of the phases formed in the interlayer of the joint it was possible to measure their hardness and compare the effect of different joining temperatures on them, as well as, on the interfaces between the base metals and interlayer (figure 58). The effects of hardness indentations done in the first joint are illustrated in figure 59-a. Data presented in figure 58 reveal the following results;

- No crack formed during the measurement in the indentation section;
- The interface between Ti6Al4V and the interlayer shows a greater value in the first joint because it is thicker due to higher temperature and greater diffusion of Ti and Ni to form Ti_2Ni; the value of the second joint had been influenced by the adjacent phases;
- The values of TiNi and Ti_2Ni phases in both joints are similar;
- $TiNi_3$ of the second joint has smaller value due to embedding pure Ni grains, as seen in figure 47-d;
- Interface of nitinol substrate and interlayer shows same hardness values.

The effect of different joining temperatures was also evaluated by macrohardness with the smallest load; 1kgf. Figure 59-b illustrates the results of that measurement adapted on the image of the joint obtained by SEM. Grain sizes also are observed in that picture; nitinol has larger grains than Ti6Al4V. The reasons for having greater hardness for the interlayer joined at lower temperature could be;

- The amount of unwanted intermetallic phases formed at lower temperature; the more the $TiNi_3$ and Ti_2Ni (harder phases, see figure 58), the greater the hardness value;
- Needles of martensite formed at lower temperature are thinner than those formed at higher temperature.

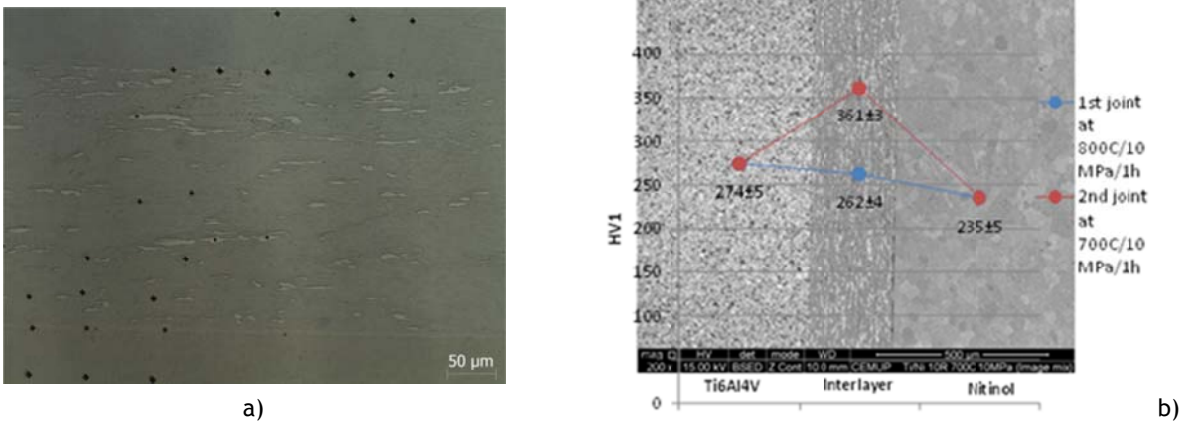

a) b)

Figure 59 - (a) Order of hardness indentations on the cross section of the 1st joint obtained by OM, (b) values of the macrohardness accompanied with SEM image at low magnification

Macroscopic hardness measurement was not performed on bonded areas using interlayers of 10 cycles and 15 cycles joined at 700 °C/3h and 800 °C/1h, respectively, because they contained small cracks along the cross section that affected the measured hardness values.

Chapter five: conclusions and suggestions

It is possible to classify the conclusions of this research work as the followings;

5.1 deformation process

Roll bonding is greatly influenced by the primary surface scratches and cleanliness of the surface. Better results obtained by grinding papers with 600 and 1000 mesh for Ti and Ni, respectively;

Deterioration of the roll bonding occurs due to any stop during multilayer fabrication;

A little fragmentation of Ni and Ti has formed in the multilayer during the ARB process;

Thickness reduction is not uniform and layers are fluctuated;

High strain rate does not deteriorate the ARB process in the case of Ni/Ti system;

Increase of the number of cutting and rolling cycles improves the bonding and reduction process, i.e. the greater the number of passes, the lower the amount of delamination;

Solid state diffusion has occurred within the layers during ARB and it is promoted by the increase of the number of cycles;

Ultrafine Ni grains form in the layers having thicknesses in micro scale;

Ti/Ni system requires a primary reduction greater than 50% otherwise foils will slide over each other and material loss increases;

Temperature of the roll mills greatly affect both the roll bonding and the thickness reduction of the strip, i.e. the hotter the rollers the better the bonds and the thinner the final foil;

The greater the number of R&C cycles, the harder the multilayer foil;

The higher the strain rate, the sooner the achievement of the ultrafine multilayer foils;

Reducing the dimensions of the foil during the process is less expensive and time consuming than using intermediate heat treatment to decrease the strength of the foil to continue the rolling;

Precautions should be taken during the ARB process due to the probability of foil explosion;

Material loss occurs during ARB process due to formation and separation of brittle chips on the sides of the strip.

Annealed Ni/Ti could tolerate reduction of almost 70% without failure;

Repeating a cycle will improve the bond if any bond has already established;

5.2 Heating processes

Distribution of Kirkendall voids is proportion with the distribution of the deformation and strain across the section of the rolled strip;

Selection of any temperature to do any stress relief should be considered by the results of the DSC test;

Applying pressure decreases the Kirkendall voids;

The higher the annealing temperature, the greater the number of Kirkendall voids;

The higher the temperature, the less the formation of $TiNi_3$ and Ti_2Ni;

The influence of temperature on the phase formation is greater than that of the time;

5.3 Diffusion bonding

Using ultrafine multilayer of Ni and Ti in DB process has decreased the joining temperature of the Ti6Al4V and nitinol alloys, 800 ºC and 700 ºC, close to the half of their melting points, 1660 ºC and 1300 ºC, respectively;

Good joint has been conducted between interlayer and Ti6Al4V while there are some voids between that aid bond and nitinol;

Temperature rise does not greatly influence the joint between the interlayer and the nitinol;

The greater the temperature, the better the joint in the interface of Ti6Al4V;

The temperature of the DB process has increased the grain size of the ultrafine/nano multilayer to the micron scale;

Rising the interval time could compensate the temperature reduction while the quality of the joint could be preserved and more diffusion will provide more TiNi phase;

Using a harder interlayer, foil of greater cycles, might increase the formation of cracks at the joint interface;

Surface scratches on the interlayer greatly influence the DB process so it is better to grind hard foils with 240 mesh grinding paper.

5.4 Crack division

Cracks observed in this work could be classified into the following order;

Delaminated portion of a layer during roll bonding due to the presence of any oxide, inclusion and no surface roughness;

Interfacial cracks caused during heating stages due to the difference of thermal expansion coefficient between Ni and Ti and affecting weak bonded regions;

Cracks caused by the accumulation of Kirkendall voids;

Defect cracks with sharp points caused by the lack of stress release due to the larger thickness of the layer or caused by the brittleness of the phase.

5.5 Ideas of complimentary works to improve the products for prospect jobs

Conducting microhardness on the joint zones of the third and fourth welds;

Avoiding any fluctuation to the primary foils provides better surface preparation and good roll bonded interfaces so it is better to prepare the primary foils by a cutting mould than scissors to obtain a flat strip, it increases the points of contact between each layer;

Applying stress relieving after 10 cycles and 15 cycles at 350 ºC and 300 ºC, respectively, could improve the ductility of the foil that it can face less crack formation during ARB process and could fill the gap between the non-parallel substrates;

Homogenizing treatment in order to reduce the voids, e.g. 40h can provoke the vacancy mechanism and improve the inter diffusivity of nickel and titanium [17].

Applying a primary diffusion bonding could provide uniform deformation for both Ni and Ti in the primary rolling stage and also could reduce the fluctuation of layers;

Specifying the rolling machine during the period of producing multilayer to keep the gap between the roll mills constant;

Providing longer batches to produce longer product so that it would be possible to use more similar interlayer in various conditions of D.B process;

Using wire cut/ diamond cutter than Discotom-Wheels to cut Ti6Al4V alloy to obtain parallel surfaces;

Doing shear tests to evaluate the strength of the bond and the effect of those phases in the strength of the bond;

Heating stage XRD could be useful to determine the effect of the layer thickness on the formation and elimination of any intermetallic phases to reduce the number of SEM evaluations.

It could be possible to apply long interval heat treating on the joined parts to find an interlayer composed of TiNi phase but it would not be cost effective.

It will be possible to exceed 15 cycles of cutting and rolling if longer primary batched are prepared. This approach could eliminate the unwanted intermediate phases and could also lower the temperature of nitinol formation.

Appendices;

Appendix A: thickness calculation of the primary foil

According to equation 1 and the properties of the pure metals presented in table 1 and 3, one mol of equiatomic nitinol weighs for 106.56 g/mol that gives the chemical composition of Ti-55.08%wtNi. To adjust the intended composition the variables are the thicknesses and the purity of the foils. Equations 3 and 4 give the ratio of the thicknesses of the Ti and Ni foils;

Equation (1) *1 mol Nitinol = 1 mol Ni + 1 mol Ti*

Equation (2) *Volume = w*L*t in which w & L are constants so;* $\frac{VNi}{VTi} = \frac{tNi}{tTi}$

Equation (3) $\rho = \frac{m}{V}$ *so according to the above equation;* $\frac{VNi}{VTi} = \frac{mNi*\rho Ti}{mTi*\rho Ni} = 0.62$

Equation (4) $\frac{tNi}{tTi} = 0.62\,\frac{Purity\ of\ Ni}{Purity\ of\ Ti}$

The purity of the constituents is not 100% so the ratio of 0.62 is affected through equation 4. *Goodfellow Cambridge Ltd* was considered as the material supplier which presents required data in its website. The thickness of one foil is calculated according to the other foil's thickness through equation 4.

Appendix B: surface preparation

It is important to avoid the presence of any impurities and inclusions within the multilayer foils and joints. There are two types of surface preparation in this work plus a vital precaution that should be implied.

The process is ARB so an acceptable surface roughness is needed to establish a good joint between the alternated metallic layers, the reasons will be explained in the discussion chapter. On the other hand, titanium is very prone to oxidize and it is required to remove the impure layer from the foil surface otherwise no bond will occur. Grinding the cut edges might be useful to decrease the probability of severe edge cracking. Before grinding, both metals are cleaned by a cotton tissue and acetone then dried to remove the finger prints. Silicon carbide grinding papers with 1000 and 600 mesh were used for nickel and titanium strips, respectively. Afterwards, they are to be cleaned like before or by ultrasonic in acetone and then they must be processed immediately.

It is also required to grind both the surface of the joining substrates and the multilayer foil by 600 mesh silicon carbide grinding papers, respectively, and then they are to be cleaned in acetone through ultrasonic.

Not only were the input materials to be cleaned and degreased by acetone but also the working table, any applied tools and any equipment utilized for both preparations and fabrication purposes plus the operators` hands should be clean. Surfaces of the rolling mills should be cleaned and degreased before and during the rolling process especially when the mills get hot. Blades of the scissors, tips of the pliers and caliper blades must be cleaned by acetone as well.

Insisting on grinding the surface is not only to remove the superficial oxide layers but also it can introduce some defects to the surface such as dislocation because it is a mechanical work. Thereby, the probability of the atomic diffusion at the interfaces increases during roll bonding process.

Appendix C: Strain rate during ARB [28]

Speed of the roll mills = 20 rpm = 1/3 per second

Circumference of the mill = 225 mm => r = 35.8 mm OA

Primary thickness = 0.325 mm

Thickness after rolling = 0.23mm to 0.09mm gives an average of 0.16 mm

Circumferential roll velocity = (1/3)*225 = 75 mm/s

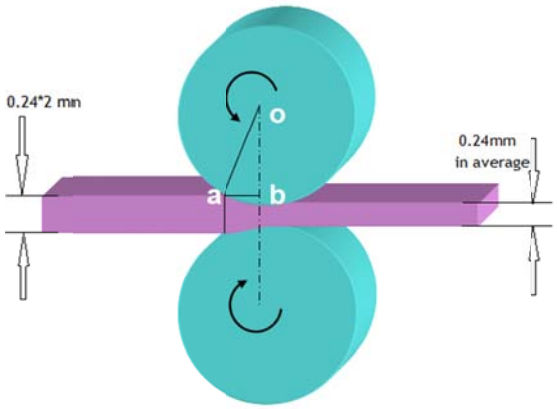

Figure 60 - position of the foil between the roll mills before and after rolling [28]

IN rectangular OAB: OB = OA – (final thickness/2) = 35.8 – (0.0.24/2) = 35.68 mm

OA2 = OB2 + AB2 => AB = $\sqrt{35.8^2 - 35.68^2}$ = 2.93 mm = $length\ of\ the\ strip\ passed$

Time of deformation = $\frac{length\ of\ the\ strip\ passed}{circumferential\ roll\ velocity}$ = $\frac{2.93}{75}$ = 0.04s

Strain level in one cycle of ARB = $\frac{2}{\sqrt{3}} \ln\frac{t}{t0} = 1.154 * \ln\frac{0.24}{0.24*2}$ = 0.8

Strain rate = $\dot{\varepsilon}$ = 0.8/0.04 = 20 s^{-1}

This is an average rate because final foil has a thickness range between 0.2 mm to 0.28 mm.

Appendix D: load calculation for DB process

Equation (5) P= $\frac{F}{A}$ => F= 10*(π*r^2) = 10*(3.14*5^2) = 785 N

Appendix E: An example of plain strain within a brass strip

As the material used for this research was expensive so some practices were done by other cheap materials to gain experience.

Rolling conditions could be adapted with compression rules. The following mentioned equations have been extracted from reference [21].

Reduction area= A= $\frac{A(i-1)-Ai}{A(i-1)}$*100, Engineering strain= e= $\frac{t(i-1)-ti}{t(i-1)}$

True strain= ε= ln$\frac{t(i-1)}{ti}$ and von Mises criterion: $\varepsilon = \frac{2}{\sqrt{3}}\ \varepsilon_3$

In those equations the variable is the thickness of the strips instead of their length because in the plain rolling condition the strain in the width condition, ε_2, is zero i.e. plain strain [21].

Table 16 – Sequence of 9 R&C cycles and strain in each cycle

Condition	Number of gear teeth	Width (average of 3 points in mm)	Thickness (average of 3 points in mm)	Reduction area	True strain	Engineering strain	von Mises criterion
Primary	Base	24.65	2.10	-	-	-	-
1st reduction	16 teeth	24.67	1.72	0.180	0.200	0.181	0.230
2nd reduction	16 teeth	24.73	1.33	0.224	0.257	0.227	0.297
3rd reduction	16 teeth	24.93	0.88	0.333	0.413	0.338	0.477
4th reduction	16 teeth	25.32	0.57	0.342	0.434	0.352	0.501
5th reduction	2 teeth	25.43	0.37	0.348	0.432	0.351	0.499
6th reduction	1 tooth	25.60	0.33	0.102	0.114	0.108	0.132
7th reduction	1 tooth	25.65	0.28	0.150	0.164	0.151	0.190
8th reduction	1 tooth	25.75	0.25	0.104	0.113	0.107	0.131
9th reduction	1 tooth	25.88	0.23*	0.075	0.083	0.080	0.096

- * means that in this thickness the gap between the roll mills is closed tightly.

Appendix F: a sort of justification of results presented in Table 8

Another method to ensure the correctness of calculating root presented in table 8 could be in the following;

Thickness of primary batch = 0.325 mm

Thickness of the multilayer after 15 cycles = 0.240 mm (measured)

Number of couples after 15 cycles = 16384

An imaginary stack composed of 16384 of primary couple = 16384*0.325 = 5324.8 mm

The strain to have a foil of 0.24 mm from a stack of 5324.8 mm thick = ln (5324.8/0.24)= 10

That value is similar to the value presented in the last column and raw of table 8.

Appendix G:

Equations 6 to 8 have been extracted from reference [14], the Gibbs free energy of formation of three intended intermetallic phases between 627 ºC and 927 ºC is in the following;

Equation (6) $\Delta_f G°_{TiNi} = -41.6 - 0.2329T$ (kJ/mol)

Equation 7) $\Delta_f G°_{Ti2Ni} = -28.32 - 0.3669T$ (kJ/mol)

Equation(8) $\Delta_f G°_{TiNi3} = -32.2 - 0.4709T$ (kJ/mol)

Another paper [40] gives other values in the equations of free energy of formation of the three intermetallic compounds which are mentioned in equations 9 to 11.

Equation (9) $G(TiNi) = -54600+18.133T$(J/mol)

Equation (10) $G(TiNi_3) = -55585+15.962T$(J/mol)

Equation (11) $G(Ti_2Ni) = -49120+17.208T$(J/mol)

It should be mentioned that all the above mentioned results belong to the equilibrium conditions so the real values of any experiment done under non equilibrium conditions would differ from those values.

Appendix H:

Here, it is tried to evaluate that value through level rule;

SEM/EDS gave the weight percentage of the Ni in that region = 9.51wt%

According to the equilibrium diagram: $\%Ti_2Ni = \frac{9.51-1}{37.8-1} = 23\%$

The calculated value is almost close to 26% given by the software of SEM.

Appendix I: Results of the hardness measurements

Table 17 – Microhardness results from the primary material to the 4 cycle

Place of indentation	*HV 0.01*	*Place of indentation*	*HV 0.05*
Primary materials			
Pure Ni foil	150±3	Pure Ni foil	136±2
Pure Ti foil	152±4	Pure Ti foil	150±6
1st cycle of ARB includes 4 layers			
Ni layer on surface	242±4	Ni layer at top	272±2
Ni layer in middle	220±4	Ni layer in middle	243±10
Ti layer in middle	207±13	Ti layer in middle	222±4
Ti layer at bottom	207±3	Ti layer at bottom	213±2
1st interface of Ni/Ti	249±5	1st interface of Ni/Ti	252±6
3rd interface of Ni/Ti	261±9	3rd interface of Ni/Ti	251±4
1st cycle of ARB includes 4 layers – hardness of the interfaces			
1st interface of Ni-Ti	249±5	1st interface of Ni-Ti	252±6
3rd interface of Ni-Ti	261±8	3rd interface of Ni-Ti	251±4
4 cycles of ARB (as rolled) includes 32 layers – test position thickness = 170 µm			
Almost 35 µm from surface	258±13	Almost 35 µm from surface	283±2
Almost 85 µm from surface	247±5	Almost 85 µm from surface	272±5
Almost 135 µm from surface	249±10	Almost 135 µm from surface	276±2

Table 18 - Microhardness results of the samples experianced intermediate annealing

Place of indentation	*HV 0.01*	*Place of indentation*	*HV 0.05*
1st interval annealing after 4 cycles of ARB - includes 32 layers – test position thickness = 150 μm			
This load could cover neither all the phases nor just one phase and results had large differences e.g. a difference of 115HV was observed.		Almost 25 μm from surface	280±5
		Almost 75 μm from surface	286±29
		Almost 125 μm from surface	266±17
6 cycles after 1st interval annealing includes 1024 layers – test position thickness = 300 μm			
Phase's distribution is not homogeneous.		Almost 40 μm from surface	304±15
Grayish phase	222±9	Almost 150 μm from surface	285±9
Probably Ni layer	294±7	Almost 250 μm from surface	315±18
**2nd interval annealing after 10 cycles of ARB - includes 1024 layers – test position thickness = 150 μm*			
Phase's distribution is not homogeneous.		Almost 25 μm from surface	316±24
Matrix	289±10	Almost 75 μm from surface	330±22
White phase	608±46	Almost 125 μm from surface	331±5
1st cycle after 2nd interval annealing includes 2048 layers (exploded sample) – test position thickness = 285 μm			
Phase's distribution is not homogeneous and it is not possible to indent in one point that includes all phases.		Almost 40 μm from surface	403±22
		Almost 140 μm from surface	429±27
		Almost 240 μm from surface	421±24
Matrix	386±8	Matrix phase	335±25
White phase	661±130	White phase - probably $TiNi_3$	589±53
1st cycle after 2nd interval annealing includes 2048 layers (exploded sample) – test position thickness = 285 μm			
Place of indentation		*HV 0.1*	
Matrix excluding white phase		426±12	
Matrix including white phase		449±8	

Table 19 - Microhardness results of the as-rolled strips rolled upto 15 cycles

Place of indentation	*HV 0.01*	*Place of indentation*	*HV 0.05*
10 cycles of ARB (as rolled) includes 1024 layers – test position thickness = 265 µm			
Almost 60 µm from surface	296±15	Almost 40 µm from surface	325±9
Almost 120 µm from surface	289±10	Almost 130 µm from surface	315±5
Almost 180 µm from surface	292±6	Almost 220 µm from surface	335±20
Almost 230 µm from surface	297±32	-	-
Ti layer	299±0	-	-
Ni layer	282±11	-	-
12 cycles of ARB (as rolled) includes 4096 layers – test position thickness = 280&290 µm			
Almost 40 µm from surface	314±18	Almost 40 µm from surface	330±6
Almost 100 µm from surface	326±13	Almost 100 µm from surface	341±9
Almost 170 µm from surface	307±6	Almost 170 µm from surface	339±9
Almost 250 µm from surface	293±21	Almost 250 µm from surface	341±9
14 cycles of ARB (as rolled) includes 16384 layers			
Different positions	415±15	Different positions	438±32
15 cycles of ARB (as rolled) includes 32768 layers – test position thickness = 240 µm			
Almost 40 µm from surface	484±0.4	Almost 40 µm from surface	516±16
Almost 80 µm from surface	465±41	Almost 120 µm from surface	460±15
Almost 120 µm from surface	464±20	Almost 200 µm from surface	469±24
Almost 160 µm from surface	450±11	-	-
Almost 200 µm from surface	450±11	-	-

Table 20 - Microhardness results of the phases and interfaces of the joints

Place of indentation	*Values in HV 0.01*
1st joint between Nitinol and Ti6Al4V at 800 ºC / 10 MPa / 1h with 10 cycles R&C processed	
Base-Ti6Al4V	296±6
Interface (Ti_2Ni)	480±52
TiNi	317±23
TiNI	315±17
Ti_2Ni	524±14
$TiNi_3$	726±40
Interface without dark points	310±11
Interface including dark points	295±21
Nitinol	267±13
Place of indentation	*HV 0.1*
Matrix including all phases	295±36
2nd joint between Nitinol and Ti6Al4V at 700 ºC / 10 MPa / 1h with 10 cycles R&C processed	
Base-Ti6Al4V	296±12
Interface affected by $TiNi_3$ and adjacent region	372±97
Interface not affected by adjacent region	336±40
TiNi	297±9
$TiNi_2$	507±0
$TiNi_3$ containing pure Ni	508±23
Interface	307±23
Nitinol	267±5
Place of indentation	*HV 0.1*
Matrix including all phases	353±24

Table 21 – Macrohardness results of the joints and raw material

Macrohardness – HV1			
	Ti6Al4V	Foil	Nitinol
1st joint	274±5	186±10	235±5
2nd joint	-	289±13	-

References

[1] Y. Zhou and A. Hu, The Open Surface Science Journal 3 (2011) 32-41

[2] ASM Metals Handbook Volume 06 (Copyright 1993 - ASM INTERNATIONAL)

[3] T.P. Weihs, M. Reiss, United States Patent Application Publication (2001) US 0038029 A1

[4] M.A. Rodriguez, D.P. Adams, and R.G. Tissot, International Centre for Diffraction Data (2009) ISSN 1097-0002

[5] D.P. Adams, M.A. Rodriguez, J.P. McDonald, M.M. Bai, E. Jones, L. Brewer, and J.J. Moore, Journal of Applied Physics (2009) 106 093505

[6] Xiaotun Qiu, Reactive Multilayer Foils and Their Application in Joining, Master thesis, Louisiana State University (2007)

[7] T.P. Weihs, O. Knio, M. Reiss, D.V Heerden, United States Patent Application Publication (2005) US 6,863,992 B2

[8] C.C. Koch, Nano Structured Materials (2nd edition – 2007 – William Andrew Publishing)

[9] R.C. Reed, The Superalloys: Fundamentals and Applications (1st published – 2006 - Cambridge University Press)

[10] ASM Metals Handbook Volume 04 (Copyright 2004 - ASM International)

[11] W.D. Callister, D.G. Rethwisch, Materials Science and Engineering (8th edition – 2009 - Wiley)

[12] L. Duarte, Determination of Phase Relations in the Ternary Fe-Ni-Ti and the Quaternary Fe-Ni-Ti-Al Systems, PhD thesis, University of Eidgenössische Technische Hochschule Zürich (ETH) (2009)

[13] S. MIYAZAKI, Y.Q FU, W.M. HUANG, Thin Film Shape Memory Alloys: Fundamentals and Device Applications (1st published – 2009 - Cambridge University Press)

[14] H.S Ding, J.M Lee, B.R Lee, S.B Kang, T.H Nam, Materials Science and Engineering A 408 (2005) 182–189

[15] ASM Metals Handbook volume 2 (Copyright 1990 - ASM International)

[16] ASM Metals Handbook- Volume 03 (Copyright 1992 - ASM International)

[17] H.S Ding, J.M Lee, B.R Lee, S.B Kang, T.H Nam, Materials Science and Engineering A 444 (2007) 265–270

[18] W.C Crone, A.N Yahya, and J.H Perepezko, Materials Science Forum, 386-388, (2002) 597-602

[19] K. Otsuka, X. Ren, Progress in Materials Science 50 (2005) 511–678

[20] C. Leyens, M. Peters, Titanium and Titanium Alloys: Fundamentals and Applications (1st published – 2003 – Wiley-VCH)

[21] ASM Metals Handbook volume 14 (4th printing 1996 - ASM International)

[22] R.Pederson, Microstructures and Phase Transformations of Ti6Al4V, PhD thesis, University of Lulea (2002)

[23] W.F.Smith, Principles of Materials Science and Engineering (3rd edition – 1996 – McGraw-Hill Inc.)

[24] S. Simões, F. Viana, M. Kocak, A.S Ramos, M.T Vieira, M.F. Vieira, Materials Chemistry and Physics 128 (2011) 202–207

[25] M.J. Zehetbauer, Y.T. Zhu, Bulk Nano-Structural Materials (1st published – 2009 - Wiley-VCH)

[26] D. Yang, Nanograin Metals and Metallic Multilayers Produced by Severe Plastic Deformation, PhD thesis, Deakin University (2011)

[27] J.G. Lenard, Primer on Flat Rolling (1st edition - 2007 - Elsevier)

[28] G.P.Dinda, Nonequilibrium Processing of Amorphous and Nano Structured Materials, PhD thesis, University of Saarlandes (2006)

[29] W.C. Crone, A.N. Yahya, and J. Perepezko, Influence of Grain Refinement on Superelasticity in NiTi, Proceedings of the SEM Annual Conference on Experimental Mechanics, Portland, OR (2001)

[30] H.S. Liu, B. Zhang and G.P. Zhang, J. Mater. Sci. Technol. 27(1) (2011) 15-21.

[31] H. Inoue, M. Ishio, T. Takasugi, Acta Materialia 51 (2003) 6373–6383

[32] G.F. Bastin and G.D. Rieck, Metallurgical Transactions 5 (1974) 1817-1826

[33] D. Tomus, K. Tsuchiya, M. Inuzuka, M. Sasaki, D. Imai, T. Ohmori, M. Umemoto, Scripta Materialia 48 (2003) 489–494

[34] L. Quintin1, R.M. Miranda, Soldag. Insp. São Paulo 17 Nº 3 (2012) 210-217

[35] M.Akselsen, Joining of Shape Memory Alloys, published in Shape Memory Alloys edited by Corneliu Cismasiu (2010)

[36] S. Simões, F. Viana, A.S Ramos, M.T Vieira, M.F. Vieira, Reaction Zone Formed During Diffusion Bonding of TiNi to Ti6Al4V Using Ni/Ti nanolayers (2013) unpublished work

[37] V. P. Korzhov and M. I. Karpov, Russian Metallurgy (Metally) 2011 No. 4 (2011) 76–78.

[38] ASM Metals Handbook Volume 09 (Copyright 2004)

[39] G. Costanza, M.E. Tata, C. Calisti, Sensors and Actuators A 157 (2010) 113–117

[40] P. He, D. Liu, Materials Science and Engineering A 437 (2006) 430–435

[41] P. Homporová1, C. Poletti, M. Stockinger, F. Warchomicka, Dynamic Phase Evolution in Titanium Alloy Ti-6Al-4V, The 12th World Conference on Titanium (2011)

[42] AV. Yakubovich, A.V. Verkhovtsev, M. Hanauske, A.V. Solov'yov, Computational Materials Science, in press (2013)

[43] K.J. Lee and P. Nash, Journal of Phase Equilibria 12 No. 5 (1991)